5-2005

A Validation Simulation of a Large Pool Fire

W. Reid Williams
University of Tennessee - Knoxville

To the Graduate Council:

I am submitting herewith a thesis written by W. Reid Williams entitled "A Validation Simulation of a Large Pool Fire." I have examined the final electronic copy of this thesis for form and content and recommend that it be accepted in partial fulfillment of the requirements for the degree of Master of Science, with a major in Engineering Science.

AJ Baker, Major Professor

We have read this thesis and recommend its acceptance:

DJ Icove, Charles Collins

Accepted for the Council:
Dixie L. Thompson

Vice Provost and Dean of the Graduate School

(Original signatures are on file with official student records.)

To the Graduate Council:

I am submitting herewith a thesis written by W. Reid Williams entitled "A Validation Simulation of a Large Pool Fire." I have examined the final electronic copy of this thesis for form and content and recommend that it be accepted in partial fulfillment of the requirements for the degree of Master of Science, with a major in Engineering Science.

A J Baker /s/

Major Professor

We have read this thesis
and recommend its acceptance:

D J Icove /s/

Charles Collins /s/

Accepted for the Council:

Anne Mayhew /s/

Vice Chancellor and
Dean of Graduate Studies

(Original signatures are on file with official student records.)

A VALIDATION SIMULATION OF A LARGE POOL FIRE

A Thesis
Presented for the
Master of Science
Degree
The University of Tennessee, Knoxville

W. Reid Williams
May 2005

ACKNOWLEDGMENTS

A. J. Baker has served as my advisor and major professor since a meeting in January 1999 to discuss graduate studies prompted by a posted notice of the two-course sequence in finite element modeling that he teaches. He encouraged me to "get my feet wet" that Winter semester with a senior level partial differential equations course included in the Engineering Science graduate curriculum. The following Fall and Spring, he introduce the concepts of finite element modeling, including discussions of grid refinement and ultimately, application of the "eye-ball norm" ... a particularly useful concept when comparing fire test data with simulation results. Dr. Baker also approved my taking a special topics course on combustion fire modeling in lieu of a course not frequently offered.

David Icove taught the combustion fire modeling course, in which he introduced an earlier version of the *Fire Dynamics Simulator* code, and served as a member of my thesis committee. The availability of this code and my familiarity with the Sandia tests from prior work-related assignments prompted the thesis proposal leading to the simulations presented herein.

Charles Collins taught a senior level numerical algebra course in a manner that was interesting, challenging, and informative. He has served as a member of my thesis committee.

Raw data from the 1983 fire tests were provided by Sandia National Laboratories in 2002. Julie Gregory, one of the authors of the report documenting those tests, *Thermal Measurements in a Series of Large Pool Fires* [SAND85-0196], directed me to Louis Gritzo, Manager, Fire Science and Technology Department. Walt Gill forwarded the data and facilitated understanding of the files received.

Financial support for graduate studies has been provided by the operating contractors of the Y-12 National Security Complex through the Educational Assistance Program: initially, Lockheed Martin Energy Systems, Inc., then BWXT Y-12, L.L.C. My supervisors have also been supportive of my studies and have accommodated impromptu changes in hours of work prompted by long nights of study.

My wife and children have encouraged and supported my studies. It has not always been easy to balance the responsibilities of home, work, and school.

ABSTRACT

The capabilities of the *Fire Dynamics Simulator (Version 3)* (FDS3) have been examined to determine whether a large pool fire test can be reasonably simulated. Activities undertaken include 2-D and 3-D pool fire modeling in the absence of wind and heat sinks within the fire principally to compare flame height predictions to established correlations, wind field modeling specifically targeted at developing initial velocity and boundary conditions to use in the simulation of an actual pool fire, and simulation of a specific pool fire test conducted by Sandia National Laboratories in 1983. Processes were developed for determining flame heights based on the criterion that flame height is defined as the height at which the flame is observed at least 50% of the time and for transforming wind field data associated with an outdoor test into initial and boundary conditions for simulating the test. It was concluded that modeling of large pool fires should be accomplished with full 3-D models, maximum burn rate should not be specified, the default radiation fraction in FDS3 should be explicitly overridden with a value of zero, and ignitors should be specified to initiate combustion. While the FDS3 simulations reflect the "highly turbulent nature of a large open pool fire and its susceptibility to winds [which] produce temperature and flow fields that are very nonuniform in both a spatial and temporal sense," further refinement of the grid in the area of the calorimeter and instrumentation modeled and reassessment of the heat of vaporization of JP-4 are expected to improve agreement between simulation results and test data. There is a significant difference between established flame height correlations and simulation results, and a potential explanation is presented. It also appears—other factors being the same—that the minimum pool dimension may be a better correlating parameter for flame height that equivalent diameter or hydraulic diameter. Several recommendations regarding potential enhancements to the FDS code are also included which, if implemented, would facilitate future modeling of outdoor fire tests.

TABLE OF CONTENTS

LIST OF TABLES

LIST OF FIGURES

ABBREVIATIONS AND SYMBOLS

Abbreviations

2-D, 3-D	two- and three-dimensional
CFR	Code of Federal Regulations
DSA	Documented Safety Analysis
DNS	Direct Numerical Simulation
DOE	U.S. Department of Energy
E, W, N, S	compass directions, east, west, north, and south
FDS3	*Fire Dynamics Simulator*, Version 3
LES	Large Eddy Simulation
RAM	random access memory
SARP	Safety Analysis Report for Packaging
SSCs	Structures, Systems, and Components

Symbols

A	surface area
A_f	horizontal burning area of the fuel
c_p	heat capacity of material
D	diameter of the fire, m
D_e	effective diameter
D_h	hydraulic diameter
F	shape factor
g	gravitational acceleration
$\Delta H_{c,eff}$	effective heat of combustion
H_f	flame height
L	pool length
m	mass of material
$\dot{m}''$	burning or mass loss rate per unit area
n, m	relative step sizes
Q	total energy gained by the material
$\dot{Q}$	heat release rate of the fire
t	time
T_{eff}	effective absolute temperature
T_i	initial wall temperature
T_r	absolute temperature at radius r from the centerline
T_R	radiation temperature
T_w	wall temperature
V	wind velocity
V_x or U	east-west component of velocity (winds from the east are negative)
V_y or V	north-south component of velocity (winds from the north are negative)
W	pool width

$_{1, 2}$	subscripts signifying the original and adjusted velocity components
δ	surface thickness
θ	direction from which wind originates
$\kappa\beta$	empirical constant
ρ	density of material
ρ_a	ambient air density
σ	Stefan-Boltzmann constant

Units

°C, C	degrees Celsius © used in figures)
°F, F	degrees Fahrenheit (F used in figures)
ft, '	foot
g	gram
GB	gigabytes
GHz	gigahertz
in., "	inch
K	Kelvins
kg	kilogram
kJ	kilo-Joule
m	meter
min	minute
mol	gram mole
s	second
W	Watt

1. INTRODUCTION

Fire analysis runs the gamut from the use of textbook correlations to complex computer modeling to various types of testing and is performed in support of design, safety analysis, and post-fire assessments. Analyses may be pursued to test hypotheses concerning fire origin and spread or be undertaken to demonstrate that a design would meet specified conditions when testing falls short of prescribed conditions. Regardless of the application, the limitations and validity of the analysis approach applied must be understood.

The analyses reported herein have been undertaken to develop a validation simulation comparing results of the *Fire Dynamics Simulator* computer code—specifically, Version 3 [FDS3-TRG; FDS3-UG]—to measured fire and calorimeter temperatures obtain from a large pool fire test. Achieving such an objective is complicated by the transient, turbulent nature of fire compounded by the effects of wind outdoors, limitations on the understanding and modeling of transport mechanisms, and computing resource limitations which affect mesh refinement from the standpoints of both adequate resolution and timely completion of runs.

This introduction presents an overview of fire analysis requirements for packaging, facility safety analysis, and design, principally for nuclear activities in Sect. 1.1; a description of the FDS3 code in Sect. 1.2; a brief introduction to pool fire tests conducted by Sandia National Laboratories in 1983 in Sect. 1.3; and a summary of inherent difficulties in fire analysis in Sect. 1.4. Chapter 2 presents material properties needed to implement the current analyses, and Chapter 3 examines radiation to thermally-thick and -thin wall models to verify heat transfer capabilities for evaluating backface temperatures in a calorimeter. Chapter 4 presents a series of two- and three-dimensional pool fire models in the absence of wind and without a calorimeter. This chapter compares standard correlations and methods for estimating flame height and compares FDS3 results to the classical methods. Chapter 5 presents the derivation of the wind field model used in the simulations of a selected Sandia pool fire that are presented in Chapter 6. Conclusions and recommendations for future modeling efforts are presented in Chapter 7.

1.1 FIRE ANALYSIS REQUIREMENTS

The following sections outline requirements that may invoke fire analysis. The requirements address safety analysis and design requirements for packaging for the transportation of nuclear materials and for nuclear facilities.

1.1.1 Safety Analysis Report for Packaging

Packaging for the transportation of nuclear materials is required to meet a specified set of tests conducted in a prescribed sequence including drop, thermal, and immersion testing. Compliance with the requirements of 10 CFR 71, *Packaging and Transportation of*

Radioactive Material [10 CFR 71], is demonstrated in a Safety Analysis Report for Packaging (SARP). The thermal test is specified 10 CFR 71.73©)(4):

> Thermal. Exposure of the specimen fully engulfed, except for a simple support system, in a hydrocarbon fuel/air fire of sufficient extent, and in sufficiently quiescent ambient conditions, to provide an average emissivity coefficient of at least 0.9, with an average flame temperature of at least 800°C (1475°F) for a period of 30 minutes, or any other thermal test that provides the equivalent total heat input to the package and which provides a time averaged environmental temperature of 800°C. The fuel source must extend horizontally at least 1 m (40 in), but may not extend more than 3 m (10 ft), beyond any external surface of the specimen, and the specimen must be positioned 1 m (40 in) above the surface of the fuel source. For purposes of calculation, the surface absorptivity coefficient must be either that value which the package may be expected to possess if exposed to the fire specified or 0.8, whichever is greater; and the convective coefficient must be that value which may be demonstrated to exist if the package were exposed to the fire specified. Artificial cooling may not be applied after cessation of external heat input, and any combustion of materials of construction, must be allowed to proceed until it terminates naturally.

Note that the regulations permit testing or calculations to demonstrate compliance. Testing may be performed in a pool fire or inside a furnace. Calculations may be used directly to simulate the thermal testing requirements or may be used as an adjunct to testing when some aspect of the testing falls short of the requirements.

When a package cannot meet the hypothetical accident conditions described in 10 CFR 71.73, an alternative approach is available which is documented in a Transportation Safety Risk Assessment [see 10 CFR 71.41©)]. This alternative approach is similar to that described in the following subsection.

1.1.2 Documented Safety Analysis[†]

A different approach is taken when analyzing accidents in nuclear facilities. In this case, accident scenarios—and, hence, specific accident characteristics reflecting facility specific conditions (i.e., accident sequence, flame temperature, duration, relative location of fuel and hazardous materials, etc.)—are defined pursuant to the preparation of a Documented Safety Analysis (DSA) for a nuclear facility [3009 CN2, p. 14]:

[†] Documented Safety Analysis is terminology introduced by 10 CFR 830, *Nuclear Safety Management*, when referring to the document evaluating the safety of a nuclear facility. One standard that is used for preparing DSAs is DOE-STD-3009. Earlier revisions of DOE-STD-3009 used the term Safety Analysis Reports which may be more familiar to readers.

> The complete spectrum of accidents are examined in hazard analysis. A limited subset of accidents ... that bound "the envelope of accident conditions to which the operation could be subjected" are carried forward to accident analysis ... These scenarios are the accidents requiring formal definition. Information obtained from specific accidents or representative accidents enveloping many small accidents are used to specify functional requirements for safety class [structures, systems, and components (SSCs)] ...

Test results introduced subsequently along with other tests documented in the test report [SAND85–0196] suggest large fires may have average temperatures exceeding those required for the preparation of SARPs. An example of the application of higher temperatures being applied in support of a DSA is provided in reports prepared by the author [WRW; WRW&JCA]. In these analyses, the principal results were estimated times to failure of cylinders containing uranium hexafluoride, with subsequent work directed at defining the consequences and specifying controls to prevent or mitigate the postulated accident.

1.1.3 Design

Design criteria for U.S. Department of Energy (DOE) nuclear facilities are specified in a DOE Order and supporting guide which draw a clear relationship between safety analysis and design. DOE O 420.1A, *Facility Safety*, states [420.1A, p. 4]:

> Detailed application of [design] requirements shall be guided by safety analyses that establish the identification and functions of safety (safety class and safety significant) [SSCs] for a facility and establish the significance to safety of functions performed by those SSCs. ... A safety analysis shall be performed at the earliest practical point in conceptual or preliminary design, so that required functional attributes of safety SSCs can be specified in the detailed design. ...

Likewise, DOE G 420.1-1, *Nonreactor Nuclear Safety Design Criteria and Explosives Safety Criteria Guide for Use with DOE O 420.1, Facility Safety*, states [G 420.1-1, pp. 5 and 6]:

> Selection and design of safety SSCs is an important part of the overall facility design process. As the facility design progresses from conceptual design through the finalization of design, designers and safety analysts must exchange information in an iterative process. ...
>
> Sufficient hazard and accident analyses must be completed during the preliminary design to verify and finalize the selection of safety SSCs. These hazard and accident analyses must be sufficiently complete to determine the design environmental and load conditions for safety SSCs. ...

While much design work is guided by established design practices, opportunities may arise for applying fire modeling simulation codes.

1.2 *FIRE DYNAMICS SIMULATOR*, VERSION 3 (FDS3)

The FDS3 code is a computational fluid dynamics model for simulation of fire-driven fluid flow developed by the National Institute of Standards and Technology. The software implements a form of the Navier-Stokes equations appropriate for low-speed, thermally-driven flow with an emphasis on smoke and heat transport from fires. The formulation of equations and numerical algorithms is described in *Fire Dynamics Simulator (Version 3) – Technical Reference Guide* [FDS3-TRG]. Guidance for preparing and executing FDS3 models is provided in *Fire Dynamics Simulator (Version 3) – User's Guide* [FDS3-UG]. The following subsections provide a high-level description of the FDS3 code.

1.2.1 Hydrodynamic Model

An approximate form of the Navier-Stokes equations appropriate for low Mach number flow is used in the model. The approximation involves filtering out acoustic waves—by replacing pressure in the state and energy equations with the background pressure—while allowing for large variations in temperature and density giving the equations an elliptic character consistent with low speed, thermal convective processes. The computation can either be treated as a Direct Numerical Simulation (DNS), in which the dissipation terms are computed directly, or as a Large Eddy Simulation (LES), in which the large-scale eddies are computed directly and the sub-grid scale dissipation processes are modeled. The choice of DNS versus LES depends primarily on the resolution of the computational grid. For example, when simulating the flow of smoke through a large, multi-room enclosure, it is not possible to resolve the combustion and transport processes directly. However, for small-scale combustion experiments, it is possible to compute transport directly and the combustion processes to some extent. The LES model, which is the default option in FDS3, is applicable to the multi-room example, while the DNS model could be used for small-scale combustion. [FDS3-TRG, pp. 3–4; FDS3-UG; p. 15]

1.2.2 Combustion Model

Two types of combustion models have been implemented in the FDS3 code. The choice depends on the resolution of the underlying grid. For a DNS calculation where the diffusion of fuel and oxygen is evaluated directly, a global one-step, finite-rate chemical reaction is most appropriate. However, in an LES calculation where the grid is not fine enough to resolve the diffusion of fuel and oxygen, a mixture fraction-based combustion model is used.

The mixture fraction combustion model assumes a mesh refinement sufficiently dense that large-scale convective and radiative transport phenomena can be simulated directly, but physical processes occurring at smaller length and time scales must be approximated. The

approximations employed reflect the spatial and temporal resolution limits of the computation and current limited understanding of the phenomena involved.

The chemical rate processes that control combustion energy release in fire scenarios are often unknown. Even if they were known, the spatial and temporal resolution limits imposed by present and foreseeable computer resources place a detailed description of combustion processes beyond reach. Thus, the model adopted in FDS3 assumes that combustion is mixing-controlled which implies that all species of interest can be described in terms of a mixture fraction Z(x, t). The mixture fraction is a conserved quantity representing the fraction of material at a given point that originated as fuel. The relations between the mass fraction of each species and the mixture fraction are known as "state relations". The state relation for the oxygen mass fraction provides the information needed to calculate the local oxygen mass consumption rate. The form of the state relation that emerges from classical laminar diffusion flame theory is a piecewise linear function. This modeling approach leads to a "flame sheet" model, where the flame is a two-dimensional surface embedded in a three-dimensional space. The local heat release rate is computed from the local oxygen consumption rate at the flame surface, assuming that the heat release rate is directly proportional to the oxygen consumption rate, independent of the fuel involved.

In the numerical algorithm implementing the mixture fraction model, the local heat release rate is computed by first locating the flame sheet, then computing the local heat release rate per unit area, and finally distributing the energy to the grid cells cut by the flame sheet. In this way, the genuinely, infinitely thin flame sheet is smeared out over the width of one grid cell, consistent with all other gas phase quantities.

The physical limitation of the mixture fraction approach to modeling combustion is the assumption that fuel and oxygen burn instantaneously when mixed. For a large-scale, well-ventilated fire, this assumption is appropriate. [FDS3-TRG, p. 8–11]

1.2.3 Radiation Transport

The default mode of radiation heat transfer assumes a non-scattering gray gas since the radiation spectrum of soot is continuous. A wide band model can be invoked (which is recommended only if the fuel is relatively non-sooting).

In calculations in which grid cells are on the order of a centimeter or larger, the average temperature of a cell cut by the flame surface may be significantly reduced from the temperature that would be associated with the flame itself with a consequent significant impact on radiation heat transfer. To compensate, the code by default assumes a fraction of the energy release by combustion within the cell is emitted as thermal radiation. This fraction can be adjusted by the user or use of the gas temperature can be forced. [FDS3-TRG, pp. 13–14; FDS3-UG, pp. 25–26, 64, 66]

1.2.4 Geometry

The governing equations solved in the FDS3 code are written in terms of a three-dimensional Cartesian coordinate system. Several options are available for refining the computational grid. One method, multiblocking, allows specification of several grids with the code giving precedence when grids overlap to the first specified mesh. Another option is to stretch the mesh, but this option is limited to two of three coordinate directions. Obstructions, vents, etc., are forced to conform with the grid(s) established by the user. Two-dimensional Cartesian or axisymmetric cylindrical models can also be developed. [FDS3-UG, pp. 1, 17–18, 64]

1.2.5 Boundary Conditions

A wide range of boundary conditions can be specified for solid surfaces, liquid fuel surfaces, and for vents. Solid surfaces may be thermally thick or thermally thin, and conduction through a wall can also be modeled. Pyrolysis characteristics can be specified for solid and liquid surfaces. Vents may be open or forced flow can be specified. Material properties associated with solids and fuels may be specified in the input file of in a database invoked from the input file. [FDS3-TRG, pp. 16–18; FDS3-UG, pp. 1, 20ff]

1.2.6 Model Accuracy

The FDS3 code is an evolving fire model originally designed to analyze industrial-scale fires. For cases where the building is relatively large in relation to the fire, the FDS3 code predicts flow velocities and temperatures to an accuracy of 10 to 20% relative to experimental measurements [FDS3-TRG, p. 41]. A comparison of predicted to experimental temperatures for large, outdoor fires is a goal of this thesis.

1.3 SANDIA FIRE TESTS

In 1983, Sandia National Laboratories conducted a series of tests in which a 5-ft-diameter, 21-ft-long, mild steel calorimeter was exposed to fire above a 30 ft by 60 ft pool. The calorimeter is similar in size to packages that are subject to the packaging requirements previously discussed. The tests were well instrumented to characterize the fire environment and the thermal response of the calorimeter. A direct comparison between one of the tests and results from an FDS3 simulation is an objective of this study. Several summaries of fire temperature results are provided in Appendix A for the three tests in the series. These summaries demonstrate the variability of the fire environment. Details of the test site are provided in Chapter 6.

1.4 INHERENT DIFFICULTIES IN FIRE ANALYSIS

A number of difficulties present themselves immediately when considering fire analysis. First, a real fire exhibits large and small scale transient, unsteady behavior. As noted in the introduction of the Sandia report [SAND85–0196, p. 7]:

> The thermal environment in an actual large open pool fire is not well-defined ... The highly turbulent nature of a large open pool fire and its susceptibility to winds produce temperature and flow fields that are very nonuniform in both a spatial and temporal sense.

For the current pool fire modeling, the preceding quote notes another complicating factor: wind ... wind direction and speed continually vary with time. Development of the wind field model used in the simulation of one of the Sandia fire tests is presented in Chapter 5. The wind field model in the absence of a fire is compared to data in Sect. 5.2.3 and in the presence of fire in Sect. 6.3.2.

Other difficulties arise with the code used to model a fire. For example, FDS3 is based on a Cartesian coordiante system, but the calorimeter to be modeled is cylindrical. Also, while the FDS3 code considers conduction perpendicular to a wall, conduction parallel to the surface is not considered.

2. MATERIAL PROPERTIES

Thermophysical properties are required for JP-4, the fuel used for the Sandia pool fire tests and the current modeling, for the A517 steel used to fabricate the large calorimeter (see Chapter 5), and for the generic steel used for the wall modeling in Chapter 3.

2.1 JP-4

JP-4 is an aviation fuel typically composed of about 50-60% gasoline and 40-50% kerosene, is highly volatile, and contains hydrocarbons in the C4-C16 range [TI#19206]. *Toxicological Profile for Jet Fuels JP-4 and JP-7* identifies a heat of combustion, an ignition temperature, a density range, and listings of hydrocarbon constituents useful for estimating an effective molecular weight, heat of vaporization, and combustion stoichiometry of JP-4 [ATSDR, Tables 3-3, 3-5, 3-6, and 3-8]. Other thermophysical properties—thermal conductivity, heat capacity, and thermal diffusivity—are based on information contained in *Perry's Chemical Engineers' Handbook* [Perry's, Tables 3-200, 3-275] and the gasoline/ kerosene composition noted previously.

Table 2.1 lists JP-4 properties used in the current analyses. Maximum burn rate and heat of vaporization are discussed further in the following paragraphs.

Maximum Burn Rate. The Sandia test report provides information for estimating average burn rate which can be set as the maximum burn rate in the FDS3 models. The initial depth of JP-4 for Tests A and B was about 8.5 in. while the depth for Test C was 7.5 in., and burn times were 35 min for the first two tests and 29 min for the third test [SAND85-0196, p. 12]. These data yield burns rates, based on the average density of JP-4, of 0.080 and 0.085 kg/m^2-s, respectively. The value for BURNING_RATE_MAX used in this report, 0.074 kg/m^2-s, was carried over from an earlier course assignment and the discrepancy was not noted until may of the cases documented herein had been executed. The anticipated impact of correcting the maximum burn rate to the average value for Test C would be an increase in temperatures and flame height [and is observed in the results for the last case considered in Chapter 6 when the burn rate is not constrained (i.e., tower flame temperatures and flame height are greater for Case C-175d than for Case C-175b)]. A more fundamental observation—that a maximum burn rate should not be set at all—is discussed in Sect. 6.3.3.

Heat of Vaporization. A heat of vaporization was estimated based on values at 25°C [Perry's, Table 3-171]; however, values reflective of the ignition or evaporation temperature would be more appropriate and lower the estimate used. Further review of *Toxicological Profile for Jet Fuels JP-4 and JP-7* indicates a flashpoint for JP-4 of -23 to 1°C and boiling points ranging from 45 to 300°C [ATSDR, Tables 3-3]. The FDS3 User's Guide states that "HEAT_OF_VAPORIZATION ... is the amount of energy required to vaporize a solid or liquid fuel once it has reached it ignition temperature TMPIGN"; therefore, a lesser heat of vaporization and an "ignition temperature" more reflective of the effective boiling point of JP-4 would be more appropriate for future modeling (see further discussion in Sect. 6.3.3).

Table 2.1. Input to FDS3 for JP-4

Property	FDS3 Variable	Value	Units	Ref.
REAC lines:				
Molecular weight	MW_FUEL	112.42	g/mol	Note 1
Ideal stoichiometric coefficients	NU_O2 NU_CO2 NU_H2O	16.06 8.03 8.03	— — —	Note 1
Fuel fraction converted to CO	CO_YIELD	0.012	—	Note 2
Fuel fraction converted to soot	SOOT_YIELD	0.019	—	Note 3
Energy release per O_2 consumed	EPUMO2	9362.5	kJ/kg	Note 4
SURF lines:				
Ignition temperature	TMPIGN	246	°C	ATSDR
Heat of vaporization	HEAT_OF_ VAPORIZATION	364	kJ/kg	See text, § 2.1.1
Heat of combustion	HEAT_OF_ COMBUSTION	42800	kJ/kg	ATSDR
Maximum burn rate	BURNING_ RATE_MAX	0.074	kg/m^2-s	See text, § 2.1.1
Thickness of heated layer	DELTA	0.1	m	Note 2
Thermal conductivity	KS	0.14	W/m-K	Note 5
Thermal diffusivity	ALPHA	8.6×10^{-8}	m^2/s	Note 6

1. Molecular weight is based on listed weight fractions and molecular weights of components [ATSDR]; estimates ranged from about 112 to about 130 with a hydrogen to carbon ratio of about 2. Stoichiometric coefficients are based on complete combustion of $C_{8.03}H_{16.06}$.
2. CO_YIELD and DELTA are carried over from the FDS3 DATABASE3 file values for kerosene.
3. SOOT_YIELD is based on the value for kerosene in the FDS3 DATABASE3 file multiplied by 0.45, the mid-point composition for kerosene [TI#19206].
4. EPUMO2 is calculated from the heat of combustion and reaction stoichiometry.
5. Thermal conductivity (and heat capacity, 2.1 kJ/kg-K) are based on data from Perry's and typical composition [TI#19206].
6. ALPHA is based on KS, heat capacity cited in Note 5, and an average density of 776 kg/m^3 [ATSDR].

2.2 STEEL

Table 2.2 lists properties for the steels used in the current analyses. For the initial radiation modeling discussed in Sect. 2.2, general properties for steel were obtained from Perry's [Tables 3-133, 3-137, 3-271, and 3-274]. The large calorimeter used in the Sandia pool fire tests is constructed of A517 steel; however, material properties for A514, which is in the same product family as A517 [ISG], were used [MatWeb].

Table 2.2. Input to FDS3 for Steel

Property	FDS3 Variable	Value	Units	Ref.
SURF lines for thick and thin wall radiation model (Sect. 2.2):				
Thermal diffusivity	ALPHA	1.11×10^{-5}	m^2/s	Note 1
Thermal conductivity	KS	43.6	W/m-K	Note 1
Wall thickness	DELTA	0.03175	m	—
Backface boundary condition	BACKING	'INSULATED'	—	FDS3-UG
Product of heat capacity, wall thickness, and density	C_DELTA_RHO	120	kJ/m^2-K	Note 1
Emissivity	EMISSIVITY	1 (default)	—	FDS3-UG
SURF lines for large calorimeter (Chapter 4):				
Thermal diffusivity	ALPHA	1.31×10^{-5}	m^2/s	Note 2
Thermal conductivity	KS	46.6	W/m-K	MatWeb
Side wall thickness	DELTA	0.03175	m	Note 3
End cap thickness	DELTA	0.0127	m	Note 3
Backface boundary condition	BACKING	'INSULATED'	—	FDS3-UG
Emissivity	EMISSIVITY	0.8	—	Note 4

1. Based on properties from Perry's.
2. Based on properties for A514 from MatWeb.
3. Based on calorimeter description from SAND85-0196 [p. 8].
4. Various references indicate a wide range of emissivities—typically less than 0.8— for various steels and surface conditions. Regulations specify use of a minimum value of 0.8 for surface absorptivity [10 CFR 71.73(c)(4)].

3. RADIATION MODELING TO THICK AND THIN WALLS

An FDS3 model without combustion was developed to evaluate radiation modeling capabilities. One set of modeling results is compared to analytical results.

3.1 FDS3 MODEL FOR RADIATION TO THICK AND THIN WALLS

The FDS3 code can model four thermal boundary conditions: constant temperature surface, constant heat flux surface, thermally-thick solid yielding a temperature gradient perpendicularly into the surface, or thermally-thin sheet which yields a uniform temperature in the surface material as it is heated or cooled [FDS3-UG, p. 21]. There is no heat conduction parallel to the surface.

The FDS3 model for evaluating radiation consists of five surfaces at a fixed temperature of 800° radiating to a sixth wall initially at 20°C (default initial condition) consisting of six panels for simulating thermally-thick and -thin boundary conditions (see Fig. 3.1). The input file is provided in Appendix B.1.

3.2 ANALYTICAL MODEL FOR A THIN WALL

For a thermally-thin surface, an analytical solution is readily derived. As a material is heated,

$$Q = m\, c_p\, (T_w - T_i)\,, \qquad (1)$$

where Q = total energy gained by the material,
m = mass of material,
c_p = heat capacity of material,
T_w = wall temperature, and
T_i = initial wall temperature.

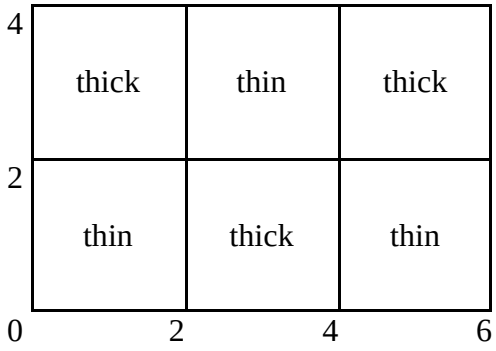

Fig. 3.1. Arrangement of thick and thin surfaces for radiation model.

The mass of the material can be expressed as:

$$m = A\,\delta\,\rho\,, \tag{2}$$

where A = surface area,
δ = surface thickness, and
ρ = density of material.

The heat flux to the surface, assuming all emissivities are 1, is given by

$$\frac{1}{A}\,\frac{dQ}{dt} = F\,\sigma\,(T_R^{\,4} - T_w^{\,4})\,, \tag{3}$$

where t = time,
F = shape factor,
σ = Stefan-Boltzmann constant, and
T_R = radiation temperature.

Taking the derivative of Eq. 1 and combining with Eqs. 2 and 3 yields

$$c_p\,\delta\,\rho\,\frac{dT_w}{dt} = F\,\sigma\,(T_R^{\,4} - T_w^{\,4})\,. \tag{4}$$

Rearranging and integrating Eq. 4 from initial conditions (0, T_i) to time t (t, T_w) yields the analytical solution:

$$\frac{4\,T_R^{\,3}\,F\,\sigma}{c_p\,\delta\,\rho}\,t = \left\{ \ln\left[\frac{1 + (T_w/T_R)}{1 - (T_w/T_R)}\right] + \arctan\,(T_w/T_R) \right\}$$

$$- \left\{ \ln\left[\frac{1 + (T_i/T_R)}{1 - (T_i/T_R)}\right] + \arctan\,(T_i/T_R) \right\}. \tag{5}$$

3.3 RADIATION MODELING RESULTS

The results of the FDS3 model and the analytical solution are plotted in Fig. 3.2. The model results plotted are the averages of the three panels (see Fig. 3.1) corresponding to each of the boundary conditions (i.e., thermally-thick and -thin). The differences between maximum and minimum values for the code results at a given time are less than 2°C. Variation between surface and backface temperatures for the thermally thick model approached 30°C. Point by point comparison between the code and analytical results for the thermally-thin model was not made, but visual observation shows reasonable consistency for the current effort.

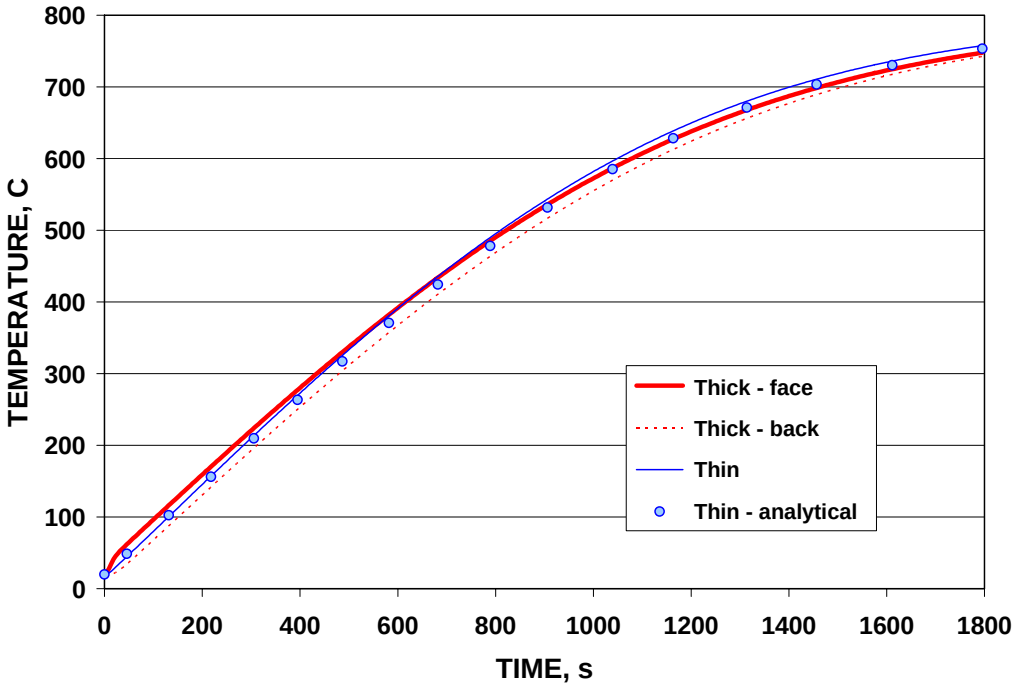

Fig. 3.2. Modeling results for radiation to thermally-thick and -thin surfaces.

4. POOL FIRE MODELING AND FLAME HEIGHT

This chapter focuses on comparing computational pool fire modeling results with established criteria and correlations for estimating flame height. Both two-dimensional axisymmetric models and three-dimensional models of square and rectangular pools are considered.

4.1 CRITERIA AND CORRELATIONS FOR ESTIMATING FLAME HEIGHT

Fire plumes may be divided into three regions: a continuous flame region, an intermittent flame region, and a thermal plume region. Visible flame tips in the intermittent region have temperatures in the range of 320 to 400°C. Flame height is defined as the height at which the flame is observed at least 50% of the time; this height is in the intermittent region. The following correlations of Heskestad and Thomas, respectively, are widely used to estimate the flame height of pool fires [NUREG-1805, pp. 3-14, 3-16 – 3-18]:

$$H_f = 0.235\, \dot{Q}^{2/5} - 1.02\, D\,, \tag{6}$$

and

$$H_f = 42\, D \left[\frac{\dot{m}''}{\rho_a (g\, D)^{0.5}} \right]^{0.61}, \tag{7}$$

where H_f = flame height, m,
$\dot{Q}$ = heat release rate of the fire, kW,
D = diameter of the fire, m,
$\dot{m}''$ = burning or mass loss rate per unit area, kg/m^2-s,
ρ_a = ambient air density, kg/m^3, and
g = gravitational acceleration, m/s^2.

The heat release rate is estimated by

$$\dot{Q} = \dot{m}'' \Delta H_{c,eff} A_f \left(1 - e^{-\kappa\beta D} \right), \tag{8}$$

where $\Delta H_{c,eff}$ = effective heat of combustion, kJ/kg, and
A_f = horizontal burning area of the fuel, m^2.
$\kappa\beta$ = empirical constant, m^{-1}

For the larger pool fires considered herein, the exponential term in Eq. 8 is negligible ($\kappa\beta$ is about 3.6 for JP-4 [NUREG-1805, p. 3-4]). For non-circular pools, the effective diameter, D_e, to be used in place of D in Eqs. 6 and 7 is defined by

$$D_e = (4\, A_f / \pi)^{0.5}\,. \tag{9}$$

While several approaches for estimating flame height from FDS3 output were consider (and will be briefly discussed in Sect. 4.2), an approach based on the 50% criterion was determined best suited for the current effort. Specifically, point measurements of heat release rates per unit volume (HRRPUV) were recorded at specified heights along the plume centerline using the THCP namelist group in FDS3. When burning occurs at the specified height, HRRPUV is positive; otherwise, the value is zero. For the purpose of evaluating these data against the 50% criterion, values less than 0.1 are assigned a zero value and all other values are assigned 1. Summing the 1s and dividing by the total number of readings yields the burn time fraction. Plotting burn time fraction against centerline height yields the flame height when the fraction falls to 0.5.

4.2 FDS3 2-D POOL FIRE MODELS AND RESULTS

Two sets of axisymmetric pool fire models were run with radii of 0.75, 1.5, 3, and 6 m, the latter radius being comparable in size to the Sandia pool fires. Horizontal grid sizes were 0.125, 0.25, and 0.5 m with vertical grid sizes equal to the horizontal grid size in the first set of cases run and three times in the second set. Simulation time was set to 600 s, and data were collected every second. When data from the 2-D series are plotted, pool radius is identified by the first three digits (equivalent to radius in cm), and grid size is determined by raising 0.5 to the power specified by the digit after the hyphen.

In the initial set of runs, temperature, heat release rate per unit volume, and mixture fraction data were collected in the r-z plane; convective heat flux was collected at specified heights; and heat release rate per unit volume was collected over specified volumes. The temperature, heat release rate, and mixture fraction data were examined to determine whether a method was available to determine flame height. Applying the temperature criterion identified in Sect. 4.1, it was expected that a plot of the maximum average temperature versus height would yield flame height when the temperatures fell to the 320 to 400°C range. (The maximum average temperature used for a given height was the maximum of the average temperatures for each radial distance at that height. Average temperatures were determined using the fds2ascii program available in the FDS3 package [FDS3-UG, p. 74].) Figure 4.1 plots data from the initial axisymmetric pool fire models, which indicate (in comparison to Eqs. 6 and 7) that excessively large flame height resulted. Other approaches considering heat release rate and cumulative fraction of heat released were dismissed because there was no sufficiently obvious change in plots of data versus height to suggest a valid criterion for flame height. Use of the stoichiometric mixture fraction as a criterion was also dismissed since the average could be easily skewed by a few large values in comparison to more numerous small values (if such were the case) and since a plot of the stoichiometric mixture fraction also appeared to yield excessive flame heights.

After dismissing these first attempts for estimating flame height, the approach to estimating lame height described at the end of Sect. 4.1 was developed from the 50% criterion Input files for the first set of runs were modified to collect heat release rate per unit volume data at specified heights along the centerline. An example of one of the input files is provided

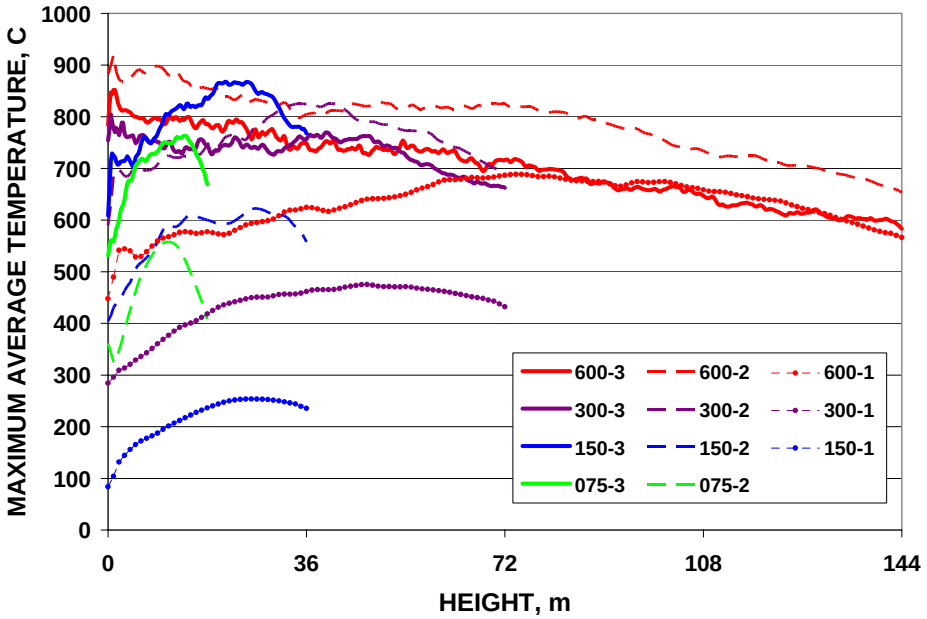

Fig. 4.1. Initial 2-D models: temperature vs height. Excessively high flame heights are anticipated relative to the criterion that flame height corresponds to an average temperature of 320 to 400°C.

in Appendix B.2. Flame height results applying the burn time fraction method are provided in Fig. 4.2. The observed heights are excessive relative to the correlations provided in Sect. 4.1. Note that initial fire development took from about one-half to almost 2 min in these simulations, so the burn time fraction is based on FDS3 output from 200 through 599 s, inclusive.

A final axisymmetric model [3-m radius (6-m diameter)] with equal horizontal and vertical grids (0.25 m) was made as a transition to the 3-D modeling. Results are presented in the next section.

4.3 FDS3 3-D Pool Fire Models and Results

Three-dimensional models of square and rectangular pools were developed for comparison to the axisymmetric models and to the correlations for flame height. These models used a 0.25-m grid above the pool and a 0.75-m grid for the balance of the computational domain, taking advantage of the multiblocking feature introduced in FDS3. An initial series of 3-D runs considered quarter-, half-, and full 3-D models of a 6 m × 6 m pool, which has the same hydraulic diameter as a 6-m diameter pool. Hydraulic diameter is defined by

$$D_h = 2 L W / (L + W) , \qquad (10)$$

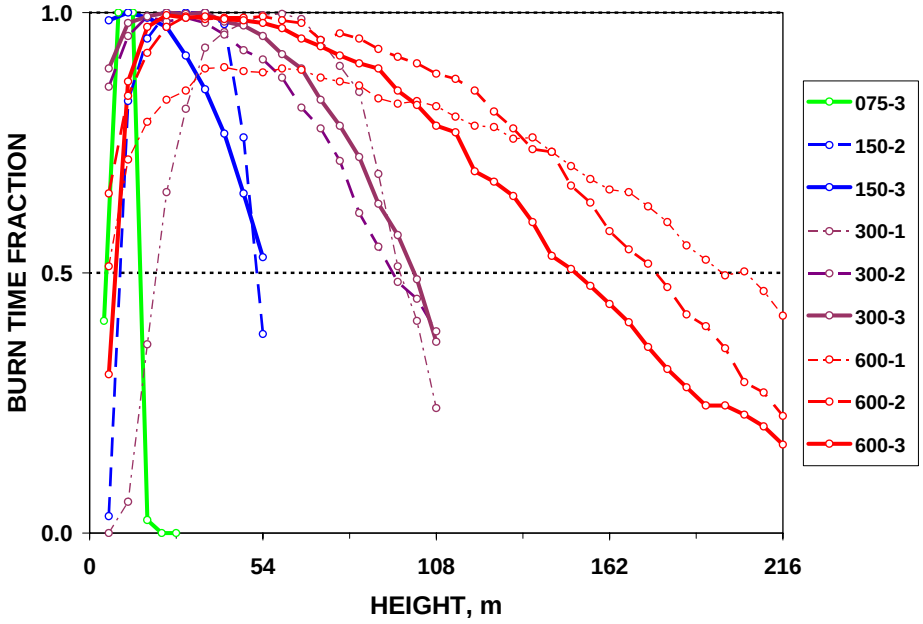

Fig. 4.2. Second set of 2-D models: burn time fraction vs height. Flame height is determined when the burn time fraction falls to 0.5. Excessively high flame heights are again indicated.

where D_h = hydraulic diameter,
L = pool length, and
W = pool width.

Flame heights for this initial sereis of 3-D runs are plotted in Fig. 4.3 along with the results for the final 2-D run (Case R6dia-2) and the earlier 300 series. The 3-D results yield a significant improvement in estimated flame heights, though they remain greater than would be predicted by Eqs. 6 and 7.

In addition to showing a significant improvement in the estimation of flame height, this initial series suggests that full three-dimensional models are preferred to quarter- or half-models ... and that invoking symmetric (mirror) boundary conditions in less than full 3-D simulations does not adequately reflect the large eddies and turbulent mixing in a fire environment. The 6 m × 6 m model (see Appendix B.3 for input data) serves as a basis for the next series of runs which includes a sequence of three models having the same hydraulic diameter ($L \times W$ = 6 × 6, 12 × 4, and 21 × 3.5; D_h = 6 m) and a second sequence of three models having the same effective diameter ($L \times W$ = 6 × 6, 12 × 3, and 24 × 1.5; D_e = 6.77 m). Results from these two sequences are provided in Fig. 4.4.

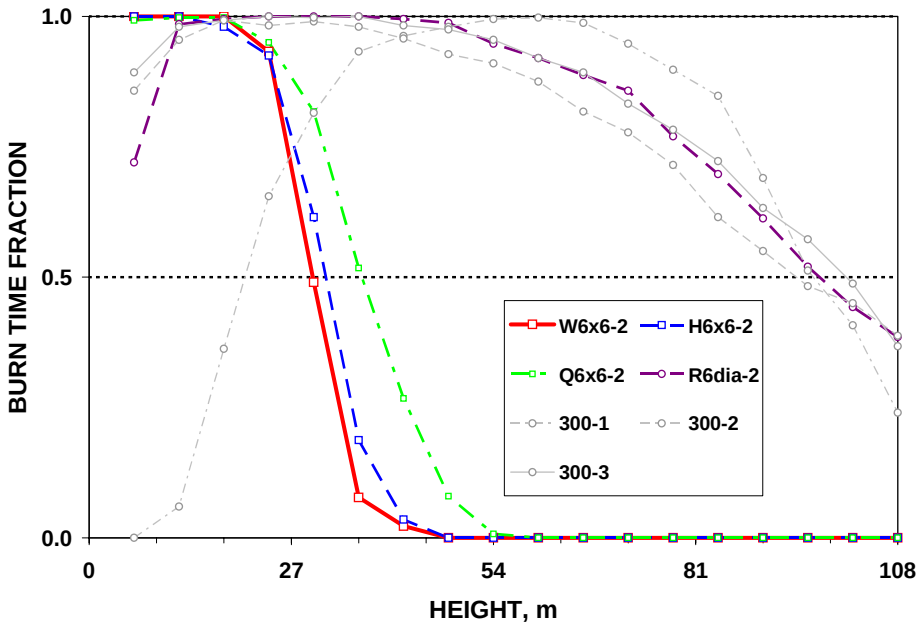

Fig. 4.3. 3-D model results for a 6 m × 6 m pool fire. 2-D 300-series results are repeated from Fig. 4.2, and results for the final 2-D case are included for comparison. All cases have the same hydraulic diameter (6 m).

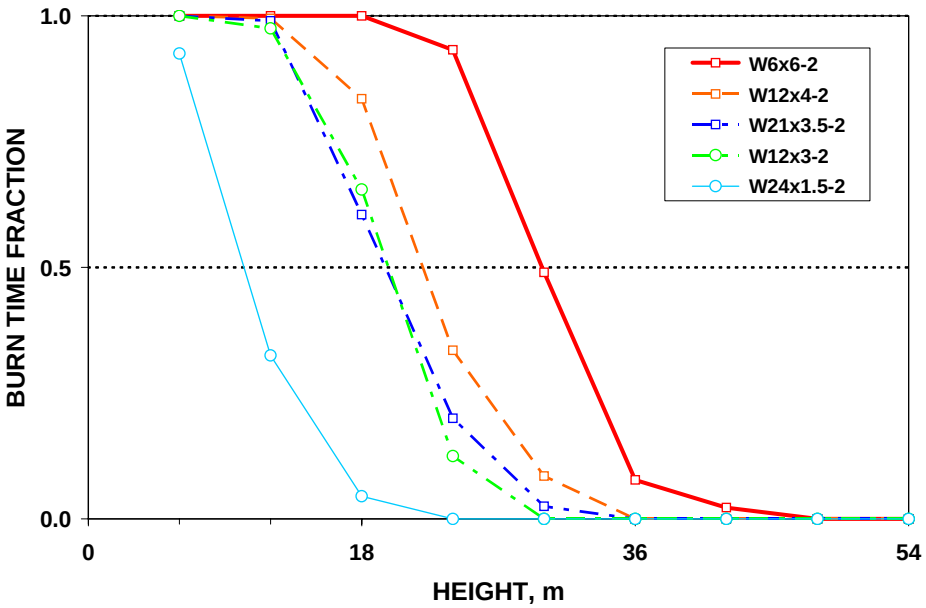

Fig. 4.4. Results for 3-D rectangular pool models. The first 3 cases identified in the legend have the same hydraulic diameter (6 m) while the first and last two cases have the same effective diameter (6.77 m).

The effect of averaging time on burn time fraction estimates is illustrated in Figs. 4.5 and 4.6. Figure 4.5 provides running averages for the indicated times which are plotted at the end of the averaging time. As averaging time increases, the variation in averages decreases, which is apparent in Fig. 4.5. This trend is presented statistically in Fig. 4.6 which provides assurance that the plume height estimates presented in this chapter, which are based on 400-s averages, are not subject to significant variation.

4.4 COMPARISON OF MODELING RESULTS AND CORRELATIONS

Figure 4.7 provides a direct comparison between flame heights predicted by FDS3 3-D pool fire models and the flame height correlations of Heskestad and Thomas (Eqs. 6 and 7). Three different bases were used for plotting the heights derived from the FDS3 models: effective diameter (Eq. 9), hydraulic diameter (Eq. 10), and the minimum pool dimension (i.e., the width). Flame height estimates derived from FDS3 models when plotted against the minimum dimension of the rectangular pool visually correlate well to twice the average of the flame height correlations. In addition to the 3-D model results already presented in this chapter, results from the Sandia pool fire simulations (Cases C-175b and C-175d) are also included. These results infer that neither effective diameter nor hydraulic diameter are

appropriate for estimating flame height for non-circular pools. Rather, the results suggest that the minimum dimension of the pool should be used.

While application of the 50% criterion yields flame height estimates from FDS3 runs that are approximately twice that expected from the correlations, an interesting result was obtained by considering the effect of a large fire on observed temperature. Following the argument that "in ... large hydrocarbon pool fires, it [is] reasonable to assume an emissivity of 1.0" since "the flames only have to be 3 to 6 feet thick to be optically opaque" [Buck and Belason], temperatures over a 1-m distance were averaged as follows:

$$T_{eff} = [(T_r^4 + 0.75\, T_{r-0.25}^4 + 0.5\, T_{r-0.50}^4 + 0.25\, T_{r-0.75}^4)/2.5]^{0.25}, \qquad (11)$$

where T_{eff} = effective absolute temperature, and
T_r = absolute temperature at radius r from the centerline.

Equation 11 was applied to time averaged temperature profiles at 13.5 and 16.25 m in the Y-Z plane from the 6 m × 6 m output. These heights correspond roughly to the heights estimated by Eqs. 7 and 6, respectively. The effective temperatures (converted from their absolute values) are plotted in Fig. 4.8 as dots at the radii of the outermost temperature considered with a bar extending toward the centerline 1 meter. The interesting result is that effective temperatures in the vicinity of 320 to 400°C are observed at 2 m from the centerline. If Eq. 11 were modified for a 2-m thickness, the effective temperature would increase. What has not been considered are the specific impacts of carbon dioxide, water vapor, and soot on the emissivity of the fire plume; however, this result suggests that if the

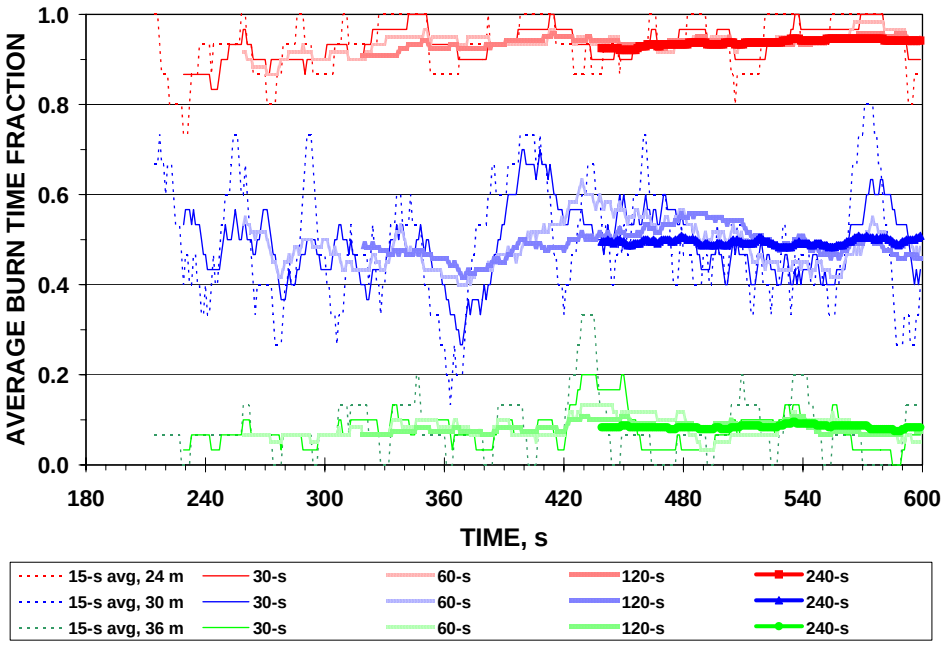

Fig. 4.5. Variation in burn time fraction estimates with averaging times. This plot corresponds to the W6x6-2 case in Figs. 4.3 and 4.4. Values are plotted at the end of the averaging time period.

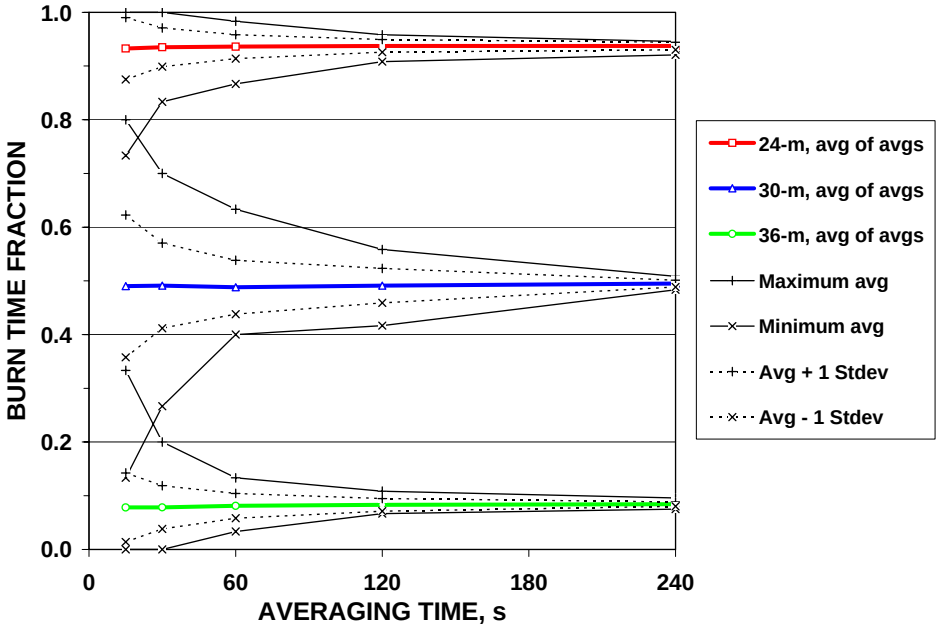

Fig. 4.6. Statistical comparison of burn time fractions vs averaging times. These results correspond to the running averages in Fig. 4.5.

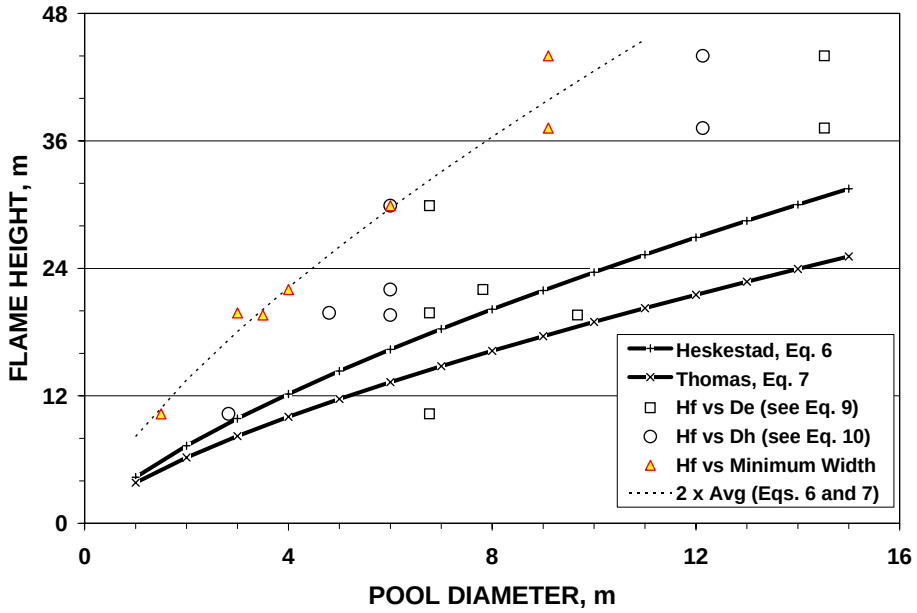

Fig. 4.7. Comparison of 3-D model results to flame height correlations. Data plotted at the same height correspond to the same run plotted against 3 different bases (D_e, D_h, and minimum width).

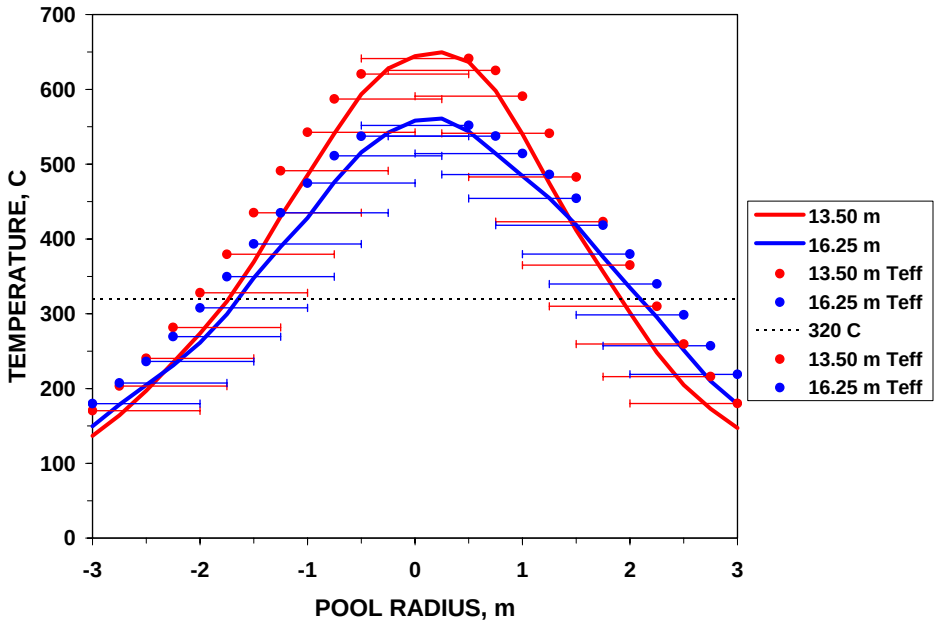

Fig. 4.8. Potential effective fire plume temperatures visible to an observer.

measurement of plume height is dependent on visual observation clouded by smoke or instrument measurements of temperature, there may be significant room for error in inferences made from observations when developing correlations of flame height. An interesting consideration for a future simulation would be to model several thin-walled surfaces aligned perpendicular to the plume centerline with a limited view factor and estimate the effective temperature of the plume from an external vantage point.

5. WIND FIELD MODELING

The development of the wind field model used in the subsequent simulation of one of the Sandia fire tests is described in this chapter. The first step is reduction of time-varying wind field data (direction and velocity) from the Sandia fire tests to a form suitable for input into the FDS3 code (i.e., velocity vectors based on a Cartesian coordinate system). The transformed data is then applied as initial and boundary conditions in a manner that yields a wind field across the domain of the model comparable to the original data.

5.1 DATA REDUCTION

The Sandia fire test report presents data for three tests including wind field data. To facilitate this current study, data from the 1983 tests were requested and received from the authors of the report. The following is a brief description of the wind patterns during each test and reflects some inferences drawn from the smoothing process presented in Sect. 5.1.1 and illustrated by application to data from Test C. Wind field data were obtained from an anemometer atop a bunker located about 120 ft (37 m) from the western edge of the pool [SAND85–0196, pp. 7, 8, and 12].

Test A: At the beginning of the test, the wind direction was from slightly north of east moving to slightly south of east over the first few minutes, then remaining slightly south of east for much of the test before shifting rapidly over the last several minutes around to the north and on to coming out of the west. This test had the most significant variations in wind speed with time. The first half the test reflected neutral or stable conditions while the last half generally reflected unstable conditions. (Daytime conditions typically reflect unstable conditions unless wind speed picks up—about 6 m/s and above—and insolation is slight [AS&PP, p. 591, T 13.2]).

Test B: Unstable conditions characterized the atmosphere during this test with significant variations in wind direction and speed both moment-by-moment and on average. Wind directions varied, on average, from north northeast around to the south, always with an easterly component.

Test C: This test reflected neutral to stable conditions throughout the test except during an early transition of wind direction from the east around to the southwest. The unstable conditions in this case were driven more by the general shift in direction over the averaging time rather than significant moment-by-moment variations. Wind speed also exhibited less moment-by-moment variations than the other tests.

Because of the more uniform stability and consistency in moment-to-moment winds, Test C was chosen as the basis for FDS3 fire simulations presented in Chapter 6.

5.1.1 Smoothing Wind Field Data

Test data were typically collected every 4.5 s although longer times between sequential data are noted. Because of the variations in time, the duration reflecting the averaging time varied from 2.85 to 3.22 min, with averaging times of 2.92 and 3.15 s being typical. Average values were directly obtained by averaging 31 data values—the datum at the specific time plus the 15 values immediately preceding and the 15 immediately following the time of interest. The goal was to use a three minute averaging time for wind field data which is in line with the range of averaging times used by various researchers correlating dispersion data [AS&PP, p. 591]. Both wind speed and direction were averaged, and—to estimate stability—the standard deviation of wind direction was also determined [AS&PP, p. 591, T 13.3]. Figure 5.1 illustrates data, average values, and stability information for Test C.

5.1.2 Transforming Smoothed Data to Velocity Vector Components

The following steps—illustrated in Fig. 5.2—were taken to obtain wind field input for the FDS3 simulation of Test C. First, a reasonable number of straight-line segments are visually overlayed on the 3-min averaged velocity and direction data, taking advantage of "significant" changes in the trend of the data. The overlays are created by specifying ordered pairs of time with velocity and direction. Next, east-west and north-south velocity components are calculated by applying the following equations to velocity and direction values interpolated from the overlays:

$$V_x = -V \cos [(90 - \theta)(\pi / 180)] , \tag{12}$$

and

$$V_y = -V \sin [(90 - \theta)(\pi / 180)] , \tag{13}$$

where V_x = east-west component of velocity (winds from the east are negative),
V_y = north-south component of velocity (winds from the north are negative),
V = absolute wind velocity (from initial overlays), and
θ = direction from which wind originates (from initial overlays), °.

The calculated values of V_x and V_y are then overlayed in the same manner as the 3-min averaged velocity. The ordered pairs of time with V_x and V_y provide the basis for the wind field model in the FDS3 simulation of Test C (see Table 5.1). Finally, as a check of the process, velocity and direction values are calculated from interpolated component overlays using the following equations to verify that the node points in the component overlays are an appropriate basis for the FDS3 simulation of Test C:

$$V = (V_y^2 + V_y^2)^{0.5} , \tag{14}$$

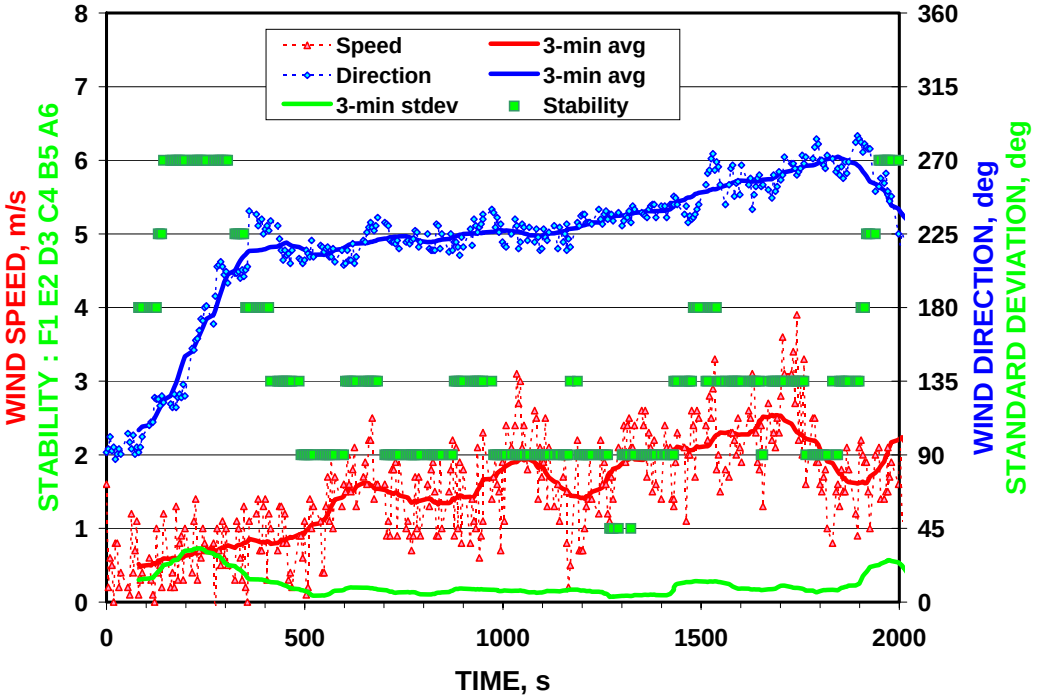

Fig. 5.1. Test C data, 3-min averaged values, and stability assessment.

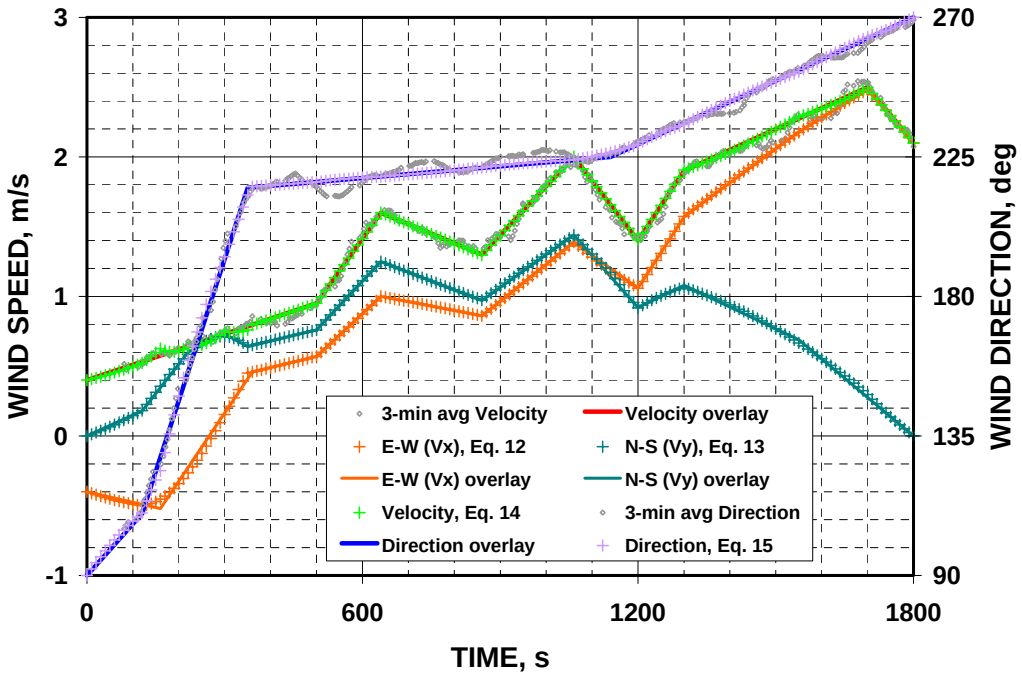

Fig. 5.2. Transforming averaged wind data to velocity vector components.

Table 5.1. Wind Field Velocity Components for Test C

Time, s	Velocity components, m/s	
	V_x	V_y
0	-0.40	0.00
120		0.18
160.	-0.52	
220		0.60
266.1	0.00	
300		0.73
350		0.64
360	0.46	
500	0.57	0.76
640	1.00	1.25
860	0.86	0.97
1060	1.39	1.44
1200	1.06	0.92
1300	1.57	1.08
1550	2.18	0.69
1700	2.48	
1800	2.10	0.00

and

$$\theta = A + B \operatorname{acos}(V_x/V) / \pi . \qquad (15)$$

where A = if $V_x > 0$ and $V_y < 0$, then 450; otherwise, 90, and
B = if $V_y < 0$, then -180; otherwise, 180.

Figure 5.2 demonstrates the process and shows a favorable comparison between the initial overlays and the values calculated form Eq. 14 and 15.

5.2 IMPLEMENTATION

The implementation process proceeded through a series of models until a model capable of providing a wind field comparable to Test C was developed for the 30-min test period. During this process, a number of the FDS3 flow field options, which are summarized in Sect. 5.2.1, were exercised. Section 5.2.2 highlights several steps in the modeling process, including the final wind field model. Results from the final wind field model are compared in Sect. 5.2.3 to the smoothed data summarized in Table 5.1.

5.2.1 FDS3 Flow Field Options

Initial Conditions. Initial velocity components— U0, V0, and W0 (m/s)—may be specified as part of the MISC namelist group. Default values are 0 m/s. [FDS3-UG, p. 16]

Velocity Boundary Conditions. Velocity boundary conditions are specified on the SURF namelist. Both normal and tangential velocities can be specified; however, because the RAMP namelist is only applied to the normal velocity, specifying the tangential velocity for a time varying wind is not useful. Therefore, only VEL (m/s) is used to specify the normal velocity. It is important to note that when VEL is specified for an external surface or the surface of an obstruction, a negative value specifies flow into the computational domain; however, when VEL is specified for flow through a free-standing VENT within a computational domain, a negatvie value specifies flow in the negative coordinate direction normal to the vent. [FDS3-UG, pp. 22, 23, 28, and 29]

Time Dependent Boundary Conditions. While several options are available in the FDS3 code for ramping initial conditions to a specified value over a specific interval of time, the approach useful in the current modeling function allows a user-defined function to vary the boundary condition as a function of the maximum value. In particular, the RAMP_V function is set equal to a character string designating a specific ramp function on a SURF namelist, then the ramp function is specified using the RAMP namelist; for example,

```
&SURF ID = 'SouthWind',      VEL = -1.44, RAMP_V = 'SouthRamp'
&SURF ID = 'SouthWind-nf', VEL =  1.44, RAMP_V = 'SouthRamp'
&RAMP ID = 'SouthRamp', T =      0., F = 0.00 /
&RAMP ID = 'SouthRamp', T =  120., F = 0.13 /
&RAMP ID = 'SouthRamp', T =  160., F = 0.24 /
                              ⋮
```

These lines, extracted from a simulation of Sandia Test C, use the same RAMP function for air coming out of the south surface into the computational domain (hence the negative value of VEL) and for air blown through vents along the east and west sides of the model (with the positive value of VEL). T specifies time and F is a value between 0 and 1, inclusive, which multiplies VEL. Negative values of F are not permitted. [FDS3-UG, pp. 23-24] (During development of wind field model, the use of negative values of F appeared to provide expected results; however, inducing flow into a boundary is not appropriate.)

Obstructions. The OBST namlist group is used to specify obstructions which are rectangular solids defined by two opposing corner points, (x_1 , y_1 , z_1) and (x_2 , y_2 , z_2). Boundary conditions on the surface of the obstruction are set by specifying surface descriptors using SURF_ID, SURF_IDS, or SURF_ID6 which, respectfully, establish the same boundary conditions on all sides of the obstruction; different boundary conditions for the top, sides (i.e., same for all sides), and bottom; or unique boundary conditions for each surface. While

SURF_ID6 was used in some early wind field models, SURF_ID is sufficient in the final modeling approach since only one of the six surfaces for a given obstruction directly affects the wind field (the other five surfaces are adjacent to other obstructions (e.g., the ground) or the boundaries of the computational domain. [FDS3-UG, pp. 27-28]

Vents. The VENT namelist group may be used to prescribe planes adjacent to obstructions (e.g., to represent a vent in a wall), an external wall or vent, or a fan within the computational domain. VENTS are also specified by opposing corner points, but two of the six coordinates must be the same (e.g., $x_1 = x_2$). SURF_ID is used to define a surface descriptor which is developed in the SURF namelist. Two SURF_ID descriptors are reserved: OPEN and MIRROR. Both OPEN and MIRROR vents can only be applied to exterior boundaries of the computational domain. The OPEN descriptor is useful in wind-field modeling. [FDS3-UG, pp. 28-29]

Creating and Removing Obstructions; Opening and Closing Vents. The ability to create and remove obstructions and to open, close, activate, and deactivate vents in an FDS3 model [FDS3-UG, pp. 55-57] facilitates complex wind field modeling since the sign on the velocity (i.e., positive or negative) cannot be changed and the multiplier F specified by the ramp function is limited to values from 0 to 1, so it cannot change the sign of the velocity value. However, some limitations are encountered in practice. For example, while obstructions can be created and removed, vents cannot. To model a shift in wind from east to west (as in Test C), an OPEN vent can be established initially for the "west" boundary of the model and an obstruction with an appropriate surface (with a negative velocity) can be specified on an obstruction for the "east" boundary. The east-boundary obstruction is removed when the east-west component of velocity shifts from west to east and an OPEN vent is activated on that boundary while an obstruction is created on the west boundary with a surface to simulate the west wind. While the use of obstructions was necessary when modeling a shift in wind direction at the boundaries of the computational domain, interior vents (i.e., fans) with a velocity of one sign can be specified to activate coincident with deactivation of a fan having a velocity of the opposite sign.

Atmospheric Profiles. The FDS3 code provides the option to specify wind profiles and temperature lapse rates. The wind profile parameters apply only to the normal velocity and the complexities introduced by applying these additional features in conjunction with variable wind direction and stability has not been pursued.

5.2.2 Modeling Wind

A series of models was developed in pursuit of a wind field model suitable for the fire simulation. While the model eventually needs to be capable of simulating wind initially coming from the east, that moves around to the south, and finally comes out of the west, initial models looked at wind coming from the south moving around to the west. All models used the RAMP function to vary the wind speed. The initial approach used only the velocity perpendicular to the south and west boundaries, which would provide the right amount of

air flow into the model domain; however, a high velocity region develops from the southwest corner in a direction determined by the relative velocities from the boundaries, while the wind velocities vary only slightly from the perpendicular velocity and direction far from the southwest corner, as illustrated in Fig. 5.3.

Since the RAMP function cannot be applied to the tangential component of velocity, the next model sought to overcome the central jet formation by stair-stepping the west and south boundaries, as illustrated in Fig. 5.4. Simply applying the perpendicular component of velocity at the boundaries still resulted in a central region of higher velocities, but the region is broader, as illustrated in Fig. 5.5.

A further refinement to the stair-stepped model modified the perpendicular velocities of adjoining sides of a particular step to maintain the total flow from those two sides while recognizing that some modification of the flows might better align flow across the entire flow field. Specifically, using the FDS3 velocity nomenclature,

$$n\,U_1 + m\,V_1 = n\,U_2 + m\,V_2 \qquad (16)$$

where n, m = relative step sizes perpendicular to the U and V velocity components,

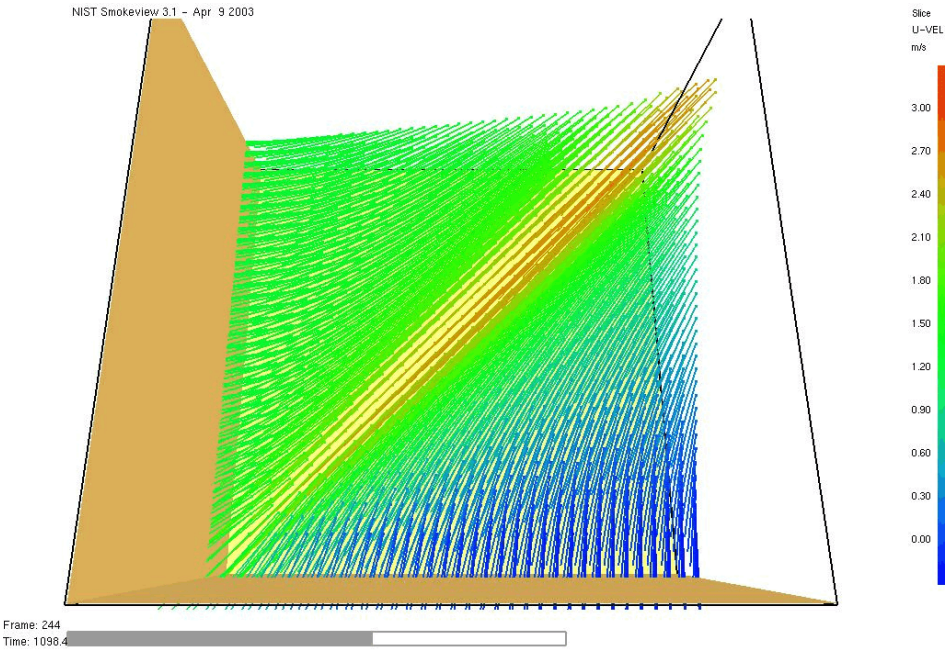

Fig. 5.3. Wind field assuming perpendicular flow from the boundaries into the modeled domain. Vectors represent relative velocity and direction while colors represent the east-west velocity component, V_x (or U in FDS3 nomenclature). Time = 1098 s.

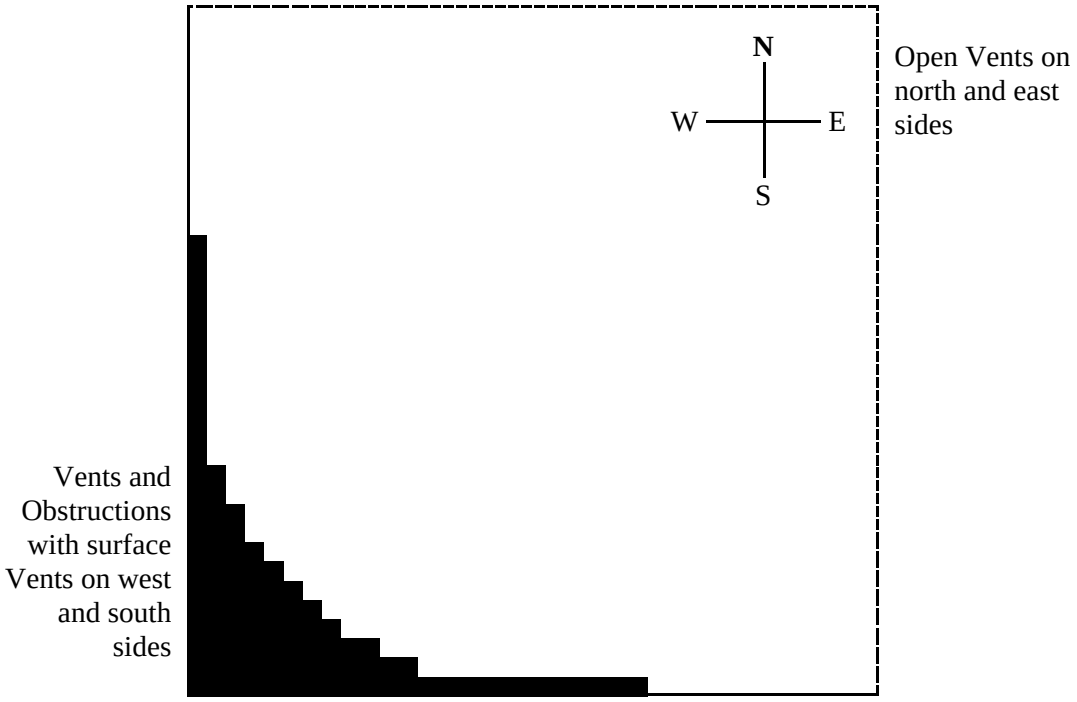

Fig. 5.4. An intermediate wind field model.

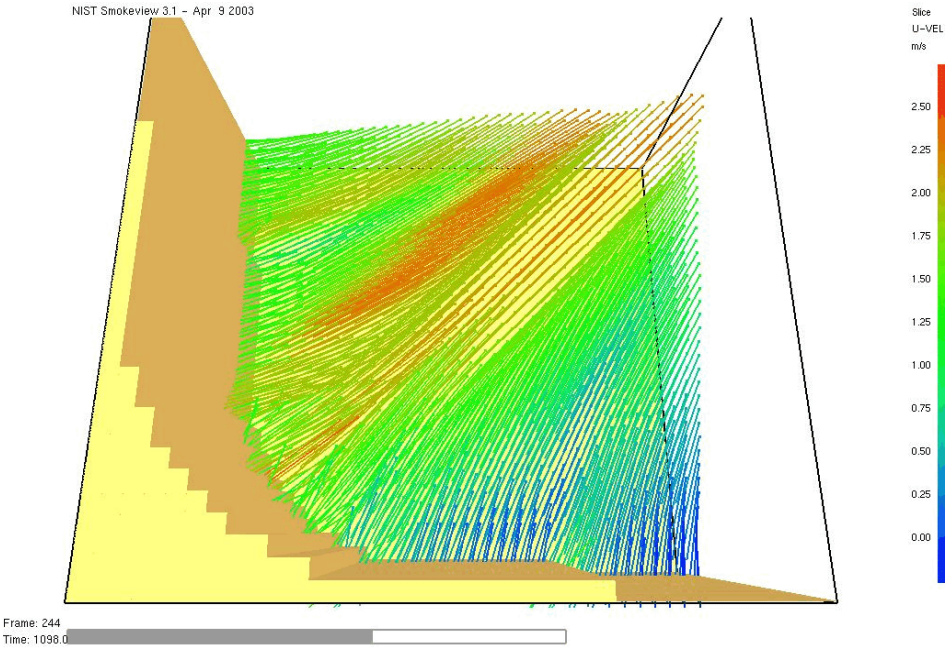

Fig. 5.5. Wind field assuming perpendicular flow from stair-stepped boundaries into the modeled domain. Time = 1098 s.

U = east-west component of velocity,
V = north-south component of velocity, and
$_{1, 2}$ = subscripts signifying the original and adjusted velocity components.

When applying Eq. 16, either U_2 or V_2 may be set and the other value can then be calculated by one of the following equations, as appropriate:

$$V_2 = (n/m)\,(U_1 - U_2) + V_1 \tag{17}$$

$$U_2 = U_1 + (m/n)\,(V_1 - V_2) \tag{18}$$

Based on the model in Fig. 5.4, the ratios of step sizes are 1:1, 2:1, and 12:1. When the step sizes are 1:1, the values of U and V are unchanged. The approach to establishing the other velocities was to take a fraction of the velocity perpendicular to the longer of the two edges, then calculate the other velocity. If one velocity is zero, the other velocity must retain its original value. Also, the calculated velocity applicable to the shorter edge should not be allowed to change excessively, so the reduction in the perpendicular velocity on the longer edge will need to be limited. Too much reduction in the velocities perpendicular to the longer edges can result in eddies in the center diagonal of the domain and a diverging wind field rather than a single converging jet at a higher velocity, as illustrated in Fig. 5.6. Less reduction in the velocities perpendicular to the longer edges can result in a central high velocity region that represents a further improvement over simply using the perpendicular components of the wind velocity, as illustrated in Fig. 5.7; nevertheless, this improved flow field is still inadequate. Also, the model shown in Fig. 5.4 cannot handle winds blowing form the east, which is the initial wind direction for Test C.

Another intermediate model was developed using columns on three sides of the domain with the surfaces providing airflow into or out of the domain or across the space between the columns based on the normal component of the wind velocity. As with the previously discussed models, winds from only the south and west were modeled. The model and results corresponding to the same time as the results presented so far in this section are provided in Fig. 5.8. This model yields more uniform results across the modeled domain, at least in the sense of direction, but air flow needs to be introduced along an entire edge to avoid the channeling observed.

Clearly, the most desirable approach would be impart to both normal and tangential components of velocity along two sides; however, as noted previously, the tangential component cannot be varied. The next approach was to specify surface vents on the east, west, and south faces with vents specified perpendicular to these outside surface vents to impart the tangential component of flow. This configuration resulted in the most uniform wind field presented so far, as illustrated in Fig. 5.9, but it still lacks the ability to model flow over the full 180° change of direction. Another concern with this model is that flow is both forced and induced which could become a problem when combustion is simulated.

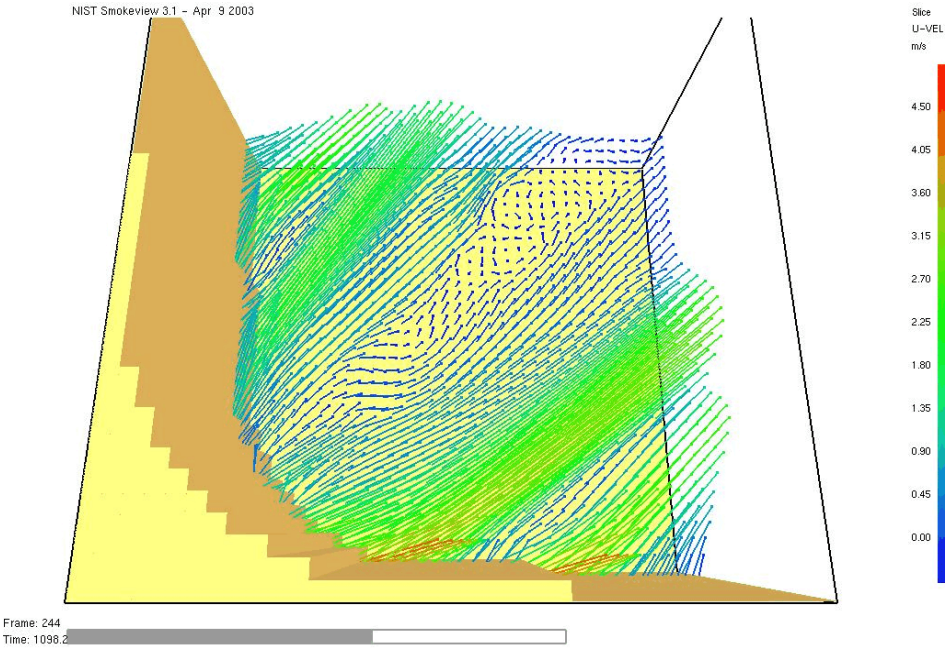

Fig. 5.6. Wind field with overly adjusted velocities that maintain air flow into the domain. Time = 1098 s.

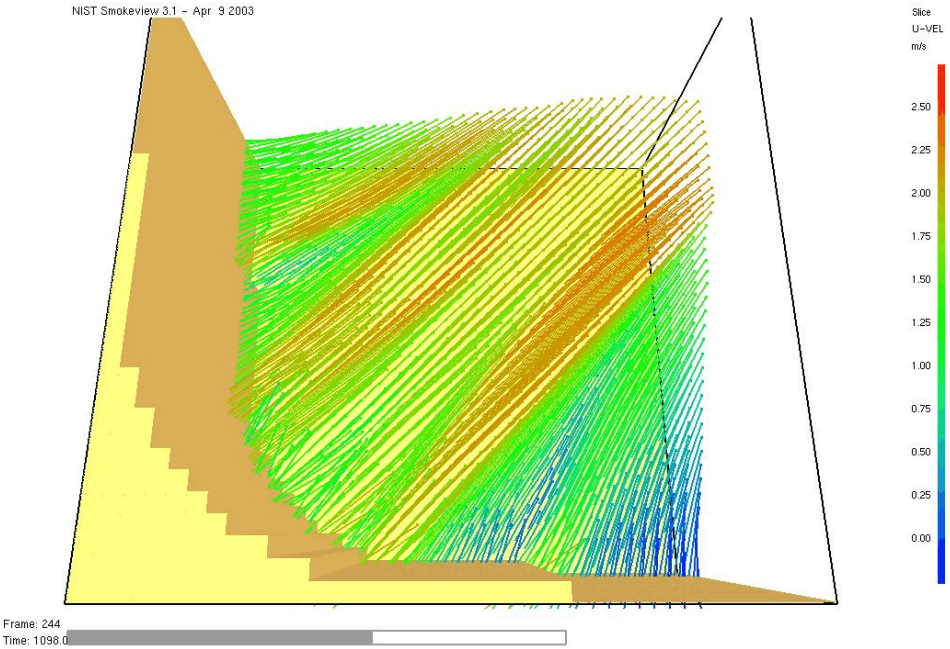

Fig. 5.7. Wind field with reasonably adjusted velocities that maintain airflow into the domain. Time = 1098 s.

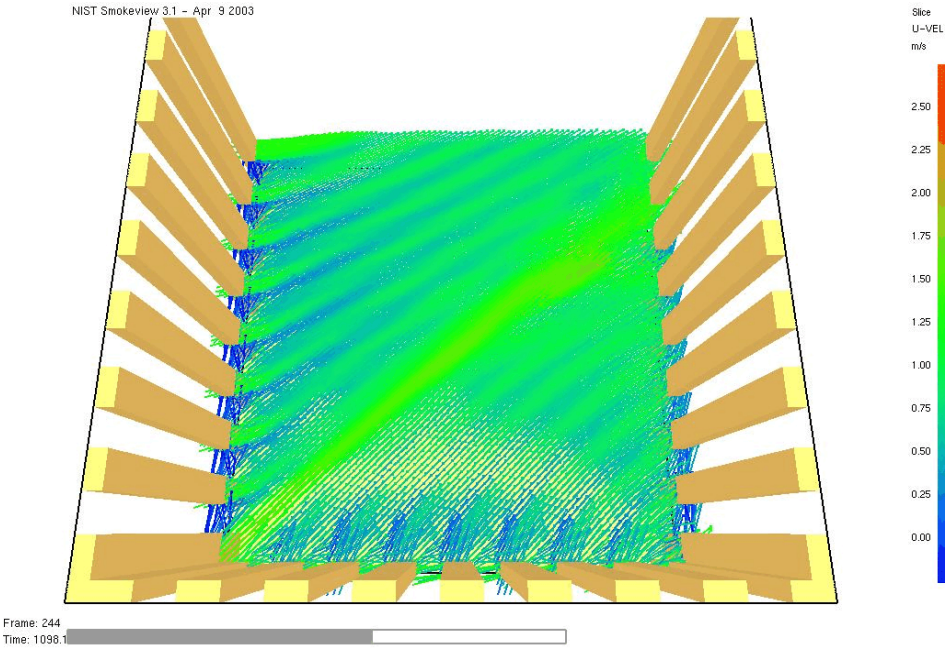

Fig. 5.8. Wind field resulting from perpendicular flow into the domain and between columns. Time = 1098 s.

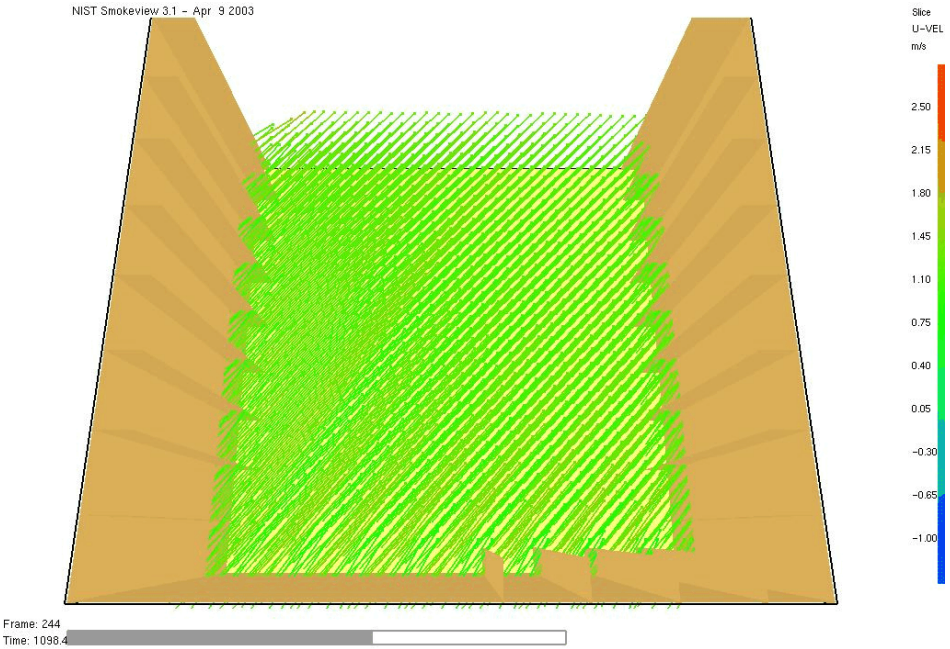

Fig. 5.9. Wind field resulting from surface vents blowing or inducing flow into the domain and short vents perpendicular to the surfaces imparting tangential flow. Time = 1098 s.

Given the uniformity of results across the domain illustrated by Fig. 5.9, as well as the need to model wind directions varying over 180°, the ability to create and remove obstructions and vents was tested and refined over several models. A general schematic of the windfiield model used for modeling the Sandia fire test is shown in Fig. 5.10. The following lines illustrate how the surface vents and obstructions are specified to yield the normal flow into the domain (there is no induced flow) and how vents perpendicular to the outer surfaces are specified to yield tangential flow:

```
 &VENT CB = YBAR0, SURF_ID = 'SouthWind'          / south face
 &VENT CB = YBAR,   SURF_ID = 'OPEN'              / north face
 &VENT CB = ZBAR,   SURF_ID = 'OPEN'              / top

 &VENT XB = -37.8,  -37.8,  -36.75, 36.75, 0, 50.4,
       SURF_ID = 'OPEN'                           / west face
 &OBST XB = -37.8,  -36.75, -36.75, 36.75, 0, 50.4,
       SURF_ID = 'WestWind-wf', T_CREATE = 266.   / west face
&OBST XB =  36.75,  37.8,  -36.75, 36.75, 0, 50.4,
       SURF_ID = 'EastWind-ef',   T_REMOVE = 266. / east face
 &VENT XB =  37.8,   37.8,  -36.75, 36.75, 0, 50.4,
       SURF_ID = 'OPEN',                T_OPEN = 266.      / east face

 &VENT XB = -33.6, -33.6, -36.75, -35.7, 0, 50.4, SURF_ID = 'EastWind-ef',
       T_DEACTIVATE = 266. /
 &VENT XB = -31.5, -31.5, -36.75, -35.7, 0, 50.4, SURF_ID = 'EastWind-ef',
       T_DEACTIVATE = 266. /
                              .
                              .
                              .
 &VENT XB = -33.6, -33.6, -36.75, -35.7, 0, 50.4, SURF_ID = 'WestWind-ef',
       T_ACTIVATE = 266. /
 &VENT XB = -31.5, -31.5, -36.75, -35.7, 0, 50.4, SURF_ID = 'WestWind-ef',
       T_ACTIVATE = 266. /
                              .
                              .
                              .
 &VENT XB = -36.75, -35.7, -33.6, -33.6, 0, 50.4, SURF_ID = 'SouthWind-nf' /
 &VENT XB = -36.75, -35.7, -31.5, -31.5, 0, 50.4, SURF_ID = 'SouthWind-nf' /
                              .
                              .
                              .
```

The first and second sets of input code preceding the vertical ellipsis are required to shift form an east wind to a west wind since the RAMP function used to vary wind speed can only be used to specify fractions between 0 and 1, inclusive. The numbers included in this illustration are specific to the final wind field model and are extracted from the complete input data file which is provided in Appendix B.4. Results from this wind field model are illustrated in Fig. 5.11 at the same time as the results in Figs. 5.3 and 5.5 through 5.9.

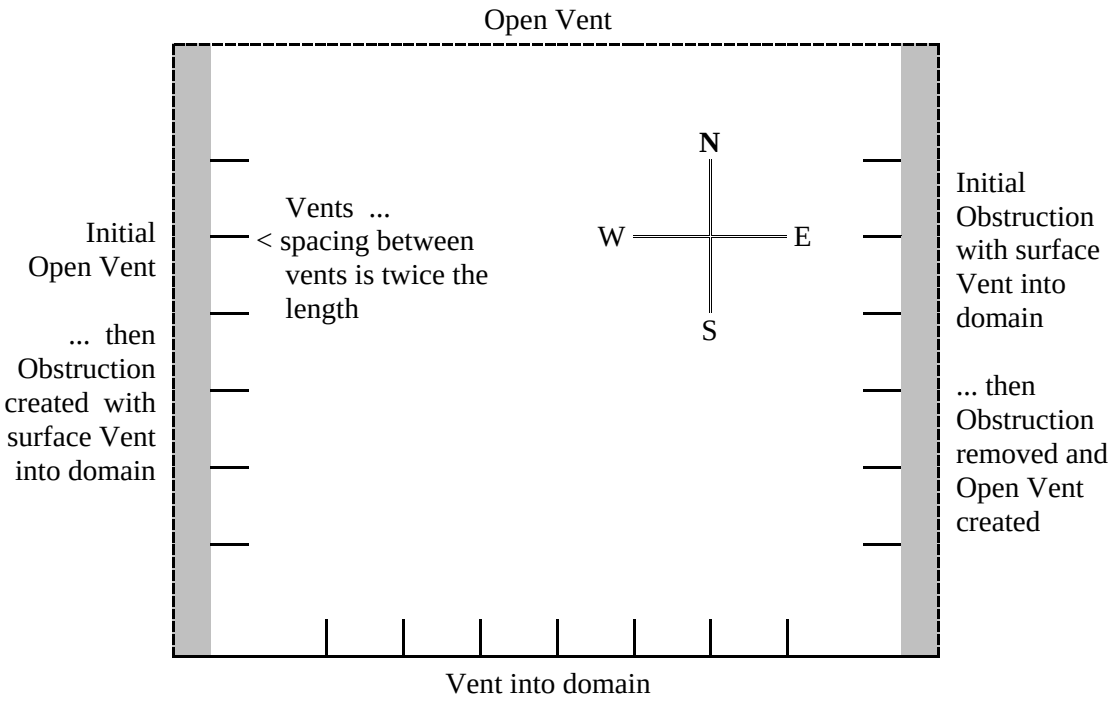

Fig. 5.10. General schematic of wind field model for Test C.

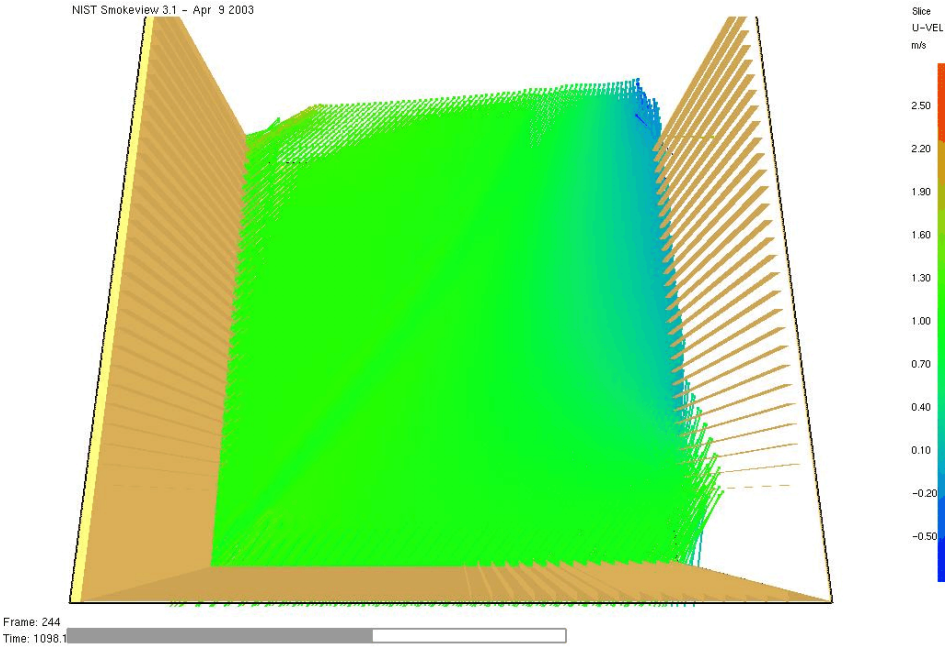

Fig. 5.11. Final wind field model which serves as the basis for the Test C wind field models. Time = 1098 s.

5.2.3 Comparison to Smoothed Input Data

Having compared qualitatively one model against another, it is also necessary to compare model results to the input data summarized in Table 5.1. This comparison is provided in Fig. 5.12. The input data, derived from measured wind field data, reflects a location about 46 m west (i.e., x = –46 m) of the vertical centerline of the model. The comparison data from the model were obtained at a height of 10 m along each axis ±20 m from the vertical centerline (10 m is typical anemometer height and is assumed throughout this report). Surfaces providing normal flow into the domain of the model are located 36.75 m from the vertical centerline on the east (x = 36.75 m), west (x = –36.75 m), and south (y = –36.75 m) sides. The obstruction providing the surface vent on the east side is removed at 266 s and is replaced by an open vent at x = 37.8 m. An open vent is initially specified on the west side at x = –37.8 m; this vent is replaced by an obstruction at 266 s providing normal flow from the west at the distance already noted.

Charts a and b in Fig. 5.12 compare the east-west and north-south components of velocity, showing general agreement with the trends of increasing and decreasing velocities, but with apparently significant differences in the magnitude of the velocity, particularly in the east-west direction. It is noted that the difference becomes less as the velocities increase. It is also noted that the deviations from the input to the simulated velocities differ most at the points farthest from the inflow boundaries. Turning attention to Fig. 5.12(c), a vertical component to flow is observed in contrast to the implicit zero vertical flow, with a significant perturbation around 300 s "measured" at the X+ location (x = 20 m). This latter flow is examined in Fig. 5.13 and is associated with the removal of the obstruction providing the initial easterly flow (i.e., wind from the east) in the model; this obstruction is seen in image a, but removed in image b. In image b a green edge is seen on the right side of the vertical flow field slices, which becomes red in successive images, moves inward, and dissipates. These images reflect a sudden influx of air from the open boundary to fill the void left by the removal of the obstruction. This sudden influx of air is diverted upwards as it meets the previously established mass of air moving to the west.

While the differences noted in Fig. 5.12 at first appear significant in comparison to actual data and derived input, the differences may not be that significant. First, there is a significant variation in wind speed and direction from moment to moment as shown in Fig. 5.1. These variations—only captured in the horizontal plane—are greater than variations in any individual trace. Second, observing the affects of wind blowing through trees or picking up dust across a play ground, there is considerable local variation in wind speed, so a ripple effect that dissipates across an almost stagnant flow field (corresponding to calm wind conditions of less than 1 m/s velocity)—albeit inadvertently introduced by the removal of an obstruction—does not seem so unreasonable. Also, the induced ripple effect essentially dissipates outside the expected region of the fire to be simulated. While it is arguably desirable for the average velocity components to more closely reflect the anticipated conditions predicated on the data reduction leading to the input parameters, the fact that the averages do converge as the wind speed increases is positive.

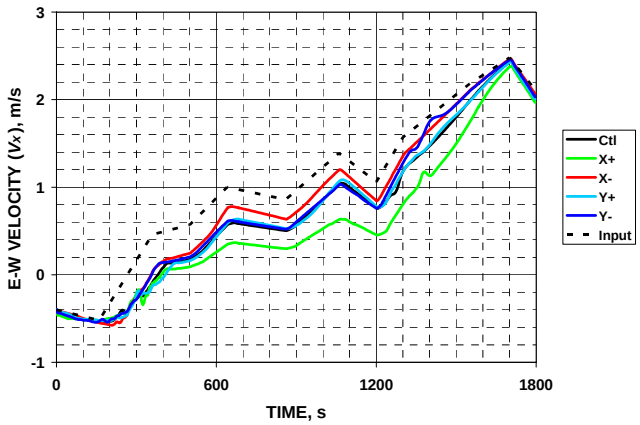

(a) Comparison of the east-west velocity component.

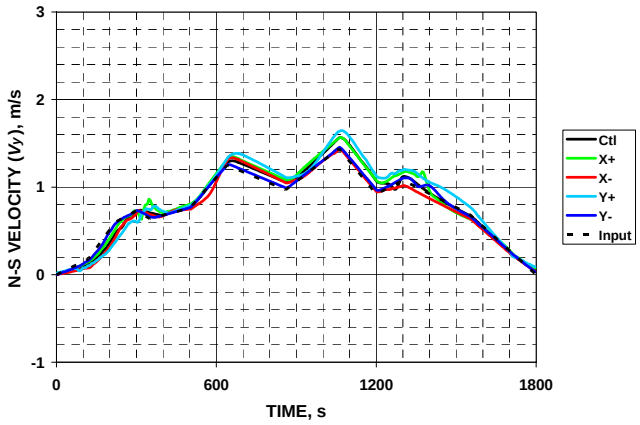

(b) Comparison of the north-south velocity component.

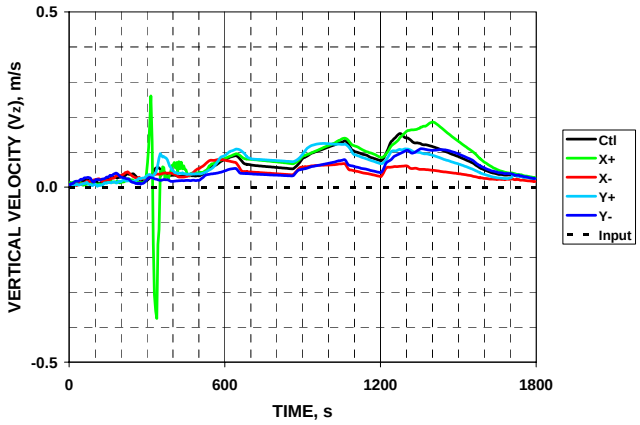

(c) Comparison of the vertical velocity component
to the implicit zero-velocity input data.

Fig. 5.12. Comparison of final wind field results to input data.

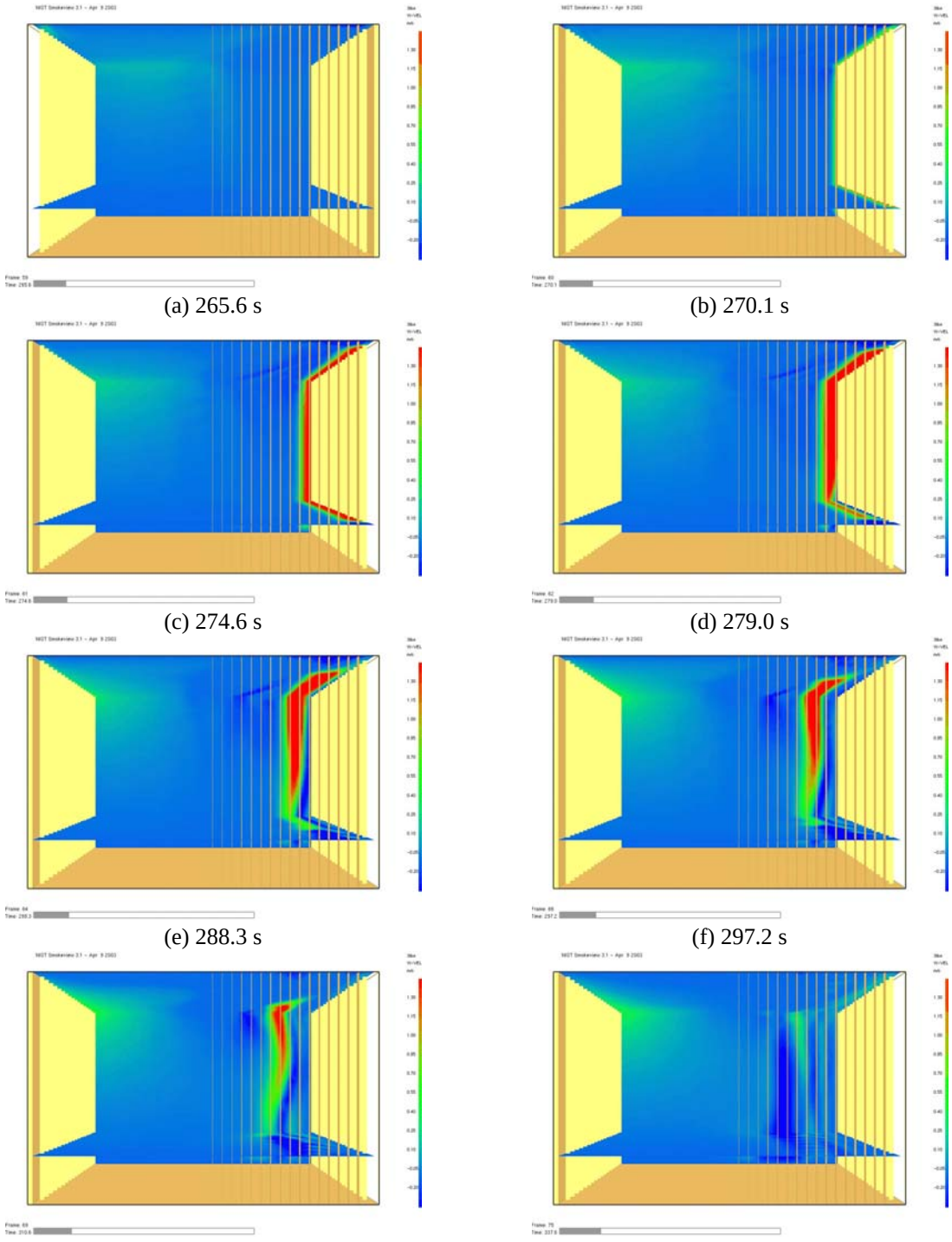

(a) 265.6 s (b) 270.1 s

(c) 274.6 s (d) 279.0 s

(e) 288.3 s (f) 297.2 s

(g) 310.6 s (h) 337.6 s

Fig. 5.13. Propagation of wind field perturbation following removal of obstruction and implementation of an open boundary on the east (right) side of the model. Images a and b show the transition. Image g corresponds to the maximum velocity in Fig. 5.12(c) and h to the minimum. Each image shows vertical velocities at y = 0 m and z = 10 and 50.4 m.

5.3 SUMMARY AND RECOMMENDATIONS

A process for reducing velocity-direction data to obtain velocity components that can be used in developing boundary conditions for a wind field model was presented in Sect. 5.1. In Sect. 5.2, available functions in FDS3 were examined and applied to implement a wind field model, with several configurations examined. This section summarizes characteristics of the final wind field model that will be utilized in simulating Sandia Fire Test C.

5.3.1 Characteristics of the Final Model

A generalized schematic of the final wind field model is illustrated in Fig. 5.10. This model provides for control of both normal and tangential time-varying flows at the boundary, and the approach allows for at least a 180° shift in wind direction. Flows are forced into the modeled domain since induced flows might adversely affect air flow downstream of a fire. The final approach does induce a flow anomaly when an obstruction is removed; however, it appears the anomaly would effectively dissipate before having an impact on a modeled fire provided the domain is sufficiently large.

5.3.2 Enhancing FDS3 Wind Field Modeling

To facilitate future modeling of wind fields, particularly in association with validation simulations, it is recommend that new boundary capabilities be introduced into the FDS3 model. Specifically, the following capabilities would be desirable:

1. Specification of time, direction, velocity triples as input data with interpolation of direction and velocity versus time. The code would determine appropriate U and V velocity components at the forced boundary.

2. Specification of north via an (x,y) ordered pair. This would allow fixed objects to be modeled in a most favorable orientation for the objects.

3. Given 1 and 2, the FDS3 code would determine the boundary to which forced flow would be applied (i.e., the normal component of the flow would be into the modeled domain). Other side boundaries and the top boundary would be open.

4. If possible, implement the capability to model the outer boundary as a circular boundary. This would permit the forced boundary to always be ±90° from the specified (or interpolated) wind direction, thus minimizing the potential impact of reversed flows at a boundary (i.e., the flow across the domain lags behind the boundary flows, so when a boundary transitions from open to forced flow, the flow field does not immediately match). An alternative to a circular boundary that might be considered is to allow the program to determine the points on the boundary corresponding to ±90° from the wind direction and allowing the transition point between forced flow and an open boundary to vary with time along the edges.

6. SIMULATION OF SANDIA FIRE TEST C

This chapter details the simulation of Sandia Fire Test C, which was selected for simulation on the basis of uniform stability and consistency in moment-to-moment winds (see Sect. 5.1). The details of the final wind field model presented in Chapter 5 are carried forward into the fire test simulations. This chapter presents details on the test site and equipment in Sect. 6.1, then provides background in Sect. 6.2 on the derivation of input for the FDS3 simulations. Results are presented in Sect. 6.3, followed by a summary and recommendations in Sect. 6.4.

6.1 FIRE TEST CONFIGURATION

This section presents information about the Sandia pool fire tests which are pertinent to this modeling effort.

6.1.1 Test Site

The Sandia fire test site consists of a concrete pool 30 ft wide × 60 ft long (in the east-west direction) × 3 ft deep (9.1 m × 18.3 m × 0.9 m). For the tests, a layer of JP-4 jet fuel about 8.5 in. (0.22 m) in depth was added on top of 26 in. (0.66 m) of water for the first two tests (Tests A and B); the fuel depth for Test C was about 7.5 in. (0.19 m). The calorimeter (described in Sect. 6.1.2) was centered over the pool and supported on a steel stand about 3 ft (0.9 m) above the fuel surface. [SAND85–0196, pp. 7 and 12]

6.1.2 Calorimeter

The large test calorimeter was 21-ft long (6.4 m), 56.5-in. outside diameter (1.4 m) A517 steel pipe with 1.25-in. thick (0.032 m) walls. Around the outside of the pipe were 2-in. (0.05 m) thick by 6-in. (0.15 m) wide reinforcing rings located on 24-in. centers (0.61 m). 0.5-in thick (0.013 m) steel plates were bolted on the ends to seal the interior of the pipe. The insides of the pipe and end caps were insulated. [SAND85–0196, p. 8]

Several smaller calorimeters—4 and 8 in. in diameter—were also installed to gather additional data from the fire. Due to limitations on grid refinement relative to their size, these small calorimeters were not modeled.

6.1.3 Instrumentation

This section describes instrumentation and locations that were subsequently modeled. Some instruments were not modeled due to limitations in FDS3 modeling capabilities and resolution that could be reasonably achieved.

Calorimeter Backface and Near-Surface Flame Temperatures. Thermocouples were placed on the inner surface (backface) of the calorimeter and two inches away from the outer

surface between the reinforcing rings at three axial locations on the top, bottom, and both sides. These thermocouple locations are identified by a four digit descriptor; the first digit (1, 2, or 3) represents the axial location from the east end of the calorimeter (1'-6", 10'-9", and 19'-6", respectively) while the last three digits (000, 090, 180, and 270) represent the radial position (the bottom, south side, top, and north side, respectively). Thermocouples were also placed inside and 2 in. outside the end caps; positions for these thermocouples are simply identified as East End Cap and West End Cap. [SAND85–0196, p. 8]

Flame Temperatures. Flame temperatures were measured at several heights on eight towers located around the calorimeter ... three on each side and one on each end. Three towers, with thermocouples at 56 and 103 in. above the initial fuel level, were located on the south and north sides of the west end of the calorimeter (Towers A and B, respectively) and on the east side of the calorimeter (Tower C). The other five towers had thermocouples at 56, 103, 216, and 440 in.; they are identified, beginning with the tower on the west end and rotating clockwise through the remaining positions, as Towers 3, 2, 7, 6, and 4. Measurements from a photograph (Fig. 2 in the Sandia report) were used to approximate the location of the towers in the east-west direction, as discussed later; north-south locations, except for Towers C and 3 were not well defined (Fig. 1 in the Sandia report is not to scale). [SAND85–0196, pp. 8 – 11]

Wind Field. Wind field data—direction and velocity—were measured at a location 120 ft (37 m) west of the pool.

6.2 FDS3 IMPLEMENTATION

This section focuses on translating the available information on the test site into information that can be used as input to an FDS3 simulation. Note that earlier chapters addressed information on thermophysical properties (Chap. 2) and the wind field (Chap. 5) That information is not repeated in this chapter. Subsection 6.2.1 addresses the modeling of the major site features: the pool and the large calorimeter. Subsections 6.2.2 and 6.2.3 address the modeling of instrumentation installed at the test site and the capture of other simulation results.

6.2.1 Modeling the Physical Configuration of the Site

The modeling the physical configuration of the pool and large calorimeter must be accomplished in the Cartesian coordinate system of the FDS3 code. The grid system established for the model must permit a reasonable approximation of the actual dimensions, and the cylindrical calorimeter must be appropriately represented within the limitations of FDS3. For the current effort, the calorimeter is represented by an obstruction having the length of the calorimeter and a square cross section having the same hydraulic diameter as the calorimeter; specifically, the edge of this cross section is the same length as the diameter (see Eq. 10). Table 6.1 identifies actual and modeled dimensions; the modeled dimensions are compatible with a grid size of 0.35 m.

Table 6.1. Physical and Modeled Dimensions of the Pool and Large Calorimeter

Description	Physical dimension		Modeled dimension, m
	ft or in.	m	
Pool length	60 ft	18.3	18.2
Pool width	30 ft	9.1	9.1
Top edge of pool to fuel surface	—	—	0.35
Calorimeter length	21 ft	6.4	6.3
Calorimeter diameter	56.5 in.	1.44	—
Modeled cross-section dimension of calorimeter (vertical and horizontal)	—	—	1.4
Elevation of bottom of calorimeter above initial fuel surface	~ 3 ft	0.9	1.05
Elevation of bottom of calorimeter above final fuel surface	—	~1.1	

The OBST namelist is used to model the ground surrounding the pool, the pool itself, and the large calorimeter. The horizontal dimensions of each of these features are centered on the vertical axis of the model. Four OBST lines are used to model the ground, with the top surface at z = 0; inert surface conditions are assumed. The pool is modeled with its top surface at z = –0.35 m; the parameter SURF_IDS is used to specify 'JP-4' for the top surface and 'INERT' for the other surfaces (see Sect. 2.1 for parameters and values invoked by specifying 'JP-4'). The calorimeter surfaces are specified using the SURF_ID6 parameter; '0.5A517' is used for those surfaces representing the end caps and '1.25A517' for the body of the calorimeter (see Sect. 2.2).

6.2.2 Modeling Instrumentation

The THCP namelist group provides several parameters for gathering temperature and flow field information. These parameters was used to capture information for comparison to the Sandia data. Appropriate values for LABEL were specified in each group to provide for easy identification of data in the output file.

Calorimeter Backface Temperatures. To track the calorimeter wall and end cap backface temperatures, the parameter QUANTITY was set to 'INSIDE_WALL_TEMPERATURE'.

Other parameters on each THCP line include XYZ to specify location; DEPTH, which was set equal to 0.03175 m for the 1.25-in. pipe walls and 0.0127 for the 0.5-in. end caps; and IOR, which is set to provide the orientation from the thermocouple to the surface. The location was specified using the coordinates corresponding to the surface of the obstruction representing the calorimeter. While Stations 1 and 3 are located a uniform distance from each end of the calorimeter, Station 2 is 3 in. off-center (x = –0.08 m in the model)..

Calorimeter Near-Surface Flame Temperatures. The location parameter XYZ of thermocouples for measuring near-surface flame temperatures was specified 0.05 m outside the surface of the calorimeter obstruction with coordinates otherwise corresponding to those for the backface thermocouples. 'TEMPERATURE' was specified for the parameter QUANTITY.

Flame Temperatures. 'TEMPERATURE' was specified for the parameter QUANTITY. The following paragraphs detail the derivation of coordinates specified by the location parameter XYZ.

Thermocouple heights on the towers were specified relative to the initial fuel surface which is about 0.9 m below the calorimeter; at the end of the fire, the fuel surface will have dropped about 0.2 m. In the model, the fuel surface is modeled at a constant 1.05 m below the modeled calorimeter, corresponding to z = –0.35 m. In this context, if a variable fuel surface were modeled, the initial fuel surface would be at z = –0.2 m. For the current model, tower thermocouple heights were converted from inches to meters, rounded to the nearest tenth of a meter, then 0.2 m was subtracted from that height to establish the value of the z coordinate.

The east-west (x) coordinates were established by scaling from the photograph mentioned previously. To accomplish the scaling, measurements were taken across the page of the horizontal location of each tower and of the length of the calorimeter. The positions of towers directly across the calorimeter from each other (e.g., Towers A and B) were averaged to establish their east-west position. For Towers 6 and 7, which had support arms for the thermocouples, it was assumed the thermocouples were located midway along the horizontal arm; these positions were averaged to represent the location of these towers.

There was insufficient information to clearly establish the north-south (y) coordinates of the towers along the side of the calorimeter, The locations were assumed to be 0.5 m from the sides of the calorimeter. The towers at each end are located at y = 0.

Wind Field Data. By specifying 'U-VELOCITY', 'V-VELOCITY', and 'Z-VELOCITY' for the parameter QUANTITY, wind field data were collected at a height of 10 m on the z-axis and on the x- and y-axes at ±20 and ±30 m. While these data do not provide a direct comparison at the location of the weather station, they do permit an assessment of the impacts of the fire on the local environment. The 10 m height is a standard elevation for gathering wind field data.

6.2.3 Other Model Output

Flame Height Data. Heat release rate data were collected along the vertical centerline by setting QUANTITY to 'HRRPUV'. These data were utilized, as outlined in Sect. 4.1, to determine flame height.

Wind Field and Temperature Data. Animated planar slices were obtained for velocities and temperatures using the SLCF namelist group. These slices were obtained along the x and y axes, at 10 m height, and at the top and open (north) side of the model

6.3 SIMULATION RESULTS

The cases initially planned and those finally executed are described in Sect. 6.3.1. Results are presented and discussed in Sects. 6.3.2 and 6.3.3.

6.3.1 Cases

Initially, a set of cases was planned to examine the impact of grid refinement on the simulation of the Test C. The region external to the fire was maintained throughout the modeling efforts with a grid size of 1.05 m, primarily because more refined models had too many nodes to execute successfully. Also, the region immediately around the calorimeter had to be modeled on a grid of no more than 0.35 m to adequately represent the dimensions detailed in Table 6.1. The first case executed in the initial set used a 0.35 m grid in a region with a foot print slightly larger than the pool from the bottom to the top of the region simulated. This first case was terminated, the input data file revised to enlarge the region surrounding the fire, and restarted from the beginning ... after observing air flow patterns into the fire, it seemed reasonable that air flow into the fire should primarily result from the upwind side of the fire being drawn into the downwind side and not from air flow induced from the downwind side. The second case, C-105, limited the 0.35-m grid region to the footprint of the pool up to a height 1.05 m above the calorimeter. Both of these cases ran to the completion of the 30-min simulation. A third case, C-175 with a refined 0.175-m grid to 18.375 m inside a 0.35-m grid inside the 1.05-m wind field grid terminated at about 140 s. At the time of failure, results from the first two cases had been reviewed and indicated excessive backface temperatures, so no attempt was made to restart the C-175 case. The excessive temperatures—specifically, backface temperatures exceeding flame temperatures—resulted from the default value of 0.35 for RADIATIVE_FRACTION, a parameter in the REAC namelist. This parameter establishes a fraction of the energy released from the flame as thermal radiation independent of thermal radiation heat transfer considerations with the intent of offsetting low averaged temperatures resulting from an insufficiently refined grid. Input files for subsequent cases set RADIATIVE_FRACTION to zero.

The initial case run with RADIATIVE_FRACTION set to zero (C-175a) took over 200 s to effectively ignite. Because of this delay, the run was stopped and two ignitors were added

to the model. These ignitors were modeled as 0.35-m square cross-sectioned obstructions running almost the full length of the pool, set back 0.35 m from each edge. A constant temperature of 1000°C was specified for the bottom surface of each ignitor. The ignitors were removed 10 s into the simulation. Successful ignition of the fire resulted from this modification. Two cases, C-175b and C-35b, used input files modified from C-175 and C-35, respectively, by setting RADIATIVE_FRACTION to zero, adding ignitors, and adjusting the extent of the grids, both horizontally and vertically.

Two additional cases, C-175c and C-175d, were executed to examine effects of burn rate and heat of vaporization. C-175c was modified from C-175b by setting the ignition temperature to the initial temperature and the heat of vaporization to 1 kJ/kg with the intent of effectively forcing the maximum burn rate. C-175d was also modified from C-175b, in this instance by deleting the maximum burn rate but retaining the ignition temperature and heat of vaporization used for all other fire simulations reported herein except C-175c. Table 6.2 summarizes the pool fire cases executed to completion that were intended to simulate Sandia Test C. A listing of C-175b is provided in Appendix B.5.

6.3.2 Results

This section compares results of the six completed FDS3 simulations of Test C to temperature and wind field data collected during the Sandia tests. Flame height results are also presented.

Calorimeter Backface Temperatures. Figures 6.1 through 6.5 present calorimeter backface temperature traces from the FDS3 simulations and data from Test C. Case C-105, which used the default radiation fraction, and Case C-35b, which used only the medium grid for the fire and a radiation fraction of 0, provide the upper and lower curves in these figures. Case C-105 typically exceeds the Test C data, with exceptions occurring early in the simulation. Case C-35 results typically exceed or lie in the vicinity of the data, but this result reflects the default radiation fraction. The three cases run with a fine grid—C-175b, C-175c, and C-175d—yield temperatures sometimes above and sometimes below the data. Of these latter cases, C-175c, which was intended to push the burn rate toward the specified maximum value by minimizing the ignition temperature and heat of vaporization, yields the maximum temperature trace. The other two fine grid cases—C-175b and C-175d—yield similar temperature traces which might suggested the simulated burn rate is near the maximum and that with adequate refinement and setting the radiation fraction to zero, the fuel burn rate can be properly determined by the basic principals of heat transfer encoded in FDS3. One final observation is that some data and simulation traces for the fine grid cases almost appear reversed; in other words, better agreement might be inferred if the data traces in Figs. 6.2 and 6.4 were exchanged while the simulation traces were retrained.

Calorimeter Near-Surface Flame Temperatures. Some trends seen in the backface results are observed in the near-surface temperature results presented in Fig. 6.6 ... Case C-35b having the lowest temperatures ... C-175b and C-175d yielding comparable results ... C-175c

Table 6.2. Variations in Input Data Files for Test C

Parameter	C-35	C-105	C-35b	C-175b	C-175c	C-175d
Fine grid, 0.175 m						
X, extent	No fine grid			±9.45		
Y, extent				±4.725		
Z, maximum				16.975		
Medium grid, 0.35 m						
X, extent	±10.5	±9.1		–10.15 / +10.85		
Y, extent	±7.0	±4.55		±7.0		
Z, maximum	49.35	3.15		40.95		
Wind field grid, 1.05 m						
X, extent	±47.25			±47.25		
Y, extent	–46.2 / +37.8			–46.2 / +37.8		
Z, maximum	49.35			40.95		
Fine grid, 0.175 m						
IBAR	No fine grid			108		
JBAR				54		
KBAR				100		
Medium grid, 0.35 m						
IBAR	60	52		60		
JBAR	40	26		40		
KBAR	144	12		120		
Wind field grid, 1.05 m						
IBAR	90			90		
JBAR	80			80		
KBAR	48			40		
Radiative fraction	0.35 (default)			0.		
Ignitors	No			Yes		
Ignition temperature, °C	264.				20.	264.
Heat of vaporization, kJ/kg	364.				1.	364.
Maximum burn rate, kg/m^2-s	0.074					No limit

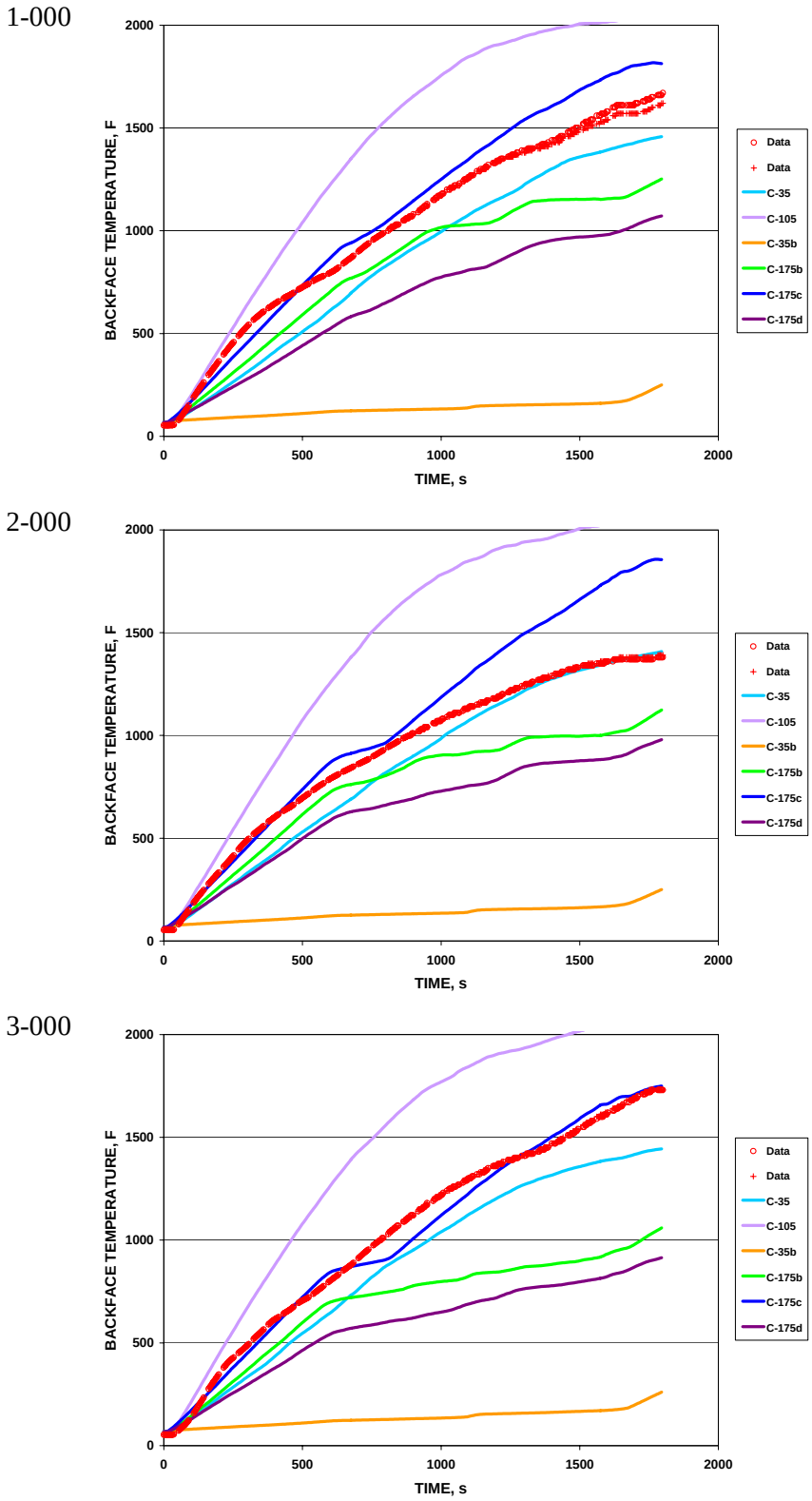

Fig. 6.1. Backface temperatures on the bottom of the calorimeter.

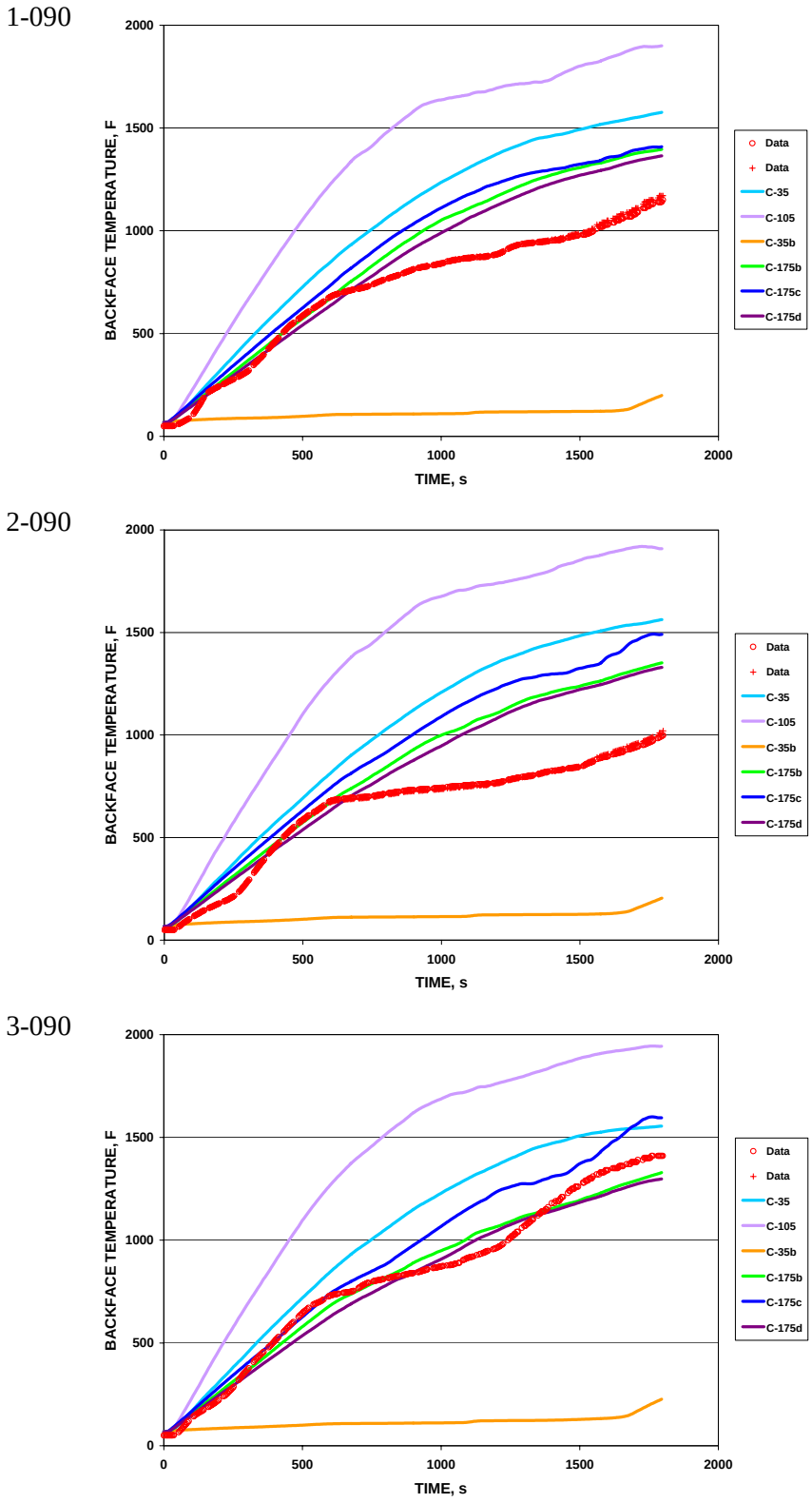

Fig. 6.2. Backface temperatures on the south side of the calorimeter.

1-180

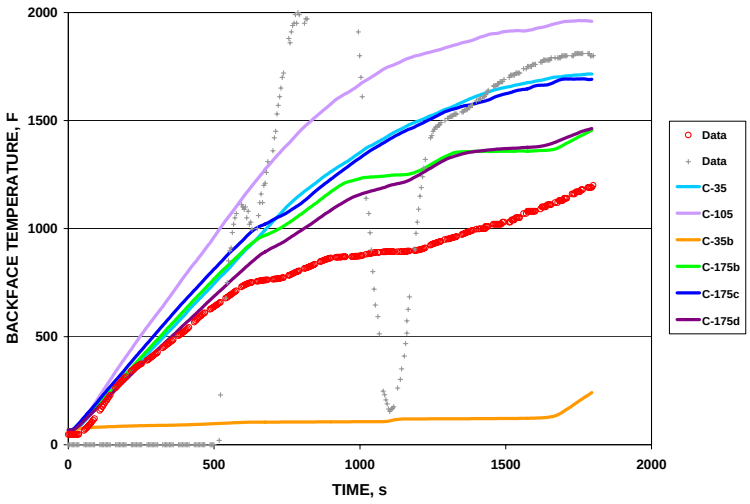

2-180

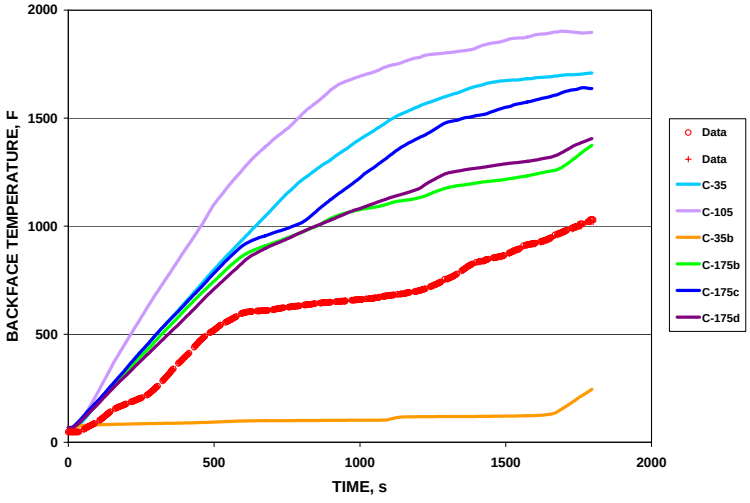

3-180

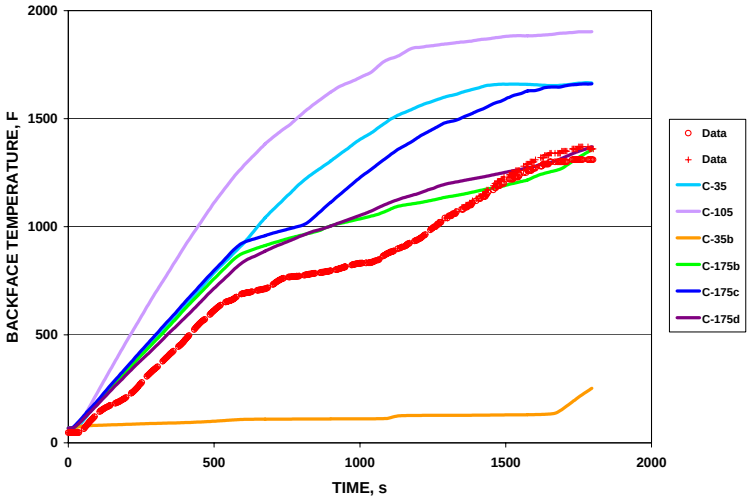

Fig. 6.3. Backface temperatures on the top of the calorimeter.

1-270

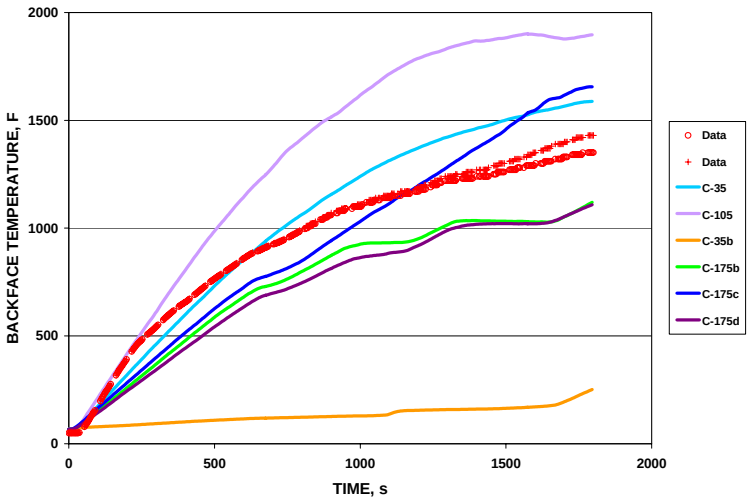

2-270

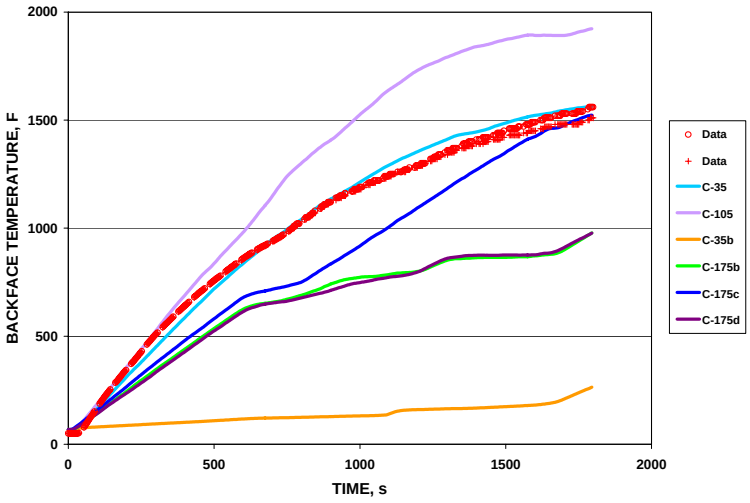

3-270

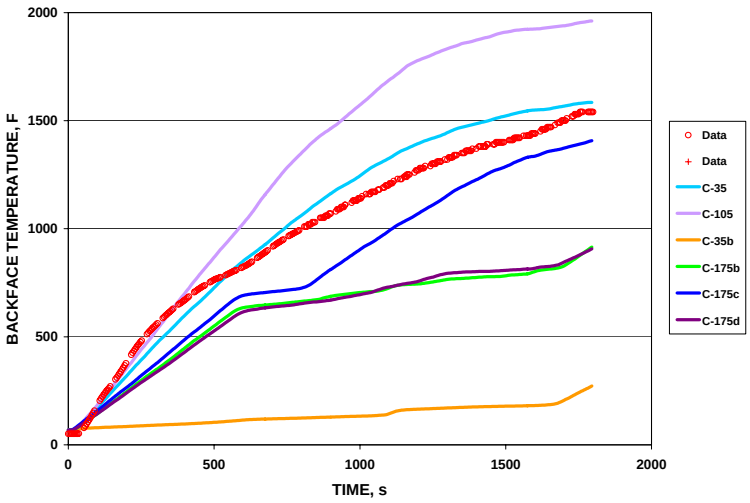

Fig. 6.4. Backface temperatures on the north side of the calorimeter.

East

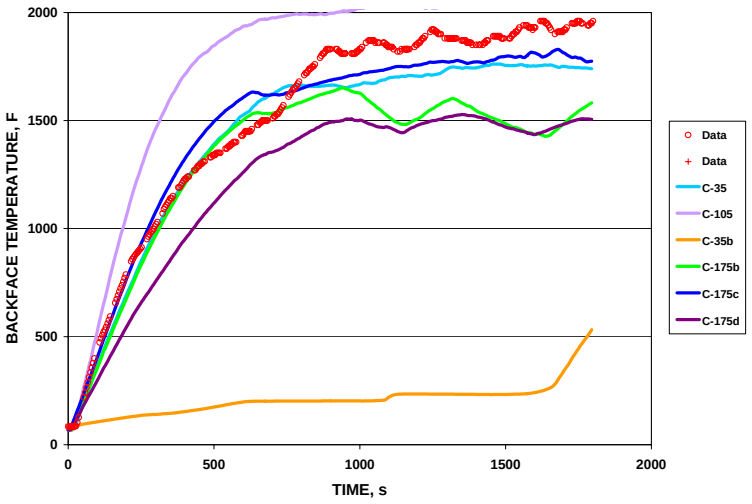

West

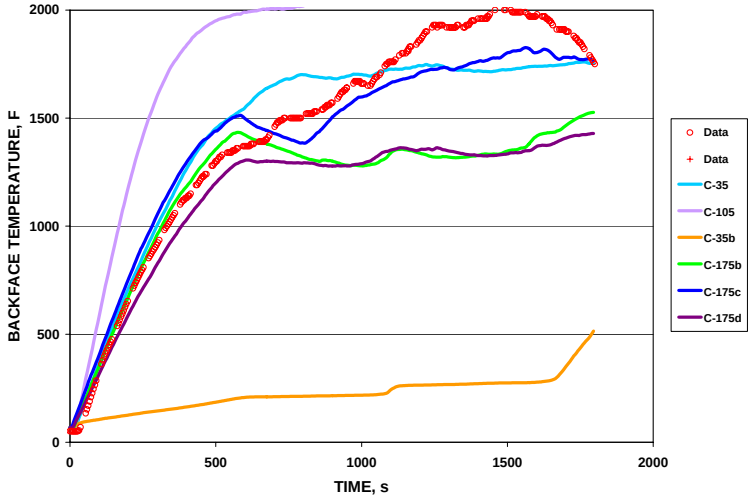

Fig. 6.5. Backface temperatures of the calorimeter end caps.

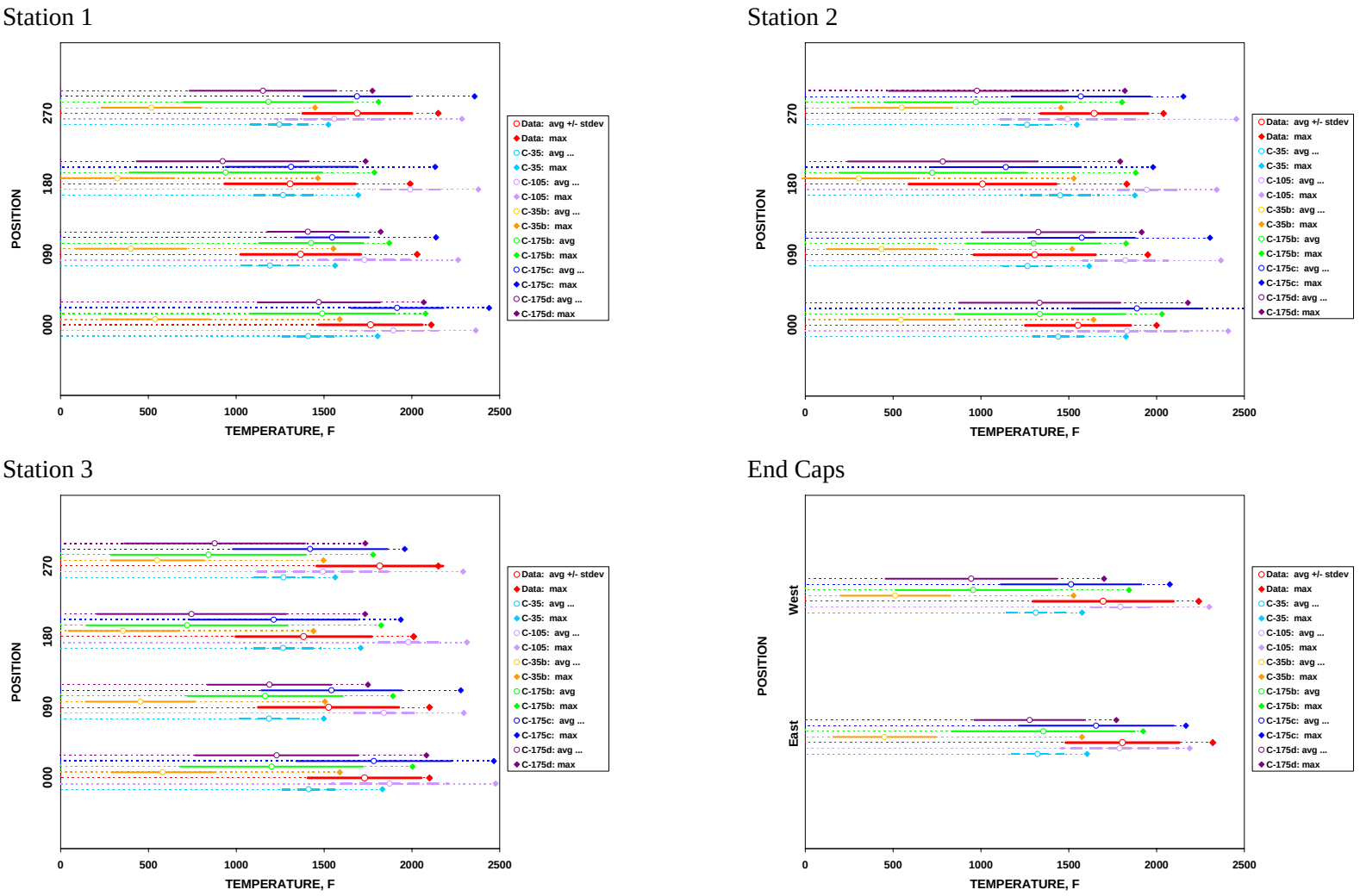

Fig. 6.6. Flame temperatures 2 in. from calorimeter surface. Data points show average and maximum temperatures. Heavy solid and dashed lines reflect standard deviations in temperatures.

yielding higher temperatures than C-175b and C-175d. While some results from Cases C-35 and C-105 appear favorable, they are compromised by the default radiative fraction. The results from Cases C-175b, C-175c, and C-175d are often favorable; however, there are also significant differences between the averages of the simulation results and the data. Comparing standard deviations often indicates similar variability in simulations and data. The impact of the square cross section of the modeled calorimeter versus the actual cross section is not known.

Flame Temperatures. Figures 6.7, 6.8, and 6.9 summarize and compare simulation results and Test C data from the tower thermocouples. Figure 6.8 also provides a schematic of tower locations around the calorimeter. A trend noted in these results is that averaged temperatures from the simulations seem more uniform with height than the Test C data, which typically decrease with increasing thermocouple height. It is noted that while Cases C-175b and C-175d yield similar results at the lowest thermal couple height, the differences between averaged temperatures for Cases C-175d and C-175b become greater with height (C-175d temperatures being the greater). Also, temperatures for Case C-175c exceed those for the other fine grid cases at the lower heights, with the difference decreasing sufficiently that at the greatest height temperatures are consistent with or fall below the averaged temperatures of Cases C-175d and C-175b. These trends may be explained by the treatment of burn rate and heat of vaporization, as subsequently discussed. As with the near-surface temperature comparisons, it is noted that standard deviations typically indicate similar variability in simulations and data.

Since tower locations in the east-west direction were estimated from a photograph and since there was no clear basis for estimating the north-south location, averaged temperatures as a function of location along the mid-planes were extracted from FDS3 slice files at heights approximating the locations of the tower thermocouples. These averaged temperatures are plotted in Fig. 6.10, with Test C data plotted at the distance specified in input files; horizontal lines enable a comparison of data to the simulated traces for considering whether specifying different tower locations in the input files could have improved the comparison of simulation results to Test C data. It is not immediately apparent that adjusting tower locations would improve the comparisons.

Wind Field. Original wind field data and the modeled input are presented in Chapter 5—see specifically Figs. 5.1 and 5.2, respectively. Wind field measurements from case C-175d are presented in Figs. 6.11 and 6.12. Results from 20 and 30 m east and west of the center of the pool are given in Fig. 6.11, with similar results to the north and south in Fig. 6.12. The effects of the fire environment are evident with results nearest the forced boundaries most nearly reflecting the input wind field, while those nearer, around, and downwind of the fire exhibit the effects of air flow into the fire. As the wind shifts from east to west, upwind transition occurs fairly quickly (before 400 s) while downwind effects evolve more slowly (over several minutes) before reflecting a somewhat more uniform—albeit erratic—behavior.

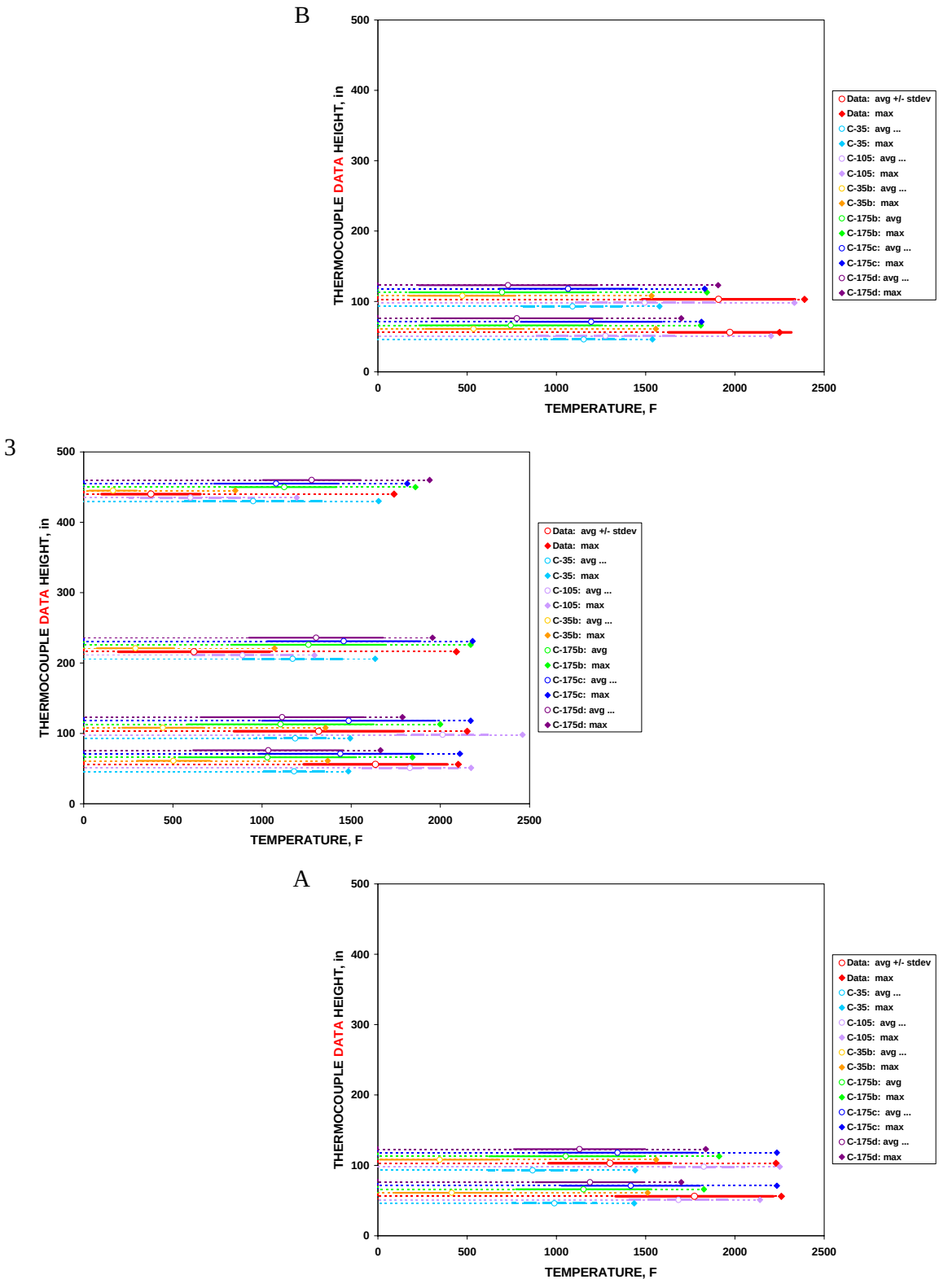

Fig. 6.7. Flame temperatures around the west end of the calorimeter.

2

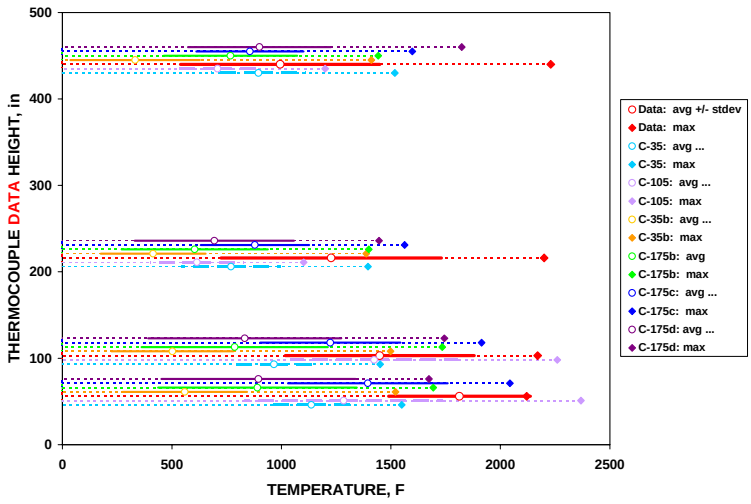

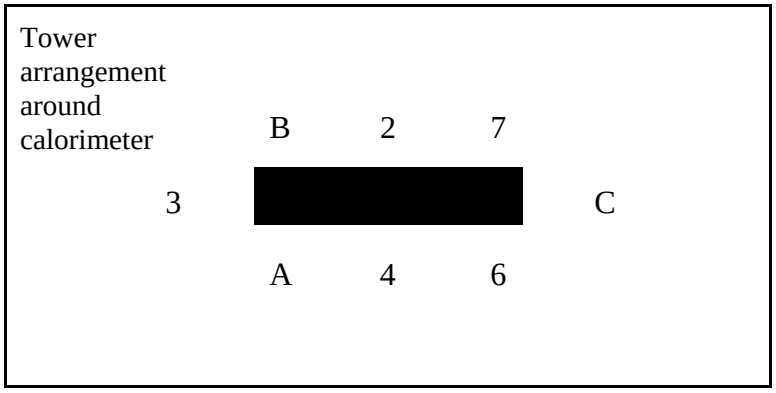

4

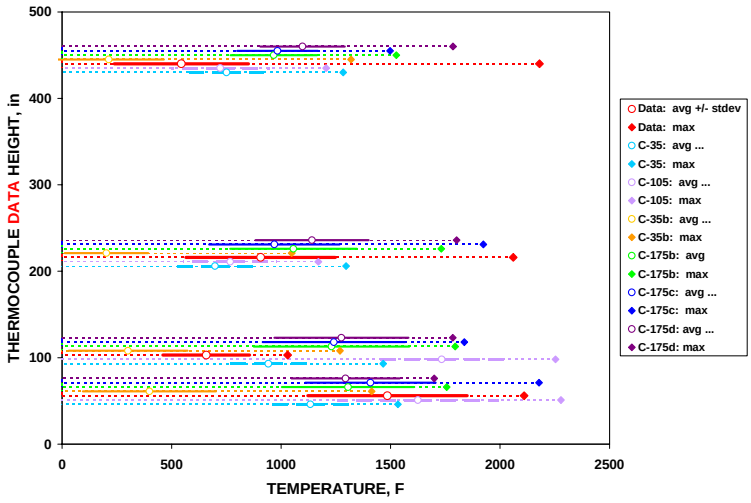

Fig. 6.8. Flame temperatures north and south of calorimeter and tower locations.

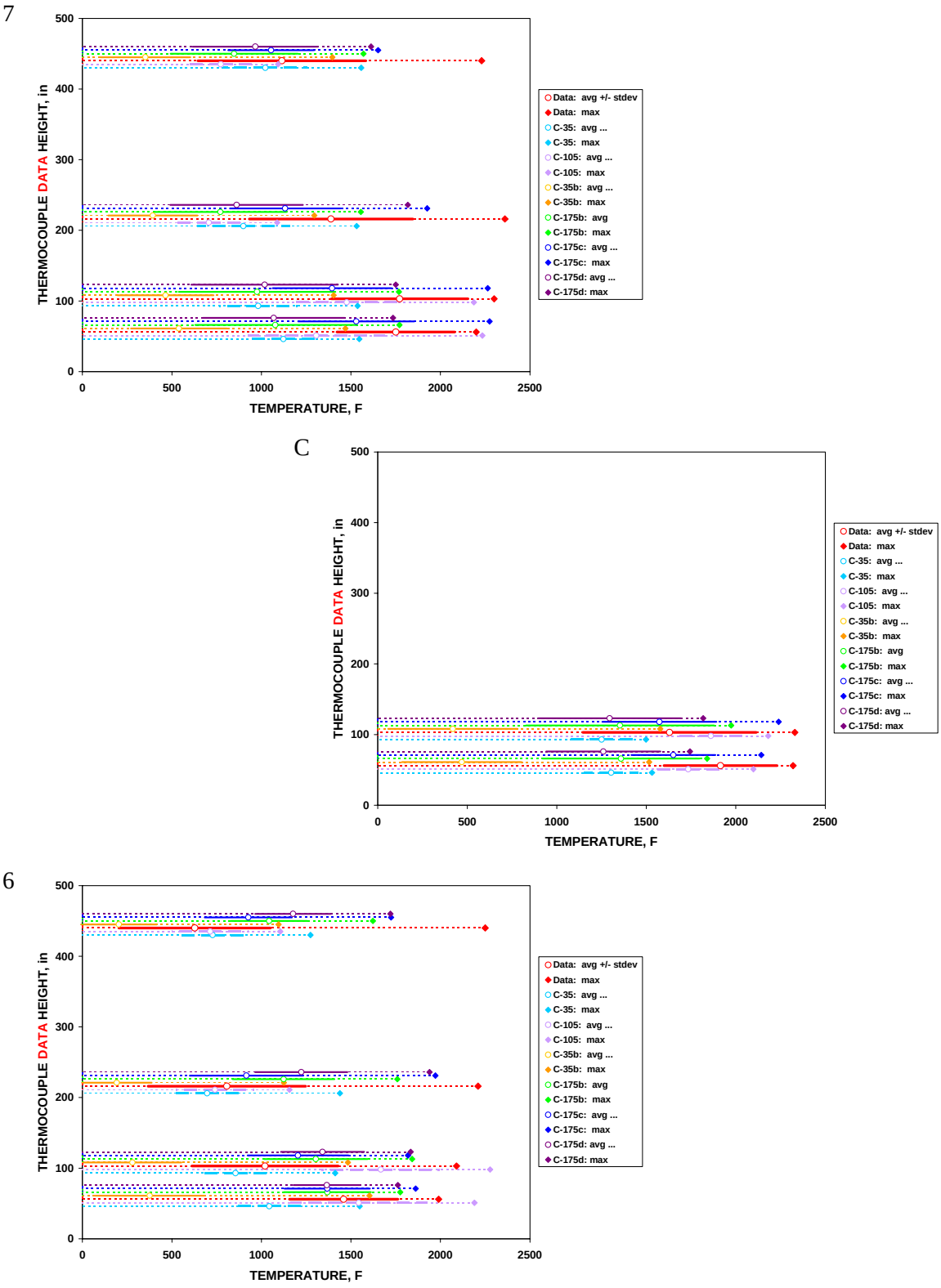

Fig. 6.9. Flame temperatures around the east end of the calorimeter.

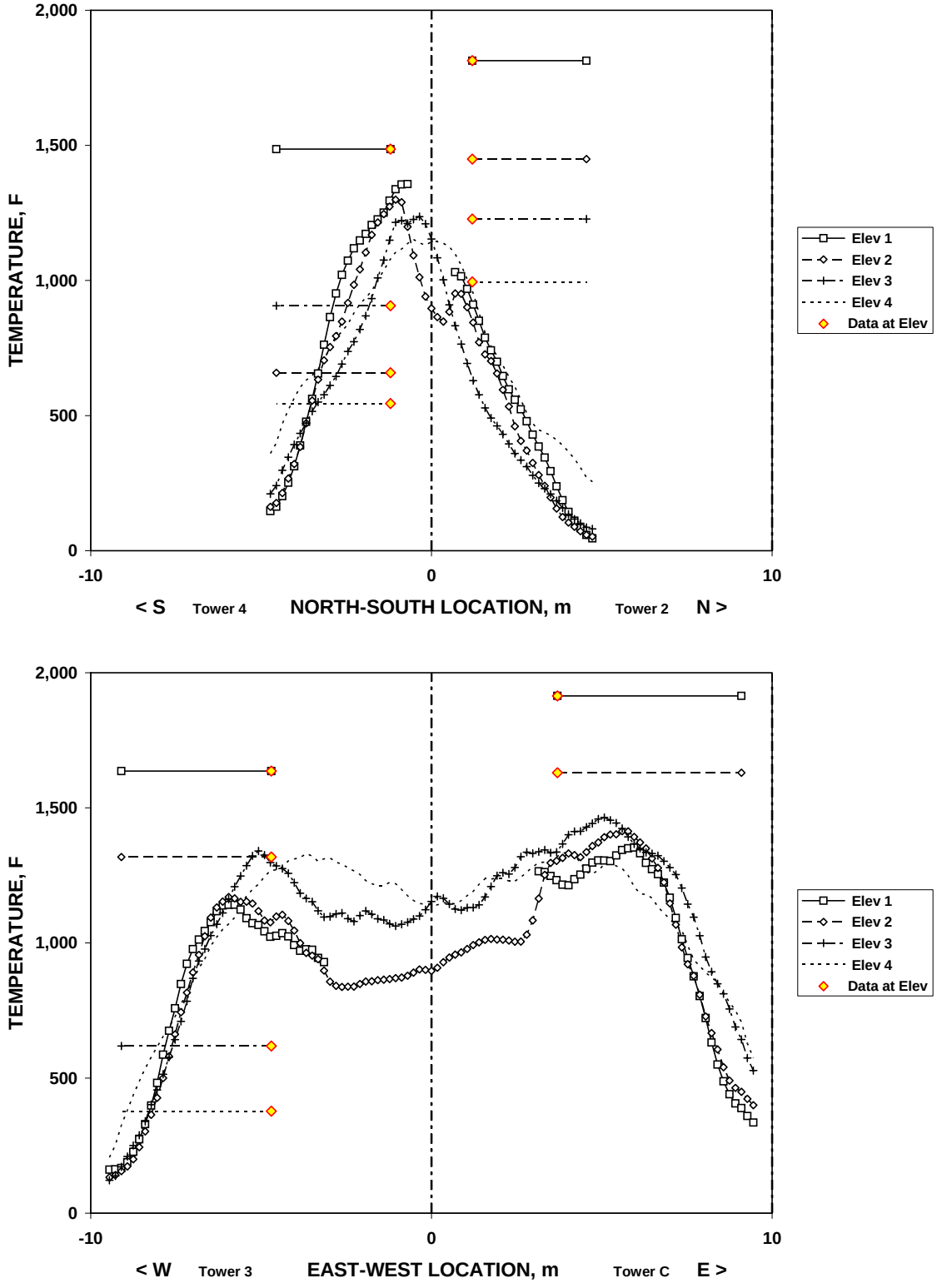

Fig. 6.10. Comparison of averaged midplane flame temperature for C-175d to data.

20 m West

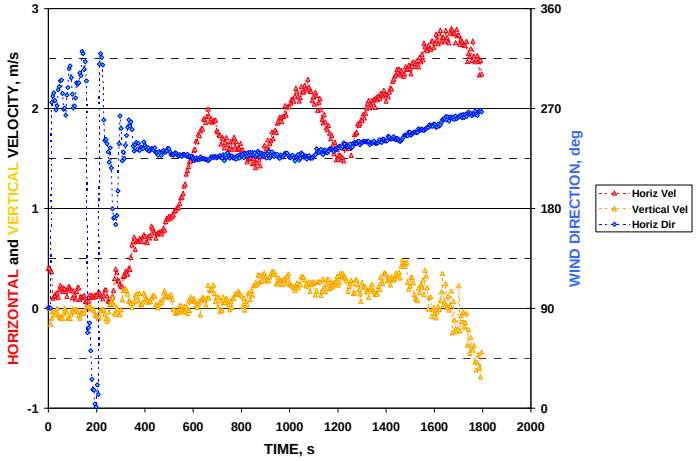

20 m East

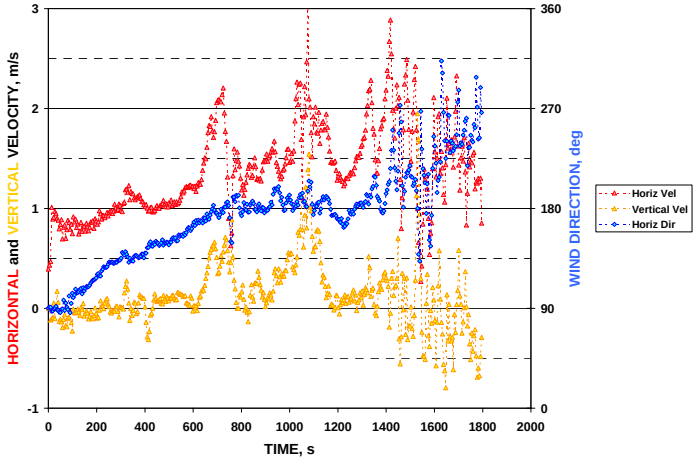

30 m West

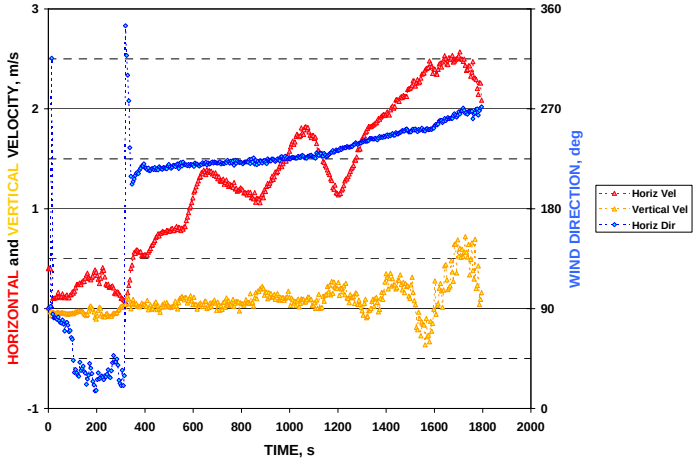

30 m East

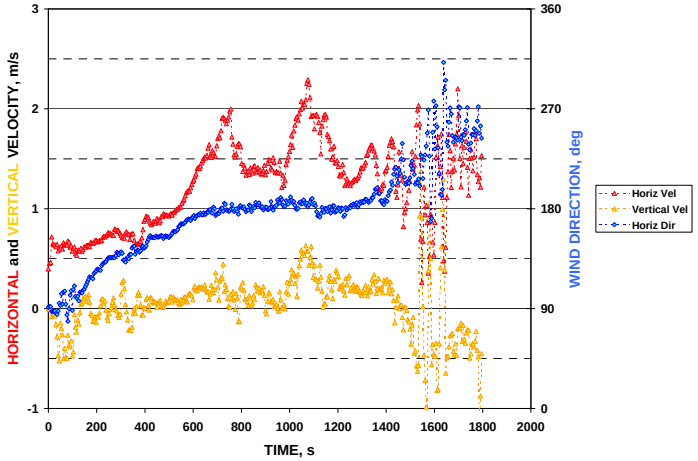

Fig. 6.11. Wind field results for C-175d (west and east of the pool center).

20 m South

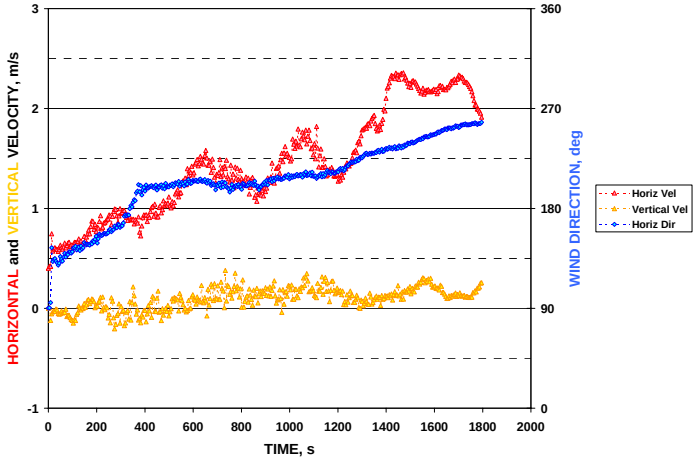

20 m North

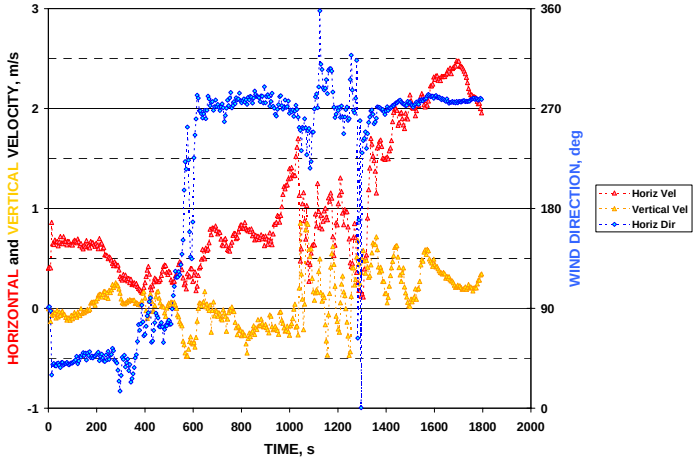

30 m South

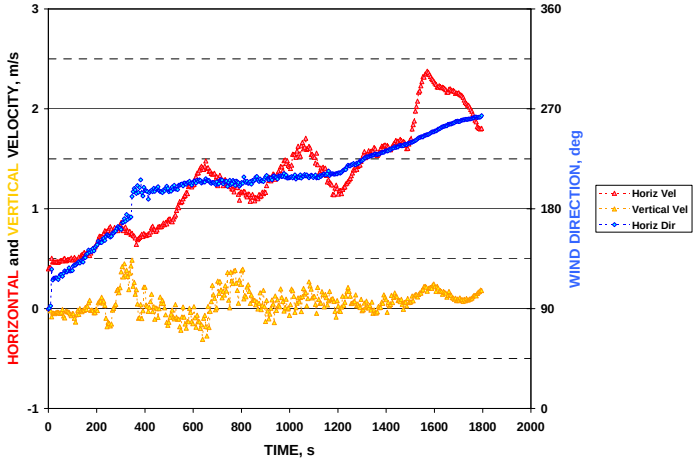

30 m North

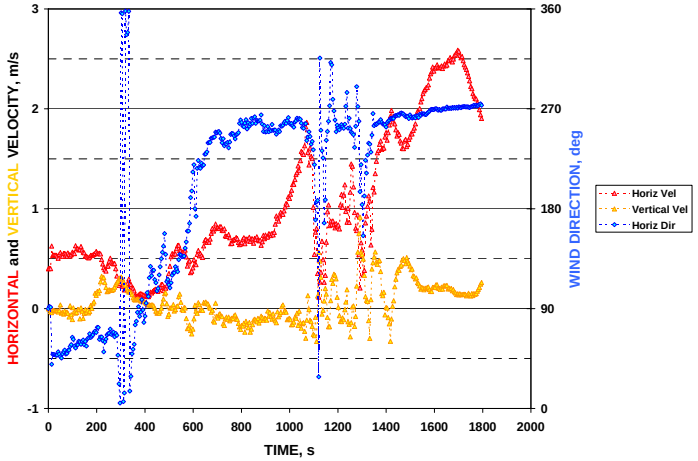

Fig. 6.12. Wind field results for C-175d (south and north of the pool center)

Flame Height. Burntime fraction versus plume height for the six simulations of Test C are presented in Fig. 6.13; the flame heights marked are based on the criterion that burntime fraction equals 0.50. The flame height for Case C-175b is also plotted in Fig. 4.7 in the comparison of flame height correlations and the results from simulations reported herein. Except for Case C-175d, for which a flame height was not determined by interpolation of simulation results but was estimated at about 44 m from Fig. 6.13, all cases considered reflect the same maximum burn rate (however, simulated burn rates may be less; see subsequent discussion). This latter greater flame height (in comparison to the C-175b and C-175c) may indicate that greater burn rates occurred when the maximum burn rate was removed as a limiting parameter. Figure 6.14 shows that the vertical velocity at the surface of the pool was greater for the case without a maximum burn rate; by Eq. 6 and 7, a greater mass release or heat release rate leads to greater flame heights. While Fig. 6.14 suggests there should be a difference in flame heights for Cases C-175b and C-175c, the lack of difference is probably well within the bounds of uncertainty. The fact that more energy from the fire would be available in C-175c for heating the fire plume in the absence of heating and evaporating the liquid fuel from the pool may lead to increased turbulence in the plume, with greater fuel-air mixing resulting in the observed results.

Direct Comparison of Simulation Results and Data. Appendix C provides a direct comparison between data from Test C and the FDS3 simulation results Case C-175d.

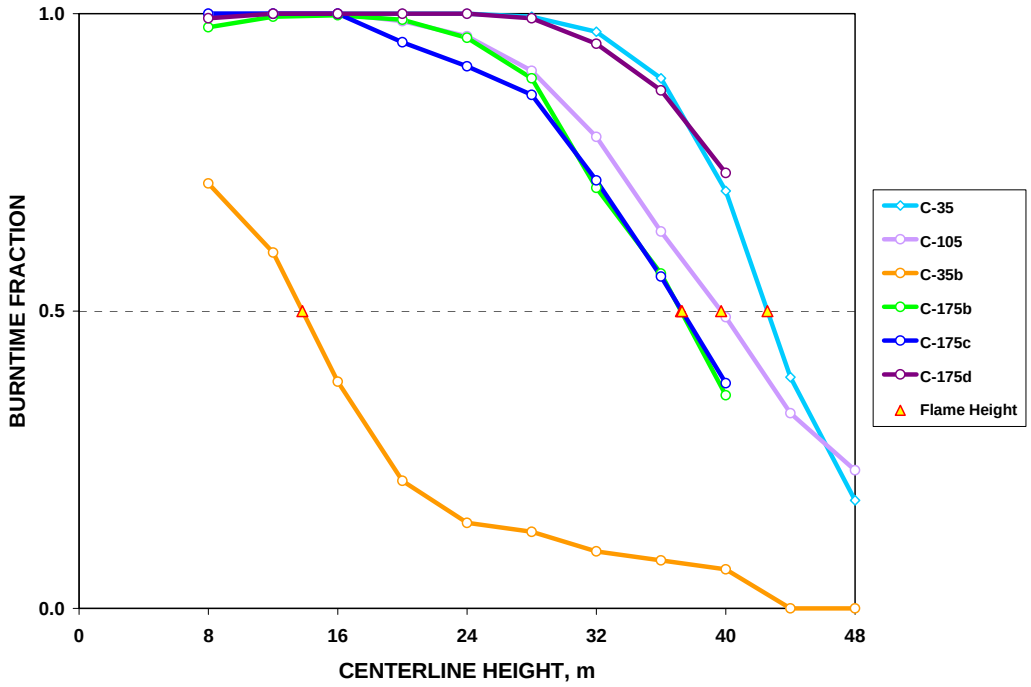

Fig. 6.13. Flame height for Test C simulations. A burntime fraction of 0.5 is the criterion for flame height.

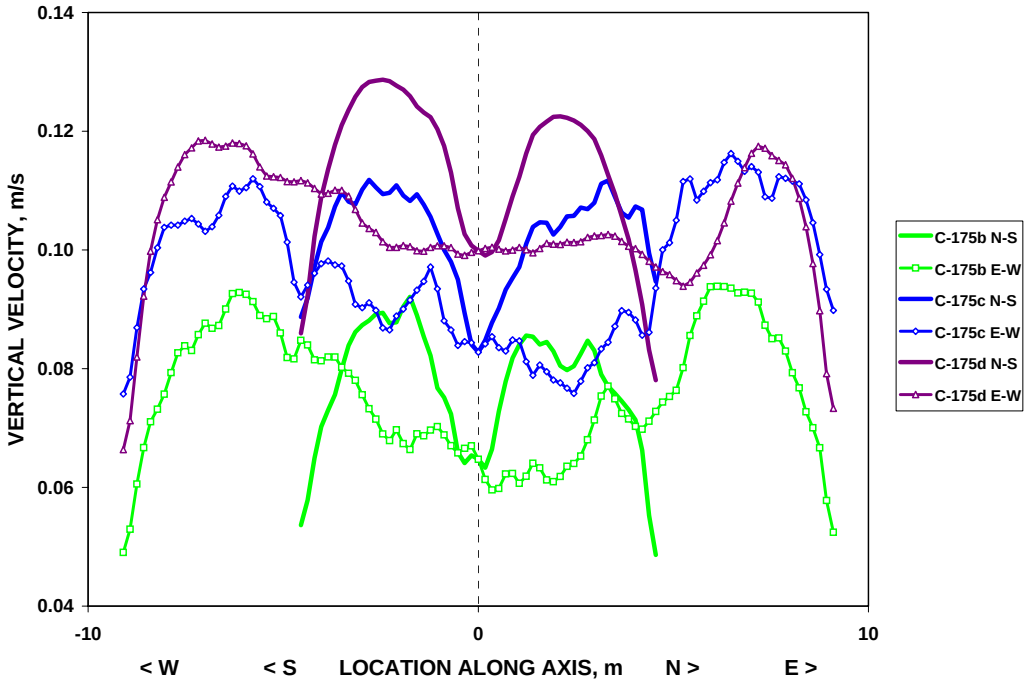

Fig. 6.14. Vertical velocity from the pool surface for Cases C-175b, c, and d.

6.3.3 Discussion of Results

Several issues arose during the evolution of the Test C simulations and the review of results during and after those cases were executed. An early concern was the observation of excessive backface temperatures which was traced to the default radiation fraction. Subsequent to this observation, the radiation fraction was set to zero; however, ignitors, which were removed after 10 s of simulation, had to be modeled to initiate combustion. Consideration of the final three cases warrant further discussion with respect to maximum burn rate, heat of vaporization, and grid refinement. It is noted that neither Test C nor the simulations would meet the thermal test temperature requirements for packaging ... "... an average temperature of at least 800°C (1475°F) for a period of 30 minutes ..." (see Sect. 1.1.1). On the other hand, the FDS3 simulations do reflect the "highly turbulent nature of a large open pool fire and its susceptibility to winds [which] produce temperature and flow fields that are very nonuniform in both a spatial and temporal sense" (cf, Sect. 1.4).

Maximum Burn Rate. All cases reported herein—except Case C-175d—erroneously utilized a maximum burn rate predicated on a average derived from the time it took to burn a known depth of fuel. The error is that the burn rate is not uniform across the pool; therefore, utilizing an average as the maximum limits the material burned to a rate less than that

average observed. Removing the maximum burn rate from the input file for Case C-175d resulted in the following observations relative to Case C-175b:

1. lower backface termperatures along the bottom of the calorimeter (Fig. 6.1);

2. other backface temperatures are essentially the same, though often slightly lower (Figs. 6.2, 6.3, 6.4, and 6.5);

3. increased temperatures for the higher tower thermocouples (Figs. 6.7, 6.8, and 6.9);

4. an increased flame height (Fig. 6.13); and

5. more material released (see Fig. 6.14).

Taking an average for the velocity profiles plotted in Fig. 6.14, the burn rate is increased by about 40%. While the results presented in Chap. 4 suggested that flame heights may be underestimated by recognized correlations, Eqs. 6 and 7 can be manipulated using the height estimated for Case C-175b, the increased heat release or burning rate inferred from Fig. 6.14, and—when applying Eq. 6—an approximate diameter, to estimate an increase in flame height of about 20%. This 20% increase is comparable to the height increase observed from the simulation results. An increase in burn rate (i.e., mass loss rate from the pool surface) and the increased flame height is also consistent with the increased temperatures observed for the higher thermocouples. Finally, an increased burn rate would move the flame front away from the pool surface resulting in lower backface temperatures at the bottom of the calorimeter and lesser effects as flow proceeds up and around the calorimeter (which are more directly exposed to the flame and hot combustion gases).

Heat of Vaporization and Ignition Temperature. All cases reported—except C-175c—used the same heat of vaporization and ignition temperatures. For Case C-175c, the heat of vaporization was reduced to a negligible value and the ignition temperature was set to the ambient temperature. The intent of these changes was to maximize the burn rate by forcing it to the specified value. It is unclear whether this was actually achieved ... Relative to Case C-175b, the increased vertical velocity from the pool combined with the increased density (due to a lower ignition/evaporation temperature) would imply a higher release rate for Case C-175c; however, the flame height is the same for both cases, implying a consistent burn rate (perhaps not inconsistent with since the same maximum burn rate was specified). Temperatures resulting from Case C-175c are consistently higher than those for C-175b, which would be expected since energy typically lost from the fire to the pool to increase the liquid temperature and evaporate the fuel is now available for heating the fire plume. Further review of the appropriate ignition/evaporation temperature is warranted (i.e., is burning occurring on the pool surface or is boiling the primary mechanism to get fuel into the fire plume so that it will combust) ... and the heat of vaporization needs to reflect the ignition temperature specified. For future efforts, use of the BNDF namelist group to collect mass loss rate per unit area results via the QUANTITY, ‘BURNING_RATE’, would

facilitate understanding of the actual consequences of the parameters changed from Case C-175b to Cases C-175c and C-175d [FDS3-UG, pp. 36 and 39].

Grid Refinement. As noted previously, FDS3 models the flame as a two-dimensional surface, determines the heat release rate, and smears the energy released across the cells cut by the flame sheet, resulting in a temperatures typically less than would be actually observed. As the grid is refined—to the limits permitted by the code algorithms, computational error, and computer capacity—computed temperature averages and maximums are expected to increase, at least until the effects of smearing are off-set by the wafting of the fire sheet in the turbulent environment of the fire. With respect to the final simulations (C-175b, C-175c, and C-175d), the grids result in over a million nodes (multiply each applicable set of IBAR, JBAR, and KBAR values in Table 6.2, then sum the results), and run times were approximately 30 day for each cases on a PC having a 3.00 GHz Pentium 4 processor and 2.00 GB of RAM.

6.4 SUMMARY AND RECOMMENDATIONS

Initial simulations of the Sandia Fire Test C indicated that the default radiation fraction assumed in FDS3 could yield a significant overestimation of temperatures for a calorimeter engulfed in a fire as the grid is refined. Subsequent simulations set the radiation fraction to zero and used ignitors over the first 10 s of the simulation to initiate the fire. Later runs indicated reasonable results could be obtained with a refined grid, and the final case, C-175d, indicated that it is not necessary to limit the burn rate. It was observed that the variation in results over the course of a simulation was similar to the variation in test data. It is anticipated that further grid refinement along with adjustments to the heat of vaporization and ignition temperatures could result in further improvement in the agreement between simulation results and test data.

The following recommendations are made for future large pool fire simulations:

1. Reduce the grid size encompassing the fire itself below the 0.175 m refinement of the simulations reported herein.

2. Set the radiation fraction to zero, and use ignitors to initiate the fire.

3. Do not limit the burn rate.

4. Review and, as appropriate, adjust the heat of vaporization and ignition temperature.

7. CONCLUSIONS AND RECOMMENDATIONS

The capabilities of FDS3 have been examined to determine whether a major pool fire test can be reasonably simulated. Simulation activities were undertaken sequentially to addressed the following:

1. Radiation modeling from constant temperature walls to assess the thick and thin wall modeling capabilities of FDS3 (Chapter 3).

2. 2-D and 3-D pool fire modeling in the absence of wind and heat sinks within the fire principally to compare flame height predictions to established correlations (Chapter 4).

3. Wind field modeling specifically targeted at developing a wind field to use in the simulation of an actual pool fire (Chapter 5).

4. Simulation of a specific pool fire test (Chapter 6).

Sections 7.1 and 7.2 summarize conclusions and recommendations presented earlier in this report.

7.1 CONCLUSIONS

C1. Reasonable results are obtained from the thermally thick and thin wall boundary conditions based on visual comparison of plotted analytical results for a thin wall boundary condition and FDS3 results (Chapter 3).

C2. A process has been established to determine flame height based on the criterion that flame height is defined as the height at which the flame is observed at least 50% of the time (Chapter 4).

C3. There is a significant difference in estimated flame heights between 2-D-radial models and quarter, half, and full 3-D models that arguably represent the same fire environment (Chapter 4). Full 3-D models should be developed when simulating fires.

C4. When flame heights are plotted against equivalent diameter (Eq. 9), hydraulic diameter (Eq. 10), and minimum pool width, minimum pool width appears to provide the most consistent basis for estimating height, all other parameter being the same. When the results were plotted for comparison, a curve twice the average of the Heskestad and Thomas correlations passed through the flame heights plotted against minimum pool width. (The “factor” of two would likely increase based on the later observation that maximum burn rate should not be specified.) An argument has been presented that flame height observations—and hence correlations derived from

them—may be influenced by fire size ... since a fire is optically opaque if it is more than 1- to 2-m thick, the observed temperature or fraction of time the flame is present may be less than the actual values. (Chapter 4.)

C5. A process has been outlined and successfully implemented for transforming wind field data associated with an outdoor test into initial and boundary conditions for simulating the test (Chapters 5 and 6).

C6. When modeling large pool fires, the default radiation fraction should be overridden by explict specification of a fraction equal to zero. It will be necessary to include ignitors for a brief period at the beginning of the simulation period to ignite the fire in the absence of the default Also, maximum burn rate should not be specified. (Chapter 6.)

C7. It is anticipated that reducing the heat of vaporization to better reflect its value at the ignition temperature would improve the comparison between simulation results and data (Chapter 5).

C8. It is anticipated that further grid refinement would generally result in increased flame temperatures at the points specified in the Test C simulations, thus improving the comparison between simulation results and data. (Chapter 6).

C9. It is noted that neither Test C nor the simulations would meet the thermal test temperature requirements for packaging ... "... an average temperature of at least 800°C (1475°F) for a period of 30 minutes ..." (Chapter 6).

C10. It is noted that the FDS3 simulations do reflect the "highly turbulent nature of a large open pool fire and its susceptibility to winds [which] produce temperature and flow fields that are very nonuniform in both a spatial and temporal sense" (Chapter 6).

7.2 RECOMMENDATIONS

The following recommendations apply to users of the FDS code (FDS3 or future revisions).

R1. Full 3-D models should be used when simulating a fire (Chapter 4).

R2. The radiation fraction should be explicitly set to zero and ignitors should be modeled for a brief period to ignite the fire (Chapter 6).

R3. A maximum burn rate should not be specified (Chapter 6).

R4. When preparing to model large pool fires, care should be taken in specifying the heat of vaporization and the ignition temperature (Chapter 2 and 6).

R5. If possible, further refinement of the fine grid should be considered in the area above the pool, and sufficiently outside the pool to ensure adequate modeling of the fire. A grid size about 1 m appears adequate for the wind field beyond the pool. A transition (medium) grid extending outside the refined grid should be specified to facilitate air flow from the large wind field grid to the fine grid over the fire. (Chapter 6.)

The following recommendations are offered for consideration when correlating flame height data or enhancing the capabilities of the FDS code.

R6. The applicability of established pool fire correlations for estimating the flame height of large fires should be reviewed in light of the results presented in Chapter 4 (with the caveat noted in Conclusion 4 relative to maximum burn rate).

R7. To facilitate future modeling, several recommendations regarding potential enhancements to the FDS code were included in Sect. 5.3.2.

LIST OF REFERENCES

10 CFR 71	10 CFR PART 71, *Packaging and Transportation of Radioactive Material,* January 1, 2002.
10 CFR 830	10 CFR Part 830, *Nuclear Safety Management,* Subpart B, "Safety Basis Requirements", January 1, 2003.
3009 CN2	DOE-STD-3009-94, Change Notice 2, *Preparation Guide for U.S. Department of Energy Nonreactor Nuclear Facility Documented Safety Analyses*, U.S. Department of Energy, April 2002.
420.1A	DOE O 420.1A, *Facility Safety*, U.S. Department of Energy, May 20, 2002.
AS&PP	Darryl Randerson, Ed., *Atmospheric Science and Power Production*, DOE/TIC-27601, U.S. Department of Energy, 1984.
ATSDR	*Toxicological Profile for Jet Fuels JP-4 and JP-7*, U.S. Department of Health and Human Services, Public Health Service, Agency for Toxic Substances and Disease Registry, June 1995
Buck and Belason	Michael E. Buck and E. Bruce Belason, "ASTM Test for Effects of Large Hydrocarbon Pool Fires on Structural Members," *Plant/ Operations Progress*, Vol. 4, No. 4, pp. 225-229, October 1985.
FDS3-TRG	Kevin B. McGrattan, Howard R. Baum, Ronald G. Rehm, Anthony Hamins, Glenn P. Forney, Jason E. Floyd, Simo Hostikka, and Kuldeep Prasad, *Fire Dynamics Simulator (Version 3) – Technical Reference Guide*, NISTIR 6783, 2002 Ed., National Institute of Standards and Technology, Gaithersburg, Maryland, November 2002.
FDS3-UG	Kevin B. McGrattan, Glenn P. Forney, Jason E. Floyd, Simo Hostikka, and Kuldeep Prasad, *Fire Dynamics Simulator (Version 3) – User's Guide*, NISTIR 6784, 2002 Ed., National Institute of Standards and Technology, Gaithersburg, Maryland, November 2002.
G 420.1-1	DOE G 420.1-1, *Nonreactor Nuclear Safety Design Criteria and Explosives Safety Criteria Guide for Use with DOE O 420.1, Facility Safety*, U.S. Department of Energy, March 28, 2000.
ISG	International Steel Group, Inc., Web Site, www.intlsteel.com (see product brochure "ISG Plate A514 & T-1®," September 9, 2003, from product literature link)
MatWeb	MatWeb Material Property Data Web Site, www.matweb.com.

NUREG-1805 *Fire Dynamics Tools (FDT^s) Quantitative Fire Hazard Analysis Methods for the U.S. Nuclear Regulatory Commission Fire Protection Inspection Program*, NUREG-1805, U.S. Nuclear Regulatory Commission, Washington, DC, December 2004.

Perry's *Perry's Chemical Engineers' Handbook*, 4th Ed., McGraw-Hill Book Co., New York, 1963.

SAND85–0196 Julie J. Gregory, Roberto Mata, Jr., and Ned R. Keltner, *Thermal Measurements in a Series of Large Pool Fires*, SAND85-0196, Sandia National Laboratories, Albuquerque, New Mexico, August 1987.

TI#19206 *Petroleum Fuels: Basic Composition and Properties*, Pro_Act Fact Sheet TI#19206, Air Force Center for Environmental Excellence, February 1999.

WRW W. R. Williams, *Overview of UF_6 Cylinder-Fire Modeling with Specific Discussion of 6FIRE*, DAC-EA-710660-A001, Rev. 1, Lockheed Martin Energy Systems, Inc., Oak Ridge, Tennessee, September 1996.

WRW&JCA W. R. Williams and J. C. Anderson, *Accident Simulations Using 6FIRE and SUBLIME,* DAC-EA-710660-A003, Rev. 1, Lockheed Martin Energy Systems, Inc., Oak Ridge, Tennessee, September 1996.

APPENDICES

APPENDIX A. SANDIA FIRE TEST RESULTS

The following tables are transcribed from *Thermal Measurements in a Series of Large Pool Fires* [SAND85-0196, Tables 1, 2, and 3].

Table A.1. Average Flame Temperatures for Tower Thermocouples (°F)

	Tower B			Tower 2			Tower 7		
H_{TC}, in.	Test A	Test B	Test C	Test A	Test B	Test C	Test A	Test B	Test C
56	1483	1835	2011	1738	1797	1836	1847	1922	1773
103	1473	1641	1935	1538	1451	1476	1417	1814	1792
216				1126	1184	1244	764	1188	1401
440				577	951	1007	914	981	1133

	Tower 3						Tower C		
H_{TC}, in.	Test A	Test B	Test C				Test A	Test B	Test C
56	1410		1657		N		1806	1970	1957
103	1078	1431	1335	W	┼	E	1305	1503	1658
216	993	918	625		S				
440	1112	722	381						

	Tower A			Tower 4			Tower 6		
H_{TC}, in.	Test A	Test B	Test C	Test A	Test B	Test C	Test A	Test B	Test C
56	1145	1219	1800	1649	1577	1519	1701	1509	1505
103	962	846	1321	1431	1294		1402	1184	1048
216				990	1023	921	736	852	821
440				512	618	552	425	517	636

Table A.2. Flame Temperatures Statistics for Entire Test

	Test A	Test B	Test C
Elevation: 56 in.			
Min (°F)	600	827	344
Max (°F)	2412	2299	2323
Avg (°F)	1597	1690	1757
Std Dev (°F)	382	351	317
SD/Avg (%)	24	21	18
Elevation: 103 in.			
Min (°F)	248	454	286
Max (°F)	2376	2371	2386
Avg (°F)	1326	1396	1509
Std Dev (°F)	489	491	487
SD/Avg (%)	37	35	32
Elevation: 216 in.			
Min (°F)	163	228	255
Max (°F)	2292	2311	2356
Avg (°F)	922	1033	1003
Std Dev (°F)	484	497	507
SD/Avg (%)	52	48	51
Elevation: 440 in.			
Min (°F)	156	192	128
Max (°F)	2360	2229	2254
Avg (°F)	708	758	742
Std Dev (°F)	495	459	479
SD/Avg (%)	70	61	65

Table A.3. Flame Temperatures Statistics for Low Wind Conditions

	Test A	Test B	Test C
Elevation: 56 in.			
Min (°F)	1119	870	908
Max (°F)	2412	2244	2243
Avg (°F)	1758	1750	1793
Std Dev (°F)	235	301	286
SD/Avg (%)	13	17	16
Elevation: 103 in.			
Min (°F)	677	606	619
Max (°F)	2376	2308	2302
Avg (°F)	1577	1561	1541
Std Dev (°F)	415	431	450
SD/Avg (%)	26	28	29
Elevation: 216 in.			
Min (°F)	394	320	327
Max (°F)	2292	2311	2088
Avg (°F)	1234	1282	975
Std Dev (°F)	591	485	411
SD/Avg (%)	48	38	42
Elevation: 440 in.			
Min (°F)	297	255	153
Max (°F)	2360	2229	1980
Avg (°F)	1165	1023	611
Std Dev (°F)	609	518	356
SD/Avg (%)	52	51	58

APPENDIX B. FDS3 INPUT FILES

B.1 Radiation to Thermally-Thick and -Thin Surfaces

```
&HEAD CHID='WALL',TITLE='Thin/Thick Test Wall in Constant T Enclosure' /
&GRID IBAR=6,JBAR=6,KBAR=4 /
&PDIM XBAR0=-1,XBAR=5,YBAR0=0,YBAR=6,ZBAR0=0,ZBAR=4 /

&MISC DATABASE='c:\nist\fds\database3\database3.data',
      SURF_DEFAULT='CTWALL',
      NFRAMES=400 /
&TIME TWFIN=1800. /

&SURF ID='CTWALL', TMPWAL=800. /

&SURF ID='STEEL-thin',
      C_DELTA_RHO=120.,
      BACKING='INSULATED'/

&SURF ID='STEEL-thick    ',
      ALPHA=1.11E-5,
      KS=43.6,
      DELTA=0.03175,
      BACKING='INSULATED'/

&SURF ID='STEEL-PLATE',
      C_DELTA_RHO=120 /

&OBST XB=-1,0,0,2,0,2, SURF_ID='STEEL-thin'  /
&OBST XB=-1,0,2,4,0,2, SURF_ID='STEEL-thick' /
&OBST XB=-1,0,4,6,0,2, SURF_ID='STEEL-thin'  /
&OBST XB=-1,0,0,2,2,4, SURF_ID='STEEL-thick' /
&OBST XB=-1,0,2,4,2,4, SURF_ID='STEEL-thin'  /
&OBST XB=-1,0,4,6,2,4, SURF_ID='STEEL-thick' /

&THCP XYZ=-0.001,1,1, IOR=1, QUANTITY='WALL_TEMPERATURE', LABEL='LL-thin'  /
&THCP XYZ=-0.001,3,1, IOR=1, QUANTITY='WALL_TEMPERATURE', LABEL='LC-thick' /
&THCP XYZ=-0.001,5,1, IOR=1, QUANTITY='WALL_TEMPERATURE', LABEL='LR-thin'  /
&THCP XYZ=-0.001,1,3, IOR=1, QUANTITY='WALL_TEMPERATURE', LABEL='UL-thick' /
```

```
&THCP XYZ=-0.001,3,3, IOR=1, QUANTITY='WALL_TEMPERATURE', LABEL='UC-thin'  /
&THCP XYZ=-0.001,5,3, IOR=1, QUANTITY='WALL_TEMPERATURE', LABEL='UR-thick' /

&THCP XYZ=-0.001,1,1, IOR=1, QUANTITY='BACK_WALL_TEMPERATURE', LABEL='LL-thin'  /
&THCP XYZ=-0.001,3,1, IOR=1, QUANTITY='BACK_WALL_TEMPERATURE', LABEL='LC-thick' /
&THCP XYZ=-0.001,5,1, IOR=1, QUANTITY='BACK_WALL_TEMPERATURE', LABEL='LR-thin'  /
&THCP XYZ=-0.001,1,3, IOR=1, QUANTITY='BACK_WALL_TEMPERATURE', LABEL='UL-thick' /
&THCP XYZ=-0.001,3,3, IOR=1, QUANTITY='BACK_WALL_TEMPERATURE', LABEL='UC-thin'  /
&THCP XYZ=-0.001,5,3, IOR=1, QUANTITY='BACK_WALL_TEMPERATURE', LABEL='UR-thick' /

&BNDF QUANTITY='WALL_TEMPERATURE' /

&BNDF QUANTITY='BACK_WALL_TEMPERATURE' /
```

B.2 2-D Pool Fire Model (HRV600-3.data)

```
&HEAD CHID = 'HRV600-3', TITLE = '6-m Pool Fire w/ 0.125-m H x 0.375-m V grid' /
&GRID IBAR = 288, JBAR = 1,   KBAR = 576  /
&PDIM RBAR = 36., YBAR = 0.1, ZBAR = 216. /

&TIME TWFIN = 600. /
&MISC REACTION = 'JP-4', NFRAMES = 600 /

&REAC ID                  = 'JP-4',
      MW_FUEL             = 112.42,
      NU_O2               = 16.06,
      NU_CO2              = 8.03,
      NU_H2O              = 8.03,
      CO_YIELD            = 0.012,
      SOOT_YIELD          = 0.019,
      EPUMO2              = 9362.5 /

&SURF ID                  = 'JP-4',
      RGB                 = 0.0, 0.0, 0.5,
      TMPIGN              = 246.,
      HEAT_OF_VAPORIZATION = 364.,
      HEAT_OF_COMBUSTION  = 42800.
      BURNING_RATE_MAX    = 0.074,
      DELTA               = 0.10,
```

```
      KS                    = 0.14,
      ALPHA                 = 8.6E-8,
      PHASE                 = 'LIQUID' /

&VENT XB = 0.0, 6.0, 0.0, 0.1, 0.0, 0.0, SURF_ID = 'JP-4' /
&VENT CB = RBAR, SURF_ID = 'OPEN' /
&VENT CB = ZBAR, SURF_ID = 'OPEN' /

&THCP XYZ = 0.0, 0.0,   6., QUANTITY = 'HRRPUV', LABEL = 'HRRPUV    6' /
&THCP XYZ = 0.0, 0.0,  12., QUANTITY = 'HRRPUV', LABEL = 'HRRPUV   12' /
&THCP XYZ = 0.0, 0.0,  18., QUANTITY = 'HRRPUV', LABEL = 'HRRPUV   18' /
&THCP XYZ = 0.0, 0.0,  24., QUANTITY = 'HRRPUV', LABEL = 'HRRPUV   24' /
&THCP XYZ = 0.0, 0.0,  30., QUANTITY = 'HRRPUV', LABEL = 'HRRPUV   30' /
&THCP XYZ = 0.0, 0.0,  36., QUANTITY = 'HRRPUV', LABEL = 'HRRPUV   36' /
&THCP XYZ = 0.0, 0.0,  42., QUANTITY = 'HRRPUV', LABEL = 'HRRPUV   42' /
&THCP XYZ = 0.0, 0.0,  48., QUANTITY = 'HRRPUV', LABEL = 'HRRPUV   48' /
&THCP XYZ = 0.0, 0.0,  54., QUANTITY = 'HRRPUV', LABEL = 'HRRPUV   54' /
&THCP XYZ = 0.0, 0.0,  60., QUANTITY = 'HRRPUV', LABEL = 'HRRPUV   60' /
&THCP XYZ = 0.0, 0.0,  66., QUANTITY = 'HRRPUV', LABEL = 'HRRPUV   66' /
&THCP XYZ = 0.0, 0.0,  72., QUANTITY = 'HRRPUV', LABEL = 'HRRPUV   72' /
&THCP XYZ = 0.0, 0.0,  78., QUANTITY = 'HRRPUV', LABEL = 'HRRPUV   78' /
&THCP XYZ = 0.0, 0.0,  84., QUANTITY = 'HRRPUV', LABEL = 'HRRPUV   84' /
&THCP XYZ = 0.0, 0.0,  90., QUANTITY = 'HRRPUV', LABEL = 'HRRPUV   90' /
&THCP XYZ = 0.0, 0.0,  96., QUANTITY = 'HRRPUV', LABEL = 'HRRPUV   96' /
&THCP XYZ = 0.0, 0.0, 102., QUANTITY = 'HRRPUV', LABEL = 'HRRPUV  102' /
&THCP XYZ = 0.0, 0.0, 108., QUANTITY = 'HRRPUV', LABEL = 'HRRPUV  108' /
&THCP XYZ = 0.0, 0.0, 114., QUANTITY = 'HRRPUV', LABEL = 'HRRPUV  114' /
&THCP XYZ = 0.0, 0.0, 120., QUANTITY = 'HRRPUV', LABEL = 'HRRPUV  120' /
&THCP XYZ = 0.0, 0.0, 126., QUANTITY = 'HRRPUV', LABEL = 'HRRPUV  126' /
&THCP XYZ = 0.0, 0.0, 132., QUANTITY = 'HRRPUV', LABEL = 'HRRPUV  132' /
&THCP XYZ = 0.0, 0.0, 138., QUANTITY = 'HRRPUV', LABEL = 'HRRPUV  138' /
&THCP XYZ = 0.0, 0.0, 144., QUANTITY = 'HRRPUV', LABEL = 'HRRPUV  144' /
&THCP XYZ = 0.0, 0.0, 150., QUANTITY = 'HRRPUV', LABEL = 'HRRPUV  150' /
&THCP XYZ = 0.0, 0.0, 156., QUANTITY = 'HRRPUV', LABEL = 'HRRPUV  156' /
&THCP XYZ = 0.0, 0.0, 162., QUANTITY = 'HRRPUV', LABEL = 'HRRPUV  162' /
&THCP XYZ = 0.0, 0.0, 168., QUANTITY = 'HRRPUV', LABEL = 'HRRPUV  168' /
&THCP XYZ = 0.0, 0.0, 174., QUANTITY = 'HRRPUV', LABEL = 'HRRPUV  174' /
&THCP XYZ = 0.0, 0.0, 180., QUANTITY = 'HRRPUV', LABEL = 'HRRPUV  180' /
&THCP XYZ = 0.0, 0.0, 186., QUANTITY = 'HRRPUV', LABEL = 'HRRPUV  186' /
&THCP XYZ = 0.0, 0.0, 192., QUANTITY = 'HRRPUV', LABEL = 'HRRPUV  192' /
```

```
&THCP XYZ = 0.0, 0.0, 198., QUANTITY = 'HRRPUV', LABEL = 'HRRPUV  198' /
&THCP XYZ = 0.0, 0.0, 204., QUANTITY = 'HRRPUV', LABEL = 'HRRPUV  204' /
&THCP XYZ = 0.0, 0.0, 210., QUANTITY = 'HRRPUV', LABEL = 'HRRPUV  210' /
&THCP XYZ = 0.0, 0.0, 216., QUANTITY = 'HRRPUV', LABEL = 'HRRPUV  216' /

&SLCF PBY = 0.0, QUANTITY = 'TEMPERATURE'      /
&SLCF PBY = 0.0, QUANTITY = 'U-VELOCITY'       /
&SLCF PBY = 0.0, QUANTITY = 'W-VELOCITY'       /
&SLCF PBY = 0.0, QUANTITY = 'HRRPUV'           /
&SLCF PBY = 0.0, QUANTITY = 'MIXTURE_FRACTION' /
&SLCF PBY = 0.0, QUANTITY = 'DIVERGENCE'       /
```

B.3 3-D Pool Fire Model (W6x6-2.data)

```
&HEAD CHID = 'W6x6-2', TITLE = 'Whl 6x6 Pool w/ 0.25 fire 0.75 domain' /

&GRID IBAR  =  30,                JBAR  =  30,                KBAR = 432  /
&PDIM XBAR0 = -3.75, XBAR = 3.75, YBAR0 = -3.75, YBAR = 3.75, ZBAR = 108. /

&GRID IBAR  =  40,                JBAR  =  40,                KBAR = 144  /
&PDIM XBAR0 = -15,   XBAR = 15.,  YBAR0 = -15,   YBAR = 15.,  ZBAR = 108. /

&TIME TWFIN = 600. /
&MISC REACTION = 'JP-4', NFRAMES = 600 /

&REAC ID                   = 'JP-4',
      MW_FUEL              = 112.42,
      NU_O2                = 16.06,
      NU_CO2               = 8.03,
      NU_H2O               = 8.03,
      CO_YIELD             = 0.012,
      SOOT_YIELD           = 0.019,
      EPUMO2               = 9362.5 /

&SURF ID                   = 'JP-4',
      RGB                  = 0.0, 0.0, 0.5,
      TMPIGN               = 246.,
      HEAT_OF_VAPORIZATION = 364.,
      HEAT_OF_COMBUSTION   = 42800.
```

```
      BURNING_RATE_MAX     = 0.074,
      DELTA                = 0.10,
      KS                   = 0.14,
      ALPHA                = 8.6E-8,
      PHASE                = 'LIQUID' /

&VENT XB = -3.0, 3.0, -3.0, 3.0, 0.0, 0.0, SURF_ID = 'JP-4' /
&VENT CB = XBAR0, SURF_ID = 'OPEN' /
&VENT CB = XBAR,  SURF_ID = 'OPEN' /
&VENT CB = YBAR0, SURF_ID = 'OPEN' /
&VENT CB = YBAR,  SURF_ID = 'OPEN' /
&VENT CB = ZBAR,  SURF_ID = 'OPEN' /

&THCP XYZ = 0.0, 0.0,   6., QUANTITY = 'HRRPUV', LABEL = 'HRRPUV    6' /
&THCP XYZ = 0.0, 0.0,  12., QUANTITY = 'HRRPUV', LABEL = 'HRRPUV   12' /
&THCP XYZ = 0.0, 0.0,  18., QUANTITY = 'HRRPUV', LABEL = 'HRRPUV   18' /
&THCP XYZ = 0.0, 0.0,  24., QUANTITY = 'HRRPUV', LABEL = 'HRRPUV   24' /
&THCP XYZ = 0.0, 0.0,  30., QUANTITY = 'HRRPUV', LABEL = 'HRRPUV   30' /
&THCP XYZ = 0.0, 0.0,  36., QUANTITY = 'HRRPUV', LABEL = 'HRRPUV   36' /
&THCP XYZ = 0.0, 0.0,  42., QUANTITY = 'HRRPUV', LABEL = 'HRRPUV   42' /
&THCP XYZ = 0.0, 0.0,  48., QUANTITY = 'HRRPUV', LABEL = 'HRRPUV   48' /
&THCP XYZ = 0.0, 0.0,  54., QUANTITY = 'HRRPUV', LABEL = 'HRRPUV   54' /
&THCP XYZ = 0.0, 0.0,  60., QUANTITY = 'HRRPUV', LABEL = 'HRRPUV   60' /
&THCP XYZ = 0.0, 0.0,  66., QUANTITY = 'HRRPUV', LABEL = 'HRRPUV   66' /
&THCP XYZ = 0.0, 0.0,  72., QUANTITY = 'HRRPUV', LABEL = 'HRRPUV   72' /
&THCP XYZ = 0.0, 0.0,  78., QUANTITY = 'HRRPUV', LABEL = 'HRRPUV   78' /
&THCP XYZ = 0.0, 0.0,  84., QUANTITY = 'HRRPUV', LABEL = 'HRRPUV   84' /
&THCP XYZ = 0.0, 0.0,  90., QUANTITY = 'HRRPUV', LABEL = 'HRRPUV   90' /
&THCP XYZ = 0.0, 0.0,  96., QUANTITY = 'HRRPUV', LABEL = 'HRRPUV   96' /
&THCP XYZ = 0.0, 0.0, 102., QUANTITY = 'HRRPUV', LABEL = 'HRRPUV  102' /
&THCP XYZ = 0.0, 0.0, 108., QUANTITY = 'HRRPUV', LABEL = 'HRRPUV  108' /

&THCP XYZ = 0.5, 0.0,   6., QUANTITY = 'HRRPUV', LABEL = 'H X+.5    6' /
&THCP XYZ = 0.5, 0.0,  12., QUANTITY = 'HRRPUV', LABEL = 'H X+.5   12' /
&THCP XYZ = 0.5, 0.0,  18., QUANTITY = 'HRRPUV', LABEL = 'H X+.5   18' /
&THCP XYZ = 0.5, 0.0,  24., QUANTITY = 'HRRPUV', LABEL = 'H X+.5   24' /
&THCP XYZ = 0.5, 0.0,  30., QUANTITY = 'HRRPUV', LABEL = 'H X+.5   30' /
&THCP XYZ = 0.5, 0.0,  36., QUANTITY = 'HRRPUV', LABEL = 'H X+.5   36' /
&THCP XYZ = 0.5, 0.0,  42., QUANTITY = 'HRRPUV', LABEL = 'H X+.5   42' /
&THCP XYZ = 0.5, 0.0,  48., QUANTITY = 'HRRPUV', LABEL = 'H X+.5   48' /
```

```
&THCP XYZ = 0.5, 0.0,  54., QUANTITY = 'HRRPUV', LABEL = 'H X+.5   54' /
&THCP XYZ = 0.5, 0.0,  60., QUANTITY = 'HRRPUV', LABEL = 'H X+.5   60' /
&THCP XYZ = 0.5, 0.0,  66., QUANTITY = 'HRRPUV', LABEL = 'H X+.5   66' /
&THCP XYZ = 0.5, 0.0,  72., QUANTITY = 'HRRPUV', LABEL = 'H X+.5   72' /
&THCP XYZ = 0.5, 0.0,  78., QUANTITY = 'HRRPUV', LABEL = 'H X+.5   78' /
&THCP XYZ = 0.5, 0.0,  84., QUANTITY = 'HRRPUV', LABEL = 'H X+.5   84' /
&THCP XYZ = 0.5, 0.0,  90., QUANTITY = 'HRRPUV', LABEL = 'H X+.5   90' /
&THCP XYZ = 0.5, 0.0,  96., QUANTITY = 'HRRPUV', LABEL = 'H X+.5   96' /
&THCP XYZ = 0.5, 0.0, 102., QUANTITY = 'HRRPUV', LABEL = 'H X+.5  102' /
&THCP XYZ = 0.5, 0.0, 108., QUANTITY = 'HRRPUV', LABEL = 'H X+.5  108' /

&THCP XYZ = -0.5, 0.0,   6., QUANTITY = 'HRRPUV', LABEL = 'H X-.5    6' /
&THCP XYZ = -0.5, 0.0,  12., QUANTITY = 'HRRPUV', LABEL = 'H X-.5   12' /
&THCP XYZ = -0.5, 0.0,  18., QUANTITY = 'HRRPUV', LABEL = 'H X-.5   18' /
&THCP XYZ = -0.5, 0.0,  24., QUANTITY = 'HRRPUV', LABEL = 'H X-.5   24' /
&THCP XYZ = -0.5, 0.0,  30., QUANTITY = 'HRRPUV', LABEL = 'H X-.5   30' /
&THCP XYZ = -0.5, 0.0,  36., QUANTITY = 'HRRPUV', LABEL = 'H X-.5   36' /
&THCP XYZ = -0.5, 0.0,  42., QUANTITY = 'HRRPUV', LABEL = 'H X-.5   42' /
&THCP XYZ = -0.5, 0.0,  48., QUANTITY = 'HRRPUV', LABEL = 'H X-.5   48' /
&THCP XYZ = -0.5, 0.0,  54., QUANTITY = 'HRRPUV', LABEL = 'H X-.5   54' /
&THCP XYZ = -0.5, 0.0,  60., QUANTITY = 'HRRPUV', LABEL = 'H X-.5   60' /
&THCP XYZ = -0.5, 0.0,  66., QUANTITY = 'HRRPUV', LABEL = 'H X-.5   66' /
&THCP XYZ = -0.5, 0.0,  72., QUANTITY = 'HRRPUV', LABEL = 'H X-.5   72' /
&THCP XYZ = -0.5, 0.0,  78., QUANTITY = 'HRRPUV', LABEL = 'H X-.5   78' /
&THCP XYZ = -0.5, 0.0,  84., QUANTITY = 'HRRPUV', LABEL = 'H X-.5   84' /
&THCP XYZ = -0.5, 0.0,  90., QUANTITY = 'HRRPUV', LABEL = 'H X-.5   90' /
&THCP XYZ = -0.5, 0.0,  96., QUANTITY = 'HRRPUV', LABEL = 'H X-.5   96' /
&THCP XYZ = -0.5, 0.0, 102., QUANTITY = 'HRRPUV', LABEL = 'H X-.5  102' /
&THCP XYZ = -0.5, 0.0, 108., QUANTITY = 'HRRPUV', LABEL = 'H X-.5  108' /

&THCP XYZ = 0.0, 0.5,   6., QUANTITY = 'HRRPUV', LABEL = 'H Y+.5    6' /
&THCP XYZ = 0.0, 0.5,  12., QUANTITY = 'HRRPUV', LABEL = 'H Y+.5   12' /
&THCP XYZ = 0.0, 0.5,  18., QUANTITY = 'HRRPUV', LABEL = 'H Y+.5   18' /
&THCP XYZ = 0.0, 0.5,  24., QUANTITY = 'HRRPUV', LABEL = 'H Y+.5   24' /
&THCP XYZ = 0.0, 0.5,  30., QUANTITY = 'HRRPUV', LABEL = 'H Y+.5   30' /
&THCP XYZ = 0.0, 0.5,  36., QUANTITY = 'HRRPUV', LABEL = 'H Y+.5   36' /
&THCP XYZ = 0.0, 0.5,  42., QUANTITY = 'HRRPUV', LABEL = 'H Y+.5   42' /
&THCP XYZ = 0.0, 0.5,  48., QUANTITY = 'HRRPUV', LABEL = 'H Y+.5   48' /
&THCP XYZ = 0.0, 0.5,  54., QUANTITY = 'HRRPUV', LABEL = 'H Y+.5   54' /
&THCP XYZ = 0.0, 0.5,  60., QUANTITY = 'HRRPUV', LABEL = 'H Y+.5   60' /
```

```
&THCP XYZ = 0.0, 0.5,  66., QUANTITY = 'HRRPUV', LABEL = 'H Y+.5   66' /
&THCP XYZ = 0.0, 0.5,  72., QUANTITY = 'HRRPUV', LABEL = 'H Y+.5   72' /
&THCP XYZ = 0.0, 0.5,  78., QUANTITY = 'HRRPUV', LABEL = 'H Y+.5   78' /
&THCP XYZ = 0.0, 0.5,  84., QUANTITY = 'HRRPUV', LABEL = 'H Y+.5   84' /
&THCP XYZ = 0.0, 0.5,  90., QUANTITY = 'HRRPUV', LABEL = 'H Y+.5   90' /
&THCP XYZ = 0.0, 0.5,  96., QUANTITY = 'HRRPUV', LABEL = 'H Y+.5   96' /
&THCP XYZ = 0.0, 0.5, 102., QUANTITY = 'HRRPUV', LABEL = 'H Y+.5  102' /
&THCP XYZ = 0.0, 0.5, 108., QUANTITY = 'HRRPUV', LABEL = 'H Y+.5  108' /

&THCP XYZ = 0.0, -0.5,   6., QUANTITY = 'HRRPUV', LABEL = 'H Y-.5    6' /
&THCP XYZ = 0.0, -0.5,  12., QUANTITY = 'HRRPUV', LABEL = 'H Y-.5   12' /
&THCP XYZ = 0.0, -0.5,  18., QUANTITY = 'HRRPUV', LABEL = 'H Y-.5   18' /
&THCP XYZ = 0.0, -0.5,  24., QUANTITY = 'HRRPUV', LABEL = 'H Y-.5   24' /
&THCP XYZ = 0.0, -0.5,  30., QUANTITY = 'HRRPUV', LABEL = 'H Y-.5   30' /
&THCP XYZ = 0.0, -0.5,  36., QUANTITY = 'HRRPUV', LABEL = 'H Y-.5   36' /
&THCP XYZ = 0.0, -0.5,  42., QUANTITY = 'HRRPUV', LABEL = 'H Y-.5   42' /
&THCP XYZ = 0.0, -0.5,  48., QUANTITY = 'HRRPUV', LABEL = 'H Y-.5   48' /
&THCP XYZ = 0.0, -0.5,  54., QUANTITY = 'HRRPUV', LABEL = 'H Y-.5   54' /
&THCP XYZ = 0.0, -0.5,  60., QUANTITY = 'HRRPUV', LABEL = 'H Y-.5   60' /
&THCP XYZ = 0.0, -0.5,  66., QUANTITY = 'HRRPUV', LABEL = 'H Y-.5   66' /
&THCP XYZ = 0.0, -0.5,  72., QUANTITY = 'HRRPUV', LABEL = 'H Y-.5   72' /
&THCP XYZ = 0.0, -0.5,  78., QUANTITY = 'HRRPUV', LABEL = 'H Y-.5   78' /
&THCP XYZ = 0.0, -0.5,  84., QUANTITY = 'HRRPUV', LABEL = 'H Y-.5   84' /
&THCP XYZ = 0.0, -0.5,  90., QUANTITY = 'HRRPUV', LABEL = 'H Y-.5   90' /
&THCP XYZ = 0.0, -0.5,  96., QUANTITY = 'HRRPUV', LABEL = 'H Y-.5   96' /
&THCP XYZ = 0.0, -0.5, 102., QUANTITY = 'HRRPUV', LABEL = 'H Y-.5  102' /
&THCP XYZ = 0.0, -0.5, 108., QUANTITY = 'HRRPUV', LABEL = 'H Y-.5  108' /

&SLCF PBX = 0.0, QUANTITY = 'TEMPERATURE'      /
&SLCF PBX = 0.0, QUANTITY = 'U-VELOCITY'       /
&SLCF PBX = 0.0, QUANTITY = 'W-VELOCITY'       /
&SLCF PBX = 0.0, QUANTITY = 'HRRPUV'           /
&SLCF PBX = 0.0, QUANTITY = 'MIXTURE_FRACTION' /
&SLCF PBX = 0.0, QUANTITY = 'DIVERGENCE'       /

&SLCF PBY = 0.0, QUANTITY = 'TEMPERATURE'      /
&SLCF PBY = 0.0, QUANTITY = 'U-VELOCITY'       /
&SLCF PBY = 0.0, QUANTITY = 'W-VELOCITY'       /
&SLCF PBY = 0.0, QUANTITY = 'HRRPUV'           /
&SLCF PBY = 0.0, QUANTITY = 'MIXTURE_FRACTION' /
```

```
&SLCF PBY = 0.0, QUANTITY = 'DIVERGENCE'       /
```

B.4 Wind Field Model (wndfld-l.data)

```
&HEAD CHID = 'wndfld-l', TITLE = '9.1 x 18.2 Pool Fire Site w/ 1.05-m H x 2.1-m V grid' /

&GRID IBAR = 72, JBAR = 70, KBAR = 24 /
&PDIM XBAR0 = -37.8, XBAR = 37.8, YBAR0 = -36.75, YBAR = 36.75, ZBAR0 = 0., ZBAR = 50.4 /

&TIME TWFIN = 1800. /
&MISC NFRAMES = 400, U0 = -0.4 /

&VENT CB = YBAR0, SURF_ID = 'SouthWind'    / south face
&VENT CB = YBAR,  SURF_ID = 'OPEN'         / north face
&VENT CB = ZBAR,  SURF_ID = 'OPEN'         / top

&VENT XB = -37.8,  -37.8,  -36.75, 36.75, 0, 50.4, SURF_ID = 'OPEN'                        / west face
&OBST XB = -37.8,  -36.75, -36.75, 36.75, 0, 50.4, SURF_ID = 'WestWind-wf', T_CREATE = 266. / west face
&OBST XB =  36.75,  37.8,  -36.75, 36.75, 0, 50.4, SURF_ID = 'EastWind-ef', T_REMOVE = 266. / east face
&VENT XB =  37.8,   37.8,  -36.75, 36.75, 0, 50.4, SURF_ID = 'OPEN',        T_OPEN = 266.   / east face

&VENT XB = -33.6, -33.6, -36.75, -35.7, 0, 50.4, SURF_ID = 'EastWind-ef', T_DEACTIVATE = 266. /
&VENT XB = -31.5, -31.5, -36.75, -35.7, 0, 50.4, SURF_ID = 'EastWind-ef', T_DEACTIVATE = 266. /
&VENT XB = -29.4, -29.4, -36.75, -35.7, 0, 50.4, SURF_ID = 'EastWind-ef', T_DEACTIVATE = 266. /
&VENT XB = -27.3, -27.3, -36.75, -35.7, 0, 50.4, SURF_ID = 'EastWind-ef', T_DEACTIVATE = 266. /
&VENT XB = -25.2, -25.2, -36.75, -35.7, 0, 50.4, SURF_ID = 'EastWind-ef', T_DEACTIVATE = 266. /
&VENT XB = -23.1, -23.1, -36.75, -35.7, 0, 50.4, SURF_ID = 'EastWind-ef', T_DEACTIVATE = 266. /
&VENT XB = -21.0, -21.0, -36.75, -35.7, 0, 50.4, SURF_ID = 'EastWind-ef', T_DEACTIVATE = 266. /
&VENT XB = -18.9, -18.9, -36.75, -35.7, 0, 50.4, SURF_ID = 'EastWind-ef', T_DEACTIVATE = 266. /
&VENT XB = -16.8, -16.8, -36.75, -35.7, 0, 50.4, SURF_ID = 'EastWind-ef', T_DEACTIVATE = 266. /
&VENT XB = -14.7, -14.7, -36.75, -35.7, 0, 50.4, SURF_ID = 'EastWind-ef', T_DEACTIVATE = 266. /
&VENT XB = -12.6, -12.6, -36.75, -35.7, 0, 50.4, SURF_ID = 'EastWind-ef', T_DEACTIVATE = 266. /
&VENT XB = -10.5, -10.5, -36.75, -35.7, 0, 50.4, SURF_ID = 'EastWind-ef', T_DEACTIVATE = 266. /
&VENT XB =  -8.4,  -8.4, -36.75, -35.7, 0, 50.4, SURF_ID = 'EastWind-ef', T_DEACTIVATE = 266. /
&VENT XB =  -6.3,  -6.3, -36.75, -35.7, 0, 50.4, SURF_ID = 'EastWind-ef', T_DEACTIVATE = 266. /
&VENT XB =  -4.2,  -4.2, -36.75, -35.7, 0, 50.4, SURF_ID = 'EastWind-ef', T_DEACTIVATE = 266. /
&VENT XB =  -2.1,  -2.1, -36.75, -35.7, 0, 50.4, SURF_ID = 'EastWind-ef', T_DEACTIVATE = 266. /
&VENT XB =   0.0,   0.0, -36.75, -35.7, 0, 50.4, SURF_ID = 'EastWind-ef', T_DEACTIVATE = 266. /
&VENT XB =   2.1,   2.1, -36.75, -35.7, 0, 50.4, SURF_ID = 'EastWind-ef', T_DEACTIVATE = 266. /
```

```
&VENT XB =   4.2,   4.2, -36.75, -35.7, 0, 50.4, SURF_ID = 'EastWind-ef', T_DEACTIVATE = 266. /
&VENT XB =   6.3,   6.3, -36.75, -35.7, 0, 50.4, SURF_ID = 'EastWind-ef', T_DEACTIVATE = 266. /
&VENT XB =   8.2,   8.2, -36.75, -35.7, 0, 50.4, SURF_ID = 'EastWind-ef', T_DEACTIVATE = 266. /
&VENT XB =  10.5,  10.5, -36.75, -35.7, 0, 50.4, SURF_ID = 'EastWind-ef', T_DEACTIVATE = 266. /
&VENT XB =  12.6,  12.6, -36.75, -35.7, 0, 50.4, SURF_ID = 'EastWind-ef', T_DEACTIVATE = 266. /
&VENT XB =  14.7,  14.7, -36.75, -35.7, 0, 50.4, SURF_ID = 'EastWind-ef', T_DEACTIVATE = 266. /
&VENT XB =  16.8,  16.8, -36.75, -35.7, 0, 50.4, SURF_ID = 'EastWind-ef', T_DEACTIVATE = 266. /
&VENT XB =  18.9,  18.9, -36.75, -35.7, 0, 50.4, SURF_ID = 'EastWind-ef', T_DEACTIVATE = 266. /
&VENT XB =  21.0,  21.0, -36.75, -35.7, 0, 50.4, SURF_ID = 'EastWind-ef', T_DEACTIVATE = 266. /
&VENT XB =  23.1,  23.1, -36.75, -35.7, 0, 50.4, SURF_ID = 'EastWind-ef', T_DEACTIVATE = 266. /
&VENT XB =  25.2,  25.2, -36.75, -35.7, 0, 50.4, SURF_ID = 'EastWind-ef', T_DEACTIVATE = 266. /
&VENT XB =  27.3,  27.3, -36.75, -35.7, 0, 50.4, SURF_ID = 'EastWind-ef', T_DEACTIVATE = 266. /
&VENT XB =  29.4,  29.4, -36.75, -35.7, 0, 50.4, SURF_ID = 'EastWind-ef', T_DEACTIVATE = 266. /
&VENT XB =  31.5,  31.5, -36.75, -35.7, 0, 50.4, SURF_ID = 'EastWind-ef', T_DEACTIVATE = 266. /
&VENT XB =  33.6,  33.6, -36.75, -35.7, 0, 50.4, SURF_ID = 'EastWind-ef', T_DEACTIVATE = 266. /

&VENT XB = -33.6, -33.6, -36.75, -35.7, 0, 50.4, SURF_ID = 'WestWind-ef', T_ACTIVATE = 266. /
&VENT XB = -31.5, -31.5, -36.75, -35.7, 0, 50.4, SURF_ID = 'WestWind-ef', T_ACTIVATE = 266. /
&VENT XB = -29.4, -29.4, -36.75, -35.7, 0, 50.4, SURF_ID = 'WestWind-ef', T_ACTIVATE = 266. /
&VENT XB = -27.3, -27.3, -36.75, -35.7, 0, 50.4, SURF_ID = 'WestWind-ef', T_ACTIVATE = 266. /
&VENT XB = -25.2, -25.2, -36.75, -35.7, 0, 50.4, SURF_ID = 'WestWind-ef', T_ACTIVATE = 266. /
&VENT XB = -23.1, -23.1, -36.75, -35.7, 0, 50.4, SURF_ID = 'WestWind-ef', T_ACTIVATE = 266. /
&VENT XB = -21.0, -21.0, -36.75, -35.7, 0, 50.4, SURF_ID = 'WestWind-ef', T_ACTIVATE = 266. /
&VENT XB = -18.9, -18.9, -36.75, -35.7, 0, 50.4, SURF_ID = 'WestWind-ef', T_ACTIVATE = 266. /
&VENT XB = -16.8, -16.8, -36.75, -35.7, 0, 50.4, SURF_ID = 'WestWind-ef', T_ACTIVATE = 266. /
&VENT XB = -14.7, -14.7, -36.75, -35.7, 0, 50.4, SURF_ID = 'WestWind-ef', T_ACTIVATE = 266. /
&VENT XB = -12.6, -12.6, -36.75, -35.7, 0, 50.4, SURF_ID = 'WestWind-ef', T_ACTIVATE = 266. /
&VENT XB = -10.5, -10.5, -36.75, -35.7, 0, 50.4, SURF_ID = 'WestWind-ef', T_ACTIVATE = 266. /
&VENT XB =  -8.4,  -8.4, -36.75, -35.7, 0, 50.4, SURF_ID = 'WestWind-ef', T_ACTIVATE = 266. /
&VENT XB =  -6.3,  -6.3, -36.75, -35.7, 0, 50.4, SURF_ID = 'WestWind-ef', T_ACTIVATE = 266. /
&VENT XB =  -4.2,  -4.2, -36.75, -35.7, 0, 50.4, SURF_ID = 'WestWind-ef', T_ACTIVATE = 266. /
&VENT XB =  -2.1,  -2.1, -36.75, -35.7, 0, 50.4, SURF_ID = 'WestWind-ef', T_ACTIVATE = 266. /
&VENT XB =   0.0,   0.0, -36.75, -35.7, 0, 50.4, SURF_ID = 'WestWind-ef', T_ACTIVATE = 266. /
&VENT XB =   2.1,   2.1, -36.75, -35.7, 0, 50.4, SURF_ID = 'WestWind-ef', T_ACTIVATE = 266. /
&VENT XB =   4.2,   4.2, -36.75, -35.7, 0, 50.4, SURF_ID = 'WestWind-ef', T_ACTIVATE = 266. /
&VENT XB =   6.3,   6.3, -36.75, -35.7, 0, 50.4, SURF_ID = 'WestWind-ef', T_ACTIVATE = 266. /
&VENT XB =   8.2,   8.2, -36.75, -35.7, 0, 50.4, SURF_ID = 'WestWind-ef', T_ACTIVATE = 266. /
&VENT XB =  10.5,  10.5, -36.75, -35.7, 0, 50.4, SURF_ID = 'WestWind-ef', T_ACTIVATE = 266. /
&VENT XB =  12.6,  12.6, -36.75, -35.7, 0, 50.4, SURF_ID = 'WestWind-ef', T_ACTIVATE = 266. /
&VENT XB =  14.7,  14.7, -36.75, -35.7, 0, 50.4, SURF_ID = 'WestWind-ef', T_ACTIVATE = 266. /
```

```
&VENT XB =  16.8,  16.8, -36.75, -35.7, 0, 50.4, SURF_ID = 'WestWind-ef', T_ACTIVATE = 266. /
&VENT XB =  18.9,  18.9, -36.75, -35.7, 0, 50.4, SURF_ID = 'WestWind-ef', T_ACTIVATE = 266. /
&VENT XB =  21.0,  21.0, -36.75, -35.7, 0, 50.4, SURF_ID = 'WestWind-ef', T_ACTIVATE = 266. /
&VENT XB =  23.1,  23.1, -36.75, -35.7, 0, 50.4, SURF_ID = 'WestWind-ef', T_ACTIVATE = 266. /
&VENT XB =  25.2,  25.2, -36.75, -35.7, 0, 50.4, SURF_ID = 'WestWind-ef', T_ACTIVATE = 266. /
&VENT XB =  27.3,  27.3, -36.75, -35.7, 0, 50.4, SURF_ID = 'WestWind-ef', T_ACTIVATE = 266. /
&VENT XB =  29.4,  29.4, -36.75, -35.7, 0, 50.4, SURF_ID = 'WestWind-ef', T_ACTIVATE = 266. /
&VENT XB =  31.5,  31.5, -36.75, -35.7, 0, 50.4, SURF_ID = 'WestWind-ef', T_ACTIVATE = 266. /
&VENT XB =  33.6,  33.6, -36.75, -35.7, 0, 50.4, SURF_ID = 'WestWind-ef', T_ACTIVATE = 266. /

&VENT XB = -36.75, -35.7, -33.6, -33.6, 0, 50.4, SURF_ID = 'SouthWind-nf' /
&VENT XB = -36.75, -35.7, -31.5, -31.5, 0, 50.4, SURF_ID = 'SouthWind-nf' /
&VENT XB = -36.75, -35.7, -29.4, -29.4, 0, 50.4, SURF_ID = 'SouthWind-nf' /
&VENT XB = -36.75, -35.7, -27.3, -27.3, 0, 50.4, SURF_ID = 'SouthWind-nf' /
&VENT XB = -36.75, -35.7, -25.2, -25.2, 0, 50.4, SURF_ID = 'SouthWind-nf' /
&VENT XB = -36.75, -35.7, -23.1, -23.1, 0, 50.4, SURF_ID = 'SouthWind-nf' /
&VENT XB = -36.75, -35.7, -21.0, -21.0, 0, 50.4, SURF_ID = 'SouthWind-nf' /
&VENT XB = -36.75, -35.7, -18.9, -18.9, 0, 50.4, SURF_ID = 'SouthWind-nf' /
&VENT XB = -36.75, -35.7, -16.8, -16.8, 0, 50.4, SURF_ID = 'SouthWind-nf' /
&VENT XB = -36.75, -35.7, -14.7, -14.7, 0, 50.4, SURF_ID = 'SouthWind-nf' /
&VENT XB = -36.75, -35.7, -12.6, -12.6, 0, 50.4, SURF_ID = 'SouthWind-nf' /
&VENT XB = -36.75, -35.7, -10.5, -10.5, 0, 50.4, SURF_ID = 'SouthWind-nf' /
&VENT XB = -36.75, -35.7,  -8.4,  -8.4, 0, 50.4, SURF_ID = 'SouthWind-nf' /
&VENT XB = -36.75, -35.7,  -6.3,  -6.3, 0, 50.4, SURF_ID = 'SouthWind-nf' /
&VENT XB = -36.75, -35.7,  -4.2,  -4.2, 0, 50.4, SURF_ID = 'SouthWind-nf' /
&VENT XB = -36.75, -35.7,  -2.1,  -2.1, 0, 50.4, SURF_ID = 'SouthWind-nf' /
&VENT XB = -36.75, -35.7,   0.0,   0.0, 0, 50.4, SURF_ID = 'SouthWind-nf' /
&VENT XB = -36.75, -35.7,   2.1,   2.1, 0, 50.4, SURF_ID = 'SouthWind-nf' /
&VENT XB = -36.75, -35.7,   4.2,   4.2, 0, 50.4, SURF_ID = 'SouthWind-nf' /
&VENT XB = -36.75, -35.7,   6.3,   6.3, 0, 50.4, SURF_ID = 'SouthWind-nf' /
&VENT XB = -36.75, -35.7,   8.4,   8.4, 0, 50.4, SURF_ID = 'SouthWind-nf' /
&VENT XB = -36.75, -35.7,  10.5,  10.5, 0, 50.4, SURF_ID = 'SouthWind-nf' /
&VENT XB = -36.75, -35.7,  12.6,  12.6, 0, 50.4, SURF_ID = 'SouthWind-nf' /
&VENT XB = -36.75, -35.7,  14.7,  14.7, 0, 50.4, SURF_ID = 'SouthWind-nf' /
&VENT XB = -36.75, -35.7,  16.8,  16.8, 0, 50.4, SURF_ID = 'SouthWind-nf' /
&VENT XB = -36.75, -35.7,  18.9,  18.9, 0, 50.4, SURF_ID = 'SouthWind-nf' /
&VENT XB = -36.75, -35.7,  21.0,  21.0, 0, 50.4, SURF_ID = 'SouthWind-nf' /
&VENT XB = -36.75, -35.7,  23.1,  23.1, 0, 50.4, SURF_ID = 'SouthWind-nf' /
&VENT XB = -36.75, -35.7,  25.2,  25.2, 0, 50.4, SURF_ID = 'SouthWind-nf' /
&VENT XB = -36.75, -35.7,  27.3,  27.3, 0, 50.4, SURF_ID = 'SouthWind-nf' /
```

```
&VENT XB = -36.75, -35.7,  29.4,  29.4, 0, 50.4, SURF_ID = 'SouthWind-nf' /
&VENT XB = -36.75, -35.7,  31.5,  31.5, 0, 50.4, SURF_ID = 'SouthWind-nf' /
&VENT XB = -36.75, -35.7,  33.6,  33.6, 0, 50.4, SURF_ID = 'SouthWind-nf' /

&VENT XB = 35.7, 36.75, -33.6, -33.6, 0, 50.4, SURF_ID = 'SouthWind-nf' /
&VENT XB = 35.7, 36.75, -31.5, -31.5, 0, 50.4, SURF_ID = 'SouthWind-nf' /
&VENT XB = 35.7, 36.75, -29.4, -29.4, 0, 50.4, SURF_ID = 'SouthWind-nf' /
&VENT XB = 35.7, 36.75, -27.3, -27.3, 0, 50.4, SURF_ID = 'SouthWind-nf' /
&VENT XB = 35.7, 36.75, -25.2, -25.2, 0, 50.4, SURF_ID = 'SouthWind-nf' /
&VENT XB = 35.7, 36.75, -23.1, -23.1, 0, 50.4, SURF_ID = 'SouthWind-nf' /
&VENT XB = 35.7, 36.75, -21.0, -21.0, 0, 50.4, SURF_ID = 'SouthWind-nf' /
&VENT XB = 35.7, 36.75, -18.9, -18.9, 0, 50.4, SURF_ID = 'SouthWind-nf' /
&VENT XB = 35.7, 36.75, -16.8, -16.8, 0, 50.4, SURF_ID = 'SouthWind-nf' /
&VENT XB = 35.7, 36.75, -14.7, -14.7, 0, 50.4, SURF_ID = 'SouthWind-nf' /
&VENT XB = 35.7, 36.75, -12.6, -12.6, 0, 50.4, SURF_ID = 'SouthWind-nf' /
&VENT XB = 35.7, 36.75, -10.5, -10.5, 0, 50.4, SURF_ID = 'SouthWind-nf' /
&VENT XB = 35.7, 36.75,  -8.4,  -8.4, 0, 50.4, SURF_ID = 'SouthWind-nf' /
&VENT XB = 35.7, 36.75,  -6.3,  -6.3, 0, 50.4, SURF_ID = 'SouthWind-nf' /
&VENT XB = 35.7, 36.75,  -4.2,  -4.2, 0, 50.4, SURF_ID = 'SouthWind-nf' /
&VENT XB = 35.7, 36.75,  -2.1,  -2.1, 0, 50.4, SURF_ID = 'SouthWind-nf' /
&VENT XB = 35.7, 36.75,   0.0,   0.0, 0, 50.4, SURF_ID = 'SouthWind-nf' /
&VENT XB = 35.7, 36.75,   2.1,   2.1, 0, 50.4, SURF_ID = 'SouthWind-nf' /
&VENT XB = 35.7, 36.75,   4.2,   4.2, 0, 50.4, SURF_ID = 'SouthWind-nf' /
&VENT XB = 35.7, 36.75,   6.3,   6.3, 0, 50.4, SURF_ID = 'SouthWind-nf' /
&VENT XB = 35.7, 36.75,   8.4,   8.4, 0, 50.4, SURF_ID = 'SouthWind-nf' /
&VENT XB = 35.7, 36.75,  10.5,  10.5, 0, 50.4, SURF_ID = 'SouthWind-nf' /
&VENT XB = 35.7, 36.75,  12.6,  12.6, 0, 50.4, SURF_ID = 'SouthWind-nf' /
&VENT XB = 35.7, 36.75,  14.7,  14.7, 0, 50.4, SURF_ID = 'SouthWind-nf' /
&VENT XB = 35.7, 36.75,  16.8,  16.8, 0, 50.4, SURF_ID = 'SouthWind-nf' /
&VENT XB = 35.7, 36.75,  18.9,  18.9, 0, 50.4, SURF_ID = 'SouthWind-nf' /
&VENT XB = 35.7, 36.75,  21.0,  21.0, 0, 50.4, SURF_ID = 'SouthWind-nf' /
&VENT XB = 35.7, 36.75,  23.1,  23.1, 0, 50.4, SURF_ID = 'SouthWind-nf' /
&VENT XB = 35.7, 36.75,  25.2,  25.2, 0, 50.4, SURF_ID = 'SouthWind-nf' /
&VENT XB = 35.7, 36.75,  27.3,  27.3, 0, 50.4, SURF_ID = 'SouthWind-nf' /
&VENT XB = 35.7, 36.75,  29.4,  29.4, 0, 50.4, SURF_ID = 'SouthWind-nf' /
&VENT XB = 35.7, 36.75,  31.5,  31.5, 0, 50.4, SURF_ID = 'SouthWind-nf' /
&VENT XB = 35.7, 36.75,  33.6,  33.6, 0, 50.4, SURF_ID = 'SouthWind-nf' /

&SURF ID = 'EastWind-wf', VEL =  0.52 , RAMP_V = 'EastRamp' /
&SURF ID = 'EastWind-ef', VEL = -0.52 , RAMP_V = 'EastRamp' /
```

```
&RAMP ID = 'EastRamp', T =    0., F = 0.77 /
&RAMP ID = 'EastRamp', T =  120., F = 0.94 /
&RAMP ID = 'EastRamp', T =  160., F = 1.00 /
&RAMP ID = 'EastRamp', T =  220., F = 0.43 /
&RAMP ID = 'EastRamp', T =  266., F = 0.00 /
&RAMP ID = 'EastRamp', T = 1800., F = 0.00 /

&SURF ID = 'WestWind-wf', VEL = -2.48, RAMP_V = 'WestRamp' /
&SURF ID = 'WestWind-ef', VEL =  2.48, RAMP_V = 'WestRamp' /
&RAMP ID = 'WestRamp', T =    0., F = 0.00 /
&RAMP ID = 'WestRamp', T =  266., F = 0.00 /
&RAMP ID = 'WestRamp', T =  300., F = 0.07 /
&RAMP ID = 'WestRamp', T =  350., F = 0.17 /
&RAMP ID = 'WestRamp', T =  360., F = 0.19 /
&RAMP ID = 'WestRamp', T =  500., F = 0.23 /
&RAMP ID = 'WestRamp', T =  640., F = 0.40 /
&RAMP ID = 'WestRamp', T =  860., F = 0.35 /
&RAMP ID = 'WestRamp', T = 1060., F = 0.56 /
&RAMP ID = 'WestRamp', T = 1200., F = 0.43 /
&RAMP ID = 'WestRamp', T = 1300., F = 0.63 /
&RAMP ID = 'WestRamp', T = 1550., F = 0.88 /
&RAMP ID = 'WestRamp', T = 1700., F = 1.00 /
&RAMP ID = 'WestRamp', T = 1800., F = 0.85 /

&SURF ID = 'SouthWind',    VEL = -1.44, RAMP_V = 'SouthRamp' /
&SURF ID = 'SouthWind-nf', VEL =  1.44, RAMP_V = 'SouthRamp' /
&RAMP ID = 'SouthRamp', T =    0., F = 0.00 /
&RAMP ID = 'SouthRamp', T =  120., F = 0.13 /
&RAMP ID = 'SouthRamp', T =  160., F = 0.24 /
&RAMP ID = 'SouthRamp', T =  220., F = 0.42 /
&RAMP ID = 'SouthRamp', T =  266., F = 0.47 /
&RAMP ID = 'SouthRamp', T =  300., F = 0.51 /
&RAMP ID = 'SouthRamp', T =  350., F = 0.44 /
&RAMP ID = 'SouthRamp', T =  360., F = 0.45 /
&RAMP ID = 'SouthRamp', T =  500., F = 0.53 /
&RAMP ID = 'SouthRamp', T =  640., F = 0.87 /
&RAMP ID = 'SouthRamp', T =  860., F = 0.67 /
&RAMP ID = 'SouthRamp', T = 1060., F = 1.00 /
&RAMP ID = 'SouthRamp', T = 1200., F = 0.64 /
&RAMP ID = 'SouthRamp', T = 1300., F = 0.75 /
```

```
&RAMP ID = 'SouthRamp', T = 1550., F = 0.48 /
&RAMP ID = 'SouthRamp', T = 1700., F = 0.19 /
&RAMP ID = 'SouthRamp', T = 1800., F = 0.00 /

&THCP XYZ =   0,   0, 10, QUANTITY = 'U-VELOCITY', LABEL = 'U ctl'   /
&THCP XYZ =   0,   0, 10, QUANTITY = 'V-VELOCITY', LABEL = 'V ctl'   /
&THCP XYZ =   0,   0, 10, QUANTITY = 'W-VELOCITY', LABEL = 'W ctl'   /
&THCP XYZ =   0,   0, 10, QUANTITY = 'VELOCITY',   LABEL = 'Vel ctl' /

&THCP XYZ =  20,   0, 10, QUANTITY = 'U-VELOCITY', LABEL = 'U X+'    /
&THCP XYZ =  20,   0, 10, QUANTITY = 'V-VELOCITY', LABEL = 'V X+'    /
&THCP XYZ =  20,   0, 10, QUANTITY = 'W-VELOCITY', LABEL = 'W X+'    /
&THCP XYZ =  20,   0, 10, QUANTITY = 'VELOCITY',   LABEL = 'Vel X+'  /

&THCP XYZ = -20,   0, 10, QUANTITY = 'U-VELOCITY', LABEL = 'U X-'    /
&THCP XYZ = -20,   0, 10, QUANTITY = 'V-VELOCITY', LABEL = 'V X-'    /
&THCP XYZ = -20,   0, 10, QUANTITY = 'W-VELOCITY', LABEL = 'W X-'    /
&THCP XYZ = -20,   0, 10, QUANTITY = 'VELOCITY',   LABEL = 'Vel X-'  /

&THCP XYZ =   0,  20, 10, QUANTITY = 'U-VELOCITY', LABEL = 'U Y+'    /
&THCP XYZ =   0,  20, 10, QUANTITY = 'V-VELOCITY', LABEL = 'V Y+'    /
&THCP XYZ =   0,  20, 10, QUANTITY = 'W-VELOCITY', LABEL = 'W Y+'    /
&THCP XYZ =   0,  20, 10, QUANTITY = 'VELOCITY',   LABEL = 'Vel Y+'  /

&THCP XYZ =   0, -20, 10, QUANTITY = 'U-VELOCITY', LABEL = 'U Y-'    /
&THCP XYZ =   0, -20, 10, QUANTITY = 'V-VELOCITY', LABEL = 'W Y-'    /
&THCP XYZ =   0, -20, 10, QUANTITY = 'W-VELOCITY', LABEL = 'W Y-'    /
&THCP XYZ =   0, -20, 10, QUANTITY = 'VELOCITY',   LABEL = 'Vel Y-'  /

&SLCF PBX = 0.0, QUANTITY = 'U-VELOCITY', VECTOR = .TRUE. /
&SLCF PBX = 0.0, QUANTITY = 'V-VELOCITY'  /
&SLCF PBX = 0.0, QUANTITY = 'W-VELOCITY'  /
&SLCF PBX = 0.0, QUANTITY = 'VELOCITY'    /
&SLCF PBX = 0.0, QUANTITY = 'DIVERGENCE'  /

&SLCF PBY = 0.0, QUANTITY = 'U-VELOCITY'  /
&SLCF PBY = 0.0, QUANTITY = 'V-VELOCITY'  /
&SLCF PBY = 0.0, QUANTITY = 'W-VELOCITY'  /
&SLCF PBY = 0.0, QUANTITY = 'VELOCITY'    /
&SLCF PBY = 0.0, QUANTITY = 'DIVERGENCE'  /
```

```
&SLCF PBY = 36.7, QUANTITY = 'U-VELOCITY' /
&SLCF PBY = 36.7, QUANTITY = 'V-VELOCITY' /
&SLCF PBY = 36.7, QUANTITY = 'W-VELOCITY' /
&SLCF PBY = 36.7, QUANTITY = 'VELOCITY'   /
&SLCF PBY = 36.7, QUANTITY = 'DIVERGENCE' /

&SLCF PBZ = 10.0, QUANTITY = 'U-VELOCITY' /
&SLCF PBZ = 10.0, QUANTITY = 'V-VELOCITY' /
&SLCF PBZ = 10.0, QUANTITY = 'W-VELOCITY' /
&SLCF PBZ = 10.0, QUANTITY = 'VELOCITY'   /
&SLCF PBZ = 10.0, QUANTITY = 'DIVERGENCE' /

&SLCF PBZ = 50.4, QUANTITY = 'U-VELOCITY' /
&SLCF PBZ = 50.4, QUANTITY = 'V-VELOCITY' /
&SLCF PBZ = 50.4, QUANTITY = 'W-VELOCITY' /
&SLCF PBZ = 50.4, QUANTITY = 'VELOCITY'   /
&SLCF PBZ = 50.4, QUANTITY = 'DIVERGENCE' /
```

B.5 Sandia Fire Test C (C-175d.data)


```
&HEAD CHID = 'C-175d', TITLE = '9.1 x 18.2 Pool Fire w/ 0.175-m H x 0.175-m V grid' /

------
 GRID
------

&GRID IBAR = 108, JBAR = 54, KBAR = 100 /
&PDIM XBAR0 = -9.45,  XBAR =  9.45,
      YBAR0 = -4.725, YBAR =  4.725,
      ZBAR0 = -0.525, ZBAR = 16.975     /

&GRID IBAR = 60, JBAR = 40, KBAR = 120  /
&PDIM XBAR0 = -10.15, XBAR = 10.85,
      YBAR0 =  -7.0,  YBAR =  7.0,
      ZBAR0 =  -1.05, ZBAR = 40.95      /

&GRID IBAR = 90, JBAR = 80, KBAR = 40   /
&PDIM XBAR0 = -47.25, XBAR = 47.25,
      YBAR0 = -46.20, YBAR = 37.8,
```

```
      ZBAR0 =  -1.05, ZBAR = 40.95      /

&TIME TWFIN = 1800. /
&MISC REACTION = 'JP-4', NFRAMES = 400, DTCORE = 60, U0 = -0.4 /

---------------------------
 THERMOPHYSICAL PROPERTIES
---------------------------

&REAC ID                  = 'JP-4',
      MW_FUEL             = 112.42,
      NU_O2               = 16.06,
      NU_CO2              = 8.03,
      NU_H2O              = 8.03,
      CO_YIELD            = 0.012,
      SOOT_YIELD          = 0.019,
      EPUMO2              = 9362.5,
      RADIATIVE_FRACTION  = 0.      /

&SURF ID                  = 'JP-4',
      RGB                 = 0.0, 0.0, 0.5,
      TMPIGN              = 246.,
      HEAT_OF_VAPORIZATION = 364.,
      HEAT_OF_COMBUSTION  = 42800.
      DELTA               = 0.10,
      KS                  = 0.14,
      ALPHA               = 8.6E-8,
      PHASE               = 'LIQUID' / deleted BURNING_RATE_MAX

&SURF ID                  = '1.25A517',
      RGB                 = 0.5, 0.5, 0.5,
      ALPHA               = 1.31E-5,
      KS                  = 46.6,
      DELTA               = 0.03175,
      BACKING             = 'INSULATED',
      EMISSIVITY          = 0.8 /

&SURF ID                  = '0.5A517',
      RGB                 = 0.5, 0.5, 0.5,
      ALPHA               = 1.31E-5,
```

```
      KS                  = 46.6,
      DELTA               = 0.0127,
      BACKING             = 'INSULATED',
      EMISSIVITY          = 0.8 /

&SURF ID                  = 'SOURCE',
      TMPWAL              = 1000. /

--------
 GROUND
--------

&OBST XB = -47.25, -9.1, -46.2, 37.8,  -1.05, 0. /
&OBST XB =  -9.1,   9.1, -46.2, -4.55, -1.05, 0. /
&OBST XB =  -9.1,   9.1,  4.55, 37.8,  -1.05, 0. /
&OBST XB =   9.1, 47.25, -46.2, 37.8,  -1.05, 0. /

------
 POOL
------

&OBST XB = -9.1, 9.1, -4.55, 4.55, -1.05, -0.35,
      SURF_IDS = 'JP-4', 'INERT', 'INERT'        /

---------
 IGNITOR
---------

&OBST XB = -8.75, 8.75, 3.85, 4.2, 0, 0.35,
      SURF_IDS = 'INERT', 'INERT', 'SOURCE',
      RGB = 0.0, 0.0, 0.0, T_REMOVE = 10.       /

&OBST XB = -8.75, 8.75, -4.2, -3.85, 0, 0.35,
      SURF_IDS = 'INERT', 'INERT', 'SOURCE',
      RGB = 0.0, 0.0, 0.0, T_REMOVE = 10.       /

-------------------
 LARGE CALORIMETER
-------------------
```

```
&OBST XB = -3.15, 3.15, -0.7, 0.7, 0.7, 2.1,
      SURF_ID6 = '0.5A517', '0.5A517',
                 '1.25A517', '1.25A517',
                 '1.25A517', '1.25A517'          /

---------------------------------
 BOUNDARY CONDITIONS (WIND FIELD)
---------------------------------

&VENT XB = -47.25,  47.25, -46.2, -46.2,  0,    40.95,
      SURF_ID = 'SouthWind'                              / south face

&VENT XB = -47.25,  47.25,  37.8,  37.8,  0,    40.95,
      SURF_ID = 'OPEN'                                   / north face

&VENT XB = -47.25,  47.25, -46.2,  37.8, 40.95, 40.95,
      SURF_ID = 'OPEN'                                   / top

&VENT XB = -47.25, -47.25, -46.2,  37.8,  0,    40.95,
      SURF_ID = 'OPEN'                                   / west face (east wind)
&OBST XB = -47.25, -46.2,  -46.2,  37.8,  0,    40.95,
      SURF_ID = 'WestWind-wf', T_CREATE = 266.,
      BLOCK_COLOR = 'INVISIBLE'                          / west face (west wind)

&OBST XB =  46.2,   47.25, -46.2,  37.8,  0,    40.95,
      SURF_ID = 'EastWind-ef', T_REMOVE = 266.
      BLOCK_COLOR = 'INVISIBLE'                          / east face (east wind)
&VENT XB =  47.25,  47.25, -46.2,  37.8,  0,    40.95,
      SURF_ID = 'OPEN', T_OPEN = 266.                    / east face (west wind)

---------------------------------
 SOUTH FACE - EAST WIND COMPONENT
---------------------------------

&VENT XB = -44.1, -44.1, -46.2, -45.15, 0, 40.95, SURF_ID = 'EastWind-ef', T_DEACTIVATE = 266. /
&VENT XB = -42.0, -42.0, -46.2, -45.15, 0, 40.95, SURF_ID = 'EastWind-ef', T_DEACTIVATE = 266. /
&VENT XB = -39.9, -39.9, -46.2, -45.15, 0, 40.95, SURF_ID = 'EastWind-ef', T_DEACTIVATE = 266. /
&VENT XB = -37.8, -37.8, -46.2, -45.15, 0, 40.95, SURF_ID = 'EastWind-ef', T_DEACTIVATE = 266. /
&VENT XB = -35.7, -35.7, -46.2, -45.15, 0, 40.95, SURF_ID = 'EastWind-ef', T_DEACTIVATE = 266. /
&VENT XB = -33.6, -33.6, -46.2, -45.15, 0, 40.95, SURF_ID = 'EastWind-ef', T_DEACTIVATE = 266. /
```

```
&VENT XB = -31.5, -31.5, -46.2, -45.15, 0, 40.95, SURF_ID = 'EastWind-ef', T_DEACTIVATE = 266. /
&VENT XB = -29.4, -29.4, -46.2, -45.15, 0, 40.95, SURF_ID = 'EastWind-ef', T_DEACTIVATE = 266. /
&VENT XB = -27.3, -27.3, -46.2, -45.15, 0, 40.95, SURF_ID = 'EastWind-ef', T_DEACTIVATE = 266. /
&VENT XB = -25.2, -25.2, -46.2, -45.15, 0, 40.95, SURF_ID = 'EastWind-ef', T_DEACTIVATE = 266. /
&VENT XB = -23.1, -23.1, -46.2, -45.15, 0, 40.95, SURF_ID = 'EastWind-ef', T_DEACTIVATE = 266. /
&VENT XB = -21.0, -21.0, -46.2, -45.15, 0, 40.95, SURF_ID = 'EastWind-ef', T_DEACTIVATE = 266. /
&VENT XB = -18.9, -18.9, -46.2, -45.15, 0, 40.95, SURF_ID = 'EastWind-ef', T_DEACTIVATE = 266. /
&VENT XB = -16.8, -16.8, -46.2, -45.15, 0, 40.95, SURF_ID = 'EastWind-ef', T_DEACTIVATE = 266. /
&VENT XB = -14.7, -14.7, -46.2, -45.15, 0, 40.95, SURF_ID = 'EastWind-ef', T_DEACTIVATE = 266. /
&VENT XB = -12.6, -12.6, -46.2, -45.15, 0, 40.95, SURF_ID = 'EastWind-ef', T_DEACTIVATE = 266. /
&VENT XB = -10.5, -10.5, -46.2, -45.15, 0, 40.95, SURF_ID = 'EastWind-ef', T_DEACTIVATE = 266. /
&VENT XB =  -8.4,  -8.4, -46.2, -45.15, 0, 40.95, SURF_ID = 'EastWind-ef', T_DEACTIVATE = 266. /
&VENT XB =  -6.3,  -6.3, -46.2, -45.15, 0, 40.95, SURF_ID = 'EastWind-ef', T_DEACTIVATE = 266. /
&VENT XB =  -4.2,  -4.2, -46.2, -45.15, 0, 40.95, SURF_ID = 'EastWind-ef', T_DEACTIVATE = 266. /
&VENT XB =  -2.1,  -2.1, -46.2, -45.15, 0, 40.95, SURF_ID = 'EastWind-ef', T_DEACTIVATE = 266. /
&VENT XB =   0.0,   0.0, -46.2, -45.15, 0, 40.95, SURF_ID = 'EastWind-ef', T_DEACTIVATE = 266. /
&VENT XB =   2.1,   2.1, -46.2, -45.15, 0, 40.95, SURF_ID = 'EastWind-ef', T_DEACTIVATE = 266. /
&VENT XB =   4.2,   4.2, -46.2, -45.15, 0, 40.95, SURF_ID = 'EastWind-ef', T_DEACTIVATE = 266. /
&VENT XB =   6.3,   6.3, -46.2, -45.15, 0, 40.95, SURF_ID = 'EastWind-ef', T_DEACTIVATE = 266. /
&VENT XB =   8.2,   8.2, -46.2, -45.15, 0, 40.95, SURF_ID = 'EastWind-ef', T_DEACTIVATE = 266. /
&VENT XB =  10.5,  10.5, -46.2, -45.15, 0, 40.95, SURF_ID = 'EastWind-ef', T_DEACTIVATE = 266. /
&VENT XB =  12.6,  12.6, -46.2, -45.15, 0, 40.95, SURF_ID = 'EastWind-ef', T_DEACTIVATE = 266. /
&VENT XB =  14.7,  14.7, -46.2, -45.15, 0, 40.95, SURF_ID = 'EastWind-ef', T_DEACTIVATE = 266. /
&VENT XB =  16.8,  16.8, -46.2, -45.15, 0, 40.95, SURF_ID = 'EastWind-ef', T_DEACTIVATE = 266. /
&VENT XB =  18.9,  18.9, -46.2, -45.15, 0, 40.95, SURF_ID = 'EastWind-ef', T_DEACTIVATE = 266. /
&VENT XB =  21.0,  21.0, -46.2, -45.15, 0, 40.95, SURF_ID = 'EastWind-ef', T_DEACTIVATE = 266. /
&VENT XB =  23.1,  23.1, -46.2, -45.15, 0, 40.95, SURF_ID = 'EastWind-ef', T_DEACTIVATE = 266. /
&VENT XB =  25.2,  25.2, -46.2, -45.15, 0, 40.95, SURF_ID = 'EastWind-ef', T_DEACTIVATE = 266. /
&VENT XB =  27.3,  27.3, -46.2, -45.15, 0, 40.95, SURF_ID = 'EastWind-ef', T_DEACTIVATE = 266. /
&VENT XB =  29.4,  29.4, -46.2, -45.15, 0, 40.95, SURF_ID = 'EastWind-ef', T_DEACTIVATE = 266. /
&VENT XB =  31.5,  31.5, -46.2, -45.15, 0, 40.95, SURF_ID = 'EastWind-ef', T_DEACTIVATE = 266. /
&VENT XB =  33.6,  33.6, -46.2, -45.15, 0, 40.95, SURF_ID = 'EastWind-ef', T_DEACTIVATE = 266. /
&VENT XB =  35.7,  35.7, -46.2, -45.15, 0, 40.95, SURF_ID = 'EastWind-ef', T_DEACTIVATE = 266. /
&VENT XB =  37.8,  37.8, -46.2, -45.15, 0, 40.95, SURF_ID = 'EastWind-ef', T_DEACTIVATE = 266. /
&VENT XB =  39.9,  39.9, -46.2, -45.15, 0, 40.95, SURF_ID = 'EastWind-ef', T_DEACTIVATE = 266. /
&VENT XB =  42.0,  42.0, -46.2, -45.15, 0, 40.95, SURF_ID = 'EastWind-ef', T_DEACTIVATE = 266. /
&VENT XB =  44.1,  44.1, -46.2, -45.15, 0, 40.95, SURF_ID = 'EastWind-ef', T_DEACTIVATE = 266. /

---------------------------------
 SOUTH FACE - WEST WIND COMPONENT
```

```
---------------------------------

&VENT XB = -44.1, -44.1, -46.2, -45.15, 0, 40.95, SURF_ID = 'WestWind-ef', T_ACTIVATE = 266. /
&VENT XB = -42.0, -42.0, -46.2, -45.15, 0, 40.95, SURF_ID = 'WestWind-ef', T_ACTIVATE = 266. /
&VENT XB = -39.9, -39.9, -46.2, -45.15, 0, 40.95, SURF_ID = 'WestWind-ef', T_ACTIVATE = 266. /
&VENT XB = -37.8, -37.8, -46.2, -45.15, 0, 40.95, SURF_ID = 'WestWind-ef', T_ACTIVATE = 266. /
&VENT XB = -35.7, -35.7, -46.2, -45.15, 0, 40.95, SURF_ID = 'WestWind-ef', T_ACTIVATE = 266. /
&VENT XB = -33.6, -33.6, -46.2, -45.15, 0, 40.95, SURF_ID = 'WestWind-ef', T_ACTIVATE = 266. /
&VENT XB = -31.5, -31.5, -46.2, -45.15, 0, 40.95, SURF_ID = 'WestWind-ef', T_ACTIVATE = 266. /
&VENT XB = -29.4, -29.4, -46.2, -45.15, 0, 40.95, SURF_ID = 'WestWind-ef', T_ACTIVATE = 266. /
&VENT XB = -27.3, -27.3, -46.2, -45.15, 0, 40.95, SURF_ID = 'WestWind-ef', T_ACTIVATE = 266. /
&VENT XB = -25.2, -25.2, -46.2, -45.15, 0, 40.95, SURF_ID = 'WestWind-ef', T_ACTIVATE = 266. /
&VENT XB = -23.1, -23.1, -46.2, -45.15, 0, 40.95, SURF_ID = 'WestWind-ef', T_ACTIVATE = 266. /
&VENT XB = -21.0, -21.0, -46.2, -45.15, 0, 40.95, SURF_ID = 'WestWind-ef', T_ACTIVATE = 266. /
&VENT XB = -18.9, -18.9, -46.2, -45.15, 0, 40.95, SURF_ID = 'WestWind-ef', T_ACTIVATE = 266. /
&VENT XB = -16.8, -16.8, -46.2, -45.15, 0, 40.95, SURF_ID = 'WestWind-ef', T_ACTIVATE = 266. /
&VENT XB = -14.7, -14.7, -46.2, -45.15, 0, 40.95, SURF_ID = 'WestWind-ef', T_ACTIVATE = 266. /
&VENT XB = -12.6, -12.6, -46.2, -45.15, 0, 40.95, SURF_ID = 'WestWind-ef', T_ACTIVATE = 266. /
&VENT XB = -10.5, -10.5, -46.2, -45.15, 0, 40.95, SURF_ID = 'WestWind-ef', T_ACTIVATE = 266. /
&VENT XB =  -8.4,  -8.4, -46.2, -45.15, 0, 40.95, SURF_ID = 'WestWind-ef', T_ACTIVATE = 266. /
&VENT XB =  -6.3,  -6.3, -46.2, -45.15, 0, 40.95, SURF_ID = 'WestWind-ef', T_ACTIVATE = 266. /
&VENT XB =  -4.2,  -4.2, -46.2, -45.15, 0, 40.95, SURF_ID = 'WestWind-ef', T_ACTIVATE = 266. /
&VENT XB =  -2.1,  -2.1, -46.2, -45.15, 0, 40.95, SURF_ID = 'WestWind-ef', T_ACTIVATE = 266. /
&VENT XB =   0.0,   0.0, -46.2, -45.15, 0, 40.95, SURF_ID = 'WestWind-ef', T_ACTIVATE = 266. /
&VENT XB =   2.1,   2.1, -46.2, -45.15, 0, 40.95, SURF_ID = 'WestWind-ef', T_ACTIVATE = 266. /
&VENT XB =   4.2,   4.2, -46.2, -45.15, 0, 40.95, SURF_ID = 'WestWind-ef', T_ACTIVATE = 266. /
&VENT XB =   6.3,   6.3, -46.2, -45.15, 0, 40.95, SURF_ID = 'WestWind-ef', T_ACTIVATE = 266. /
&VENT XB =   8.2,   8.2, -46.2, -45.15, 0, 40.95, SURF_ID = 'WestWind-ef', T_ACTIVATE = 266. /
&VENT XB =  10.5,  10.5, -46.2, -45.15, 0, 40.95, SURF_ID = 'WestWind-ef', T_ACTIVATE = 266. /
&VENT XB =  12.6,  12.6, -46.2, -45.15, 0, 40.95, SURF_ID = 'WestWind-ef', T_ACTIVATE = 266. /
&VENT XB =  14.7,  14.7, -46.2, -45.15, 0, 40.95, SURF_ID = 'WestWind-ef', T_ACTIVATE = 266. /
&VENT XB =  16.8,  16.8, -46.2, -45.15, 0, 40.95, SURF_ID = 'WestWind-ef', T_ACTIVATE = 266. /
&VENT XB =  18.9,  18.9, -46.2, -45.15, 0, 40.95, SURF_ID = 'WestWind-ef', T_ACTIVATE = 266. /
&VENT XB =  21.0,  21.0, -46.2, -45.15, 0, 40.95, SURF_ID = 'WestWind-ef', T_ACTIVATE = 266. /
&VENT XB =  23.1,  23.1, -46.2, -45.15, 0, 40.95, SURF_ID = 'WestWind-ef', T_ACTIVATE = 266. /
&VENT XB =  25.2,  25.2, -46.2, -45.15, 0, 40.95, SURF_ID = 'WestWind-ef', T_ACTIVATE = 266. /
&VENT XB =  27.3,  27.3, -46.2, -45.15, 0, 40.95, SURF_ID = 'WestWind-ef', T_ACTIVATE = 266. /
&VENT XB =  29.4,  29.4, -46.2, -45.15, 0, 40.95, SURF_ID = 'WestWind-ef', T_ACTIVATE = 266. /
&VENT XB =  31.5,  31.5, -46.2, -45.15, 0, 40.95, SURF_ID = 'WestWind-ef', T_ACTIVATE = 266. /
&VENT XB =  33.6,  33.6, -46.2, -45.15, 0, 40.95, SURF_ID = 'WestWind-ef', T_ACTIVATE = 266. /
```

```
&VENT XB =  35.7,  35.7, -46.2, -45.15, 0, 40.95, SURF_ID = 'WestWind-ef', T_ACTIVATE = 266. /
&VENT XB =  37.8,  37.8, -46.2, -45.15, 0, 40.95, SURF_ID = 'WestWind-ef', T_ACTIVATE = 266. /
&VENT XB =  39.9,  39.9, -46.2, -45.15, 0, 40.95, SURF_ID = 'WestWind-ef', T_ACTIVATE = 266. /
&VENT XB =  42.0,  42.0, -46.2, -45.15, 0, 40.95, SURF_ID = 'WestWind-ef', T_ACTIVATE = 266. /
&VENT XB =  44.1,  44.1, -46.2, -45.15, 0, 40.95, SURF_ID = 'WestWind-ef', T_ACTIVATE = 266. /

---------------------------------
 WEST FACE - SOUTH WIND COMPONENT
---------------------------------

&VENT XB = -46.2, -45.15, -44.1, -44.1, 0, 40.95, SURF_ID = 'SouthWind-nf' /
&VENT XB = -46.2, -45.15, -42.0, -42.0, 0, 40.95, SURF_ID = 'SouthWind-nf' /
&VENT XB = -46.2, -45.15, -39.9, -39.9, 0, 40.95, SURF_ID = 'SouthWind-nf' /
&VENT XB = -46.2, -45.15, -37.8, -37.8, 0, 40.95, SURF_ID = 'SouthWind-nf' /
&VENT XB = -46.2, -45.15, -35.7, -35.7, 0, 40.95, SURF_ID = 'SouthWind-nf' /
&VENT XB = -46.2, -45.15, -33.6, -33.6, 0, 40.95, SURF_ID = 'SouthWind-nf' /
&VENT XB = -46.2, -45.15, -31.5, -31.5, 0, 40.95, SURF_ID = 'SouthWind-nf' /
&VENT XB = -46.2, -45.15, -29.4, -29.4, 0, 40.95, SURF_ID = 'SouthWind-nf' /
&VENT XB = -46.2, -45.15, -27.3, -27.3, 0, 40.95, SURF_ID = 'SouthWind-nf' /
&VENT XB = -46.2, -45.15, -25.2, -25.2, 0, 40.95, SURF_ID = 'SouthWind-nf' /
&VENT XB = -46.2, -45.15, -23.1, -23.1, 0, 40.95, SURF_ID = 'SouthWind-nf' /
&VENT XB = -46.2, -45.15, -21.0, -21.0, 0, 40.95, SURF_ID = 'SouthWind-nf' /
&VENT XB = -46.2, -45.15, -18.9, -18.9, 0, 40.95, SURF_ID = 'SouthWind-nf' /
&VENT XB = -46.2, -45.15, -16.8, -16.8, 0, 40.95, SURF_ID = 'SouthWind-nf' /
&VENT XB = -46.2, -45.15, -14.7, -14.7, 0, 40.95, SURF_ID = 'SouthWind-nf' /
&VENT XB = -46.2, -45.15, -12.6, -12.6, 0, 40.95, SURF_ID = 'SouthWind-nf' /
&VENT XB = -46.2, -45.15, -10.5, -10.5, 0, 40.95, SURF_ID = 'SouthWind-nf' /
&VENT XB = -46.2, -45.15,  -8.4,  -8.4, 0, 40.95, SURF_ID = 'SouthWind-nf' /
&VENT XB = -46.2, -45.15,  -6.3,  -6.3, 0, 40.95, SURF_ID = 'SouthWind-nf' /
&VENT XB = -46.2, -45.15,  -4.2,  -4.2, 0, 40.95, SURF_ID = 'SouthWind-nf' /
&VENT XB = -46.2, -45.15,  -2.1,  -2.1, 0, 40.95, SURF_ID = 'SouthWind-nf' /
&VENT XB = -46.2, -45.15,   0.0,   0.0, 0, 40.95, SURF_ID = 'SouthWind-nf' /
&VENT XB = -46.2, -45.15,   2.1,   2.1, 0, 40.95, SURF_ID = 'SouthWind-nf' /
&VENT XB = -46.2, -45.15,   4.2,   4.2, 0, 40.95, SURF_ID = 'SouthWind-nf' /
&VENT XB = -46.2, -45.15,   6.3,   6.3, 0, 40.95, SURF_ID = 'SouthWind-nf' /
&VENT XB = -46.2, -45.15,   8.4,   8.4, 0, 40.95, SURF_ID = 'SouthWind-nf' /
&VENT XB = -46.2, -45.15,  10.5,  10.5, 0, 40.95, SURF_ID = 'SouthWind-nf' /
&VENT XB = -46.2, -45.15,  12.6,  12.6, 0, 40.95, SURF_ID = 'SouthWind-nf' /
&VENT XB = -46.2, -45.15,  14.7,  14.7, 0, 40.95, SURF_ID = 'SouthWind-nf' /
&VENT XB = -46.2, -45.15,  16.8,  16.8, 0, 40.95, SURF_ID = 'SouthWind-nf' /
```

```
&VENT XB = -46.2, -45.15,  18.9,  18.9, 0, 40.95, SURF_ID = 'SouthWind-nf' /
&VENT XB = -46.2, -45.15,  21.0,  21.0, 0, 40.95, SURF_ID = 'SouthWind-nf' /
&VENT XB = -46.2, -45.15,  23.1,  23.1, 0, 40.95, SURF_ID = 'SouthWind-nf' /
&VENT XB = -46.2, -45.15,  25.2,  25.2, 0, 40.95, SURF_ID = 'SouthWind-nf' /
&VENT XB = -46.2, -45.15,  27.3,  27.3, 0, 40.95, SURF_ID = 'SouthWind-nf' /
&VENT XB = -46.2, -45.15,  29.4,  29.4, 0, 40.95, SURF_ID = 'SouthWind-nf' /
&VENT XB = -46.2, -45.15,  31.5,  31.5, 0, 40.95, SURF_ID = 'SouthWind-nf' /
&VENT XB = -46.2, -45.15,  33.6,  33.6, 0, 40.95, SURF_ID = 'SouthWind-nf' /
&VENT XB = -46.2, -45.15,  35.7,  35.7, 0, 40.95, SURF_ID = 'SouthWind-nf' /
&VENT XB = -46.2, -45.15,  37.8,  37.8, 0, 40.95, SURF_ID = 'SouthWind-nf' /
&VENT XB = -46.2, -45.15,  39.9,  39.9, 0, 40.95, SURF_ID = 'SouthWind-nf' /
&VENT XB = -46.2, -45.15,  42.0,  42.0, 0, 40.95, SURF_ID = 'SouthWind-nf' /
&VENT XB = -46.2, -45.15,  44.1,  44.1, 0, 40.95, SURF_ID = 'SouthWind-nf' /

---------------------------------
 EAST FACE - SOUTH WIND COMPONENT
---------------------------------

&VENT XB =  45.15,  46.2, -44.1, -44.1, 0, 40.95, SURF_ID = 'SouthWind-nf' /
&VENT XB =  45.15,  46.2, -42.0, -42.0, 0, 40.95, SURF_ID = 'SouthWind-nf' /
&VENT XB =  45.15,  46.2, -39.9, -39.9, 0, 40.95, SURF_ID = 'SouthWind-nf' /
&VENT XB =  45.15,  46.2, -37.8, -37.8, 0, 40.95, SURF_ID = 'SouthWind-nf' /
&VENT XB =  45.15,  46.2, -35.7, -35.7, 0, 40.95, SURF_ID = 'SouthWind-nf' /
&VENT XB =  45.15,  46.2, -33.6, -33.6, 0, 40.95, SURF_ID = 'SouthWind-nf' /
&VENT XB =  45.15,  46.2, -31.5, -31.5, 0, 40.95, SURF_ID = 'SouthWind-nf' /
&VENT XB =  45.15,  46.2, -29.4, -29.4, 0, 40.95, SURF_ID = 'SouthWind-nf' /
&VENT XB =  45.15,  46.2, -27.3, -27.3, 0, 40.95, SURF_ID = 'SouthWind-nf' /
&VENT XB =  45.15,  46.2, -25.2, -25.2, 0, 40.95, SURF_ID = 'SouthWind-nf' /
&VENT XB =  45.15,  46.2, -23.1, -23.1, 0, 40.95, SURF_ID = 'SouthWind-nf' /
&VENT XB =  45.15,  46.2, -21.0, -21.0, 0, 40.95, SURF_ID = 'SouthWind-nf' /
&VENT XB =  45.15,  46.2, -18.9, -18.9, 0, 40.95, SURF_ID = 'SouthWind-nf' /
&VENT XB =  45.15,  46.2, -16.8, -16.8, 0, 40.95, SURF_ID = 'SouthWind-nf' /
&VENT XB =  45.15,  46.2, -14.7, -14.7, 0, 40.95, SURF_ID = 'SouthWind-nf' /
&VENT XB =  45.15,  46.2, -12.6, -12.6, 0, 40.95, SURF_ID = 'SouthWind-nf' /
&VENT XB =  45.15,  46.2, -10.5, -10.5, 0, 40.95, SURF_ID = 'SouthWind-nf' /
&VENT XB =  45.15,  46.2,  -8.4,  -8.4, 0, 40.95, SURF_ID = 'SouthWind-nf' /
&VENT XB =  45.15,  46.2,  -6.3,  -6.3, 0, 40.95, SURF_ID = 'SouthWind-nf' /
&VENT XB =  45.15,  46.2,  -4.2,  -4.2, 0, 40.95, SURF_ID = 'SouthWind-nf' /
&VENT XB =  45.15,  46.2,  -2.1,  -2.1, 0, 40.95, SURF_ID = 'SouthWind-nf' /
&VENT XB =  45.15,  46.2,   0.0,   0.0, 0, 40.95, SURF_ID = 'SouthWind-nf' /
```

```
&VENT XB =  45.15,  46.2,   2.1,   2.1, 0, 40.95, SURF_ID = 'SouthWind-nf' /
&VENT XB =  45.15,  46.2,   4.2,   4.2, 0, 40.95, SURF_ID = 'SouthWind-nf' /
&VENT XB =  45.15,  46.2,   6.3,   6.3, 0, 40.95, SURF_ID = 'SouthWind-nf' /
&VENT XB =  45.15,  46.2,   8.4,   8.4, 0, 40.95, SURF_ID = 'SouthWind-nf' /
&VENT XB =  45.15,  46.2,  10.5,  10.5, 0, 40.95, SURF_ID = 'SouthWind-nf' /
&VENT XB =  45.15,  46.2,  12.6,  12.6, 0, 40.95, SURF_ID = 'SouthWind-nf' /
&VENT XB =  45.15,  46.2,  14.7,  14.7, 0, 40.95, SURF_ID = 'SouthWind-nf' /
&VENT XB =  45.15,  46.2,  16.8,  16.8, 0, 40.95, SURF_ID = 'SouthWind-nf' /
&VENT XB =  45.15,  46.2,  18.9,  18.9, 0, 40.95, SURF_ID = 'SouthWind-nf' /
&VENT XB =  45.15,  46.2,  21.0,  21.0, 0, 40.95, SURF_ID = 'SouthWind-nf' /
&VENT XB =  45.15,  46.2,  23.1,  23.1, 0, 40.95, SURF_ID = 'SouthWind-nf' /
&VENT XB =  45.15,  46.2,  25.2,  25.2, 0, 40.95, SURF_ID = 'SouthWind-nf' /
&VENT XB =  45.15,  46.2,  27.3,  27.3, 0, 40.95, SURF_ID = 'SouthWind-nf' /
&VENT XB =  45.15,  46.2,  29.4,  29.4, 0, 40.95, SURF_ID = 'SouthWind-nf' /
&VENT XB =  45.15,  46.2,  31.5,  31.5, 0, 40.95, SURF_ID = 'SouthWind-nf' /
&VENT XB =  45.15,  46.2,  33.6,  33.6, 0, 40.95, SURF_ID = 'SouthWind-nf' /
&VENT XB =  45.15,  46.2,  35.7,  35.7, 0, 40.95, SURF_ID = 'SouthWind-nf' /
&VENT XB =  45.15,  46.2,  37.8,  37.8, 0, 40.95, SURF_ID = 'SouthWind-nf' /
&VENT XB =  45.15,  46.2,  39.9,  39.9, 0, 40.95, SURF_ID = 'SouthWind-nf' /
&VENT XB =  45.15,  46.2,  42.0,  42.0, 0, 40.95, SURF_ID = 'SouthWind-nf' /
&VENT XB =  45.15,  46.2,  44.1,  44.1, 0, 40.95, SURF_ID = 'SouthWind-nf' /

------------------------------
 BOUNDARY SURFACE DEFINITIONS
------------------------------

&SURF ID = 'EastWind-wf', VEL =  0.52 , RAMP_V = 'EastRamp' / east wind into west face
&SURF ID = 'EastWind-ef', VEL = -0.52 , RAMP_V = 'EastRamp' / east wind out of east face
&RAMP ID = 'EastRamp', T =    0., F = 0.77 /                   and component of south face
&RAMP ID = 'EastRamp', T =  120., F = 0.94 /
&RAMP ID = 'EastRamp', T =  160., F = 1.00 /
&RAMP ID = 'EastRamp', T =  220., F = 0.43 /
&RAMP ID = 'EastRamp', T =  266., F = 0.00 /
&RAMP ID = 'EastRamp', T = 1800., F = 0.00 /

&SURF ID = 'WestWind-wf', VEL = -2.48, RAMP_V = 'WestRamp' / west wind out of west face
&SURF ID = 'WestWind-ef', VEL =  2.48, RAMP_V = 'WestRamp' / west wind into east face
&RAMP ID = 'WestRamp', T =    0., F = 0.00 /                   and component of south face
&RAMP ID = 'WestRamp', T =  266., F = 0.00 /
&RAMP ID = 'WestRamp', T =  300., F = 0.07 /
```

```
&RAMP ID = 'WestRamp', T =  350., F = 0.17 /
&RAMP ID = 'WestRamp', T =  360., F = 0.19 /
&RAMP ID = 'WestRamp', T =  500., F = 0.23 /
&RAMP ID = 'WestRamp', T =  640., F = 0.40 /
&RAMP ID = 'WestRamp', T =  860., F = 0.35 /
&RAMP ID = 'WestRamp', T = 1060., F = 0.56 /
&RAMP ID = 'WestRamp', T = 1200., F = 0.43 /
&RAMP ID = 'WestRamp', T = 1300., F = 0.63 /
&RAMP ID = 'WestRamp', T = 1550., F = 0.88 /
&RAMP ID = 'WestRamp', T = 1700., F = 1.00 /
&RAMP ID = 'WestRamp', T = 1800., F = 0.85 /

&SURF ID = 'SouthWind',    VEL = -1.44, RAMP_V = 'SouthRamp' / south wind out of south face
&SURF ID = 'SouthWind-nf', VEL =  1.44, RAMP_V = 'SouthRamp' / south wind component of
&RAMP ID = 'SouthRamp', T =    0., F = 0.00 /                   west and east face
&RAMP ID = 'SouthRamp', T =  120., F = 0.13 /
&RAMP ID = 'SouthRamp', T =  160., F = 0.24 /
&RAMP ID = 'SouthRamp', T =  220., F = 0.42 /
&RAMP ID = 'SouthRamp', T =  266., F = 0.47 /
&RAMP ID = 'SouthRamp', T =  300., F = 0.51 /
&RAMP ID = 'SouthRamp', T =  350., F = 0.44 /
&RAMP ID = 'SouthRamp', T =  360., F = 0.45 /
&RAMP ID = 'SouthRamp', T =  500., F = 0.53 /
&RAMP ID = 'SouthRamp', T =  640., F = 0.87 /
&RAMP ID = 'SouthRamp', T =  860., F = 0.67 /
&RAMP ID = 'SouthRamp', T = 1060., F = 1.00 /
&RAMP ID = 'SouthRamp', T = 1200., F = 0.64 /
&RAMP ID = 'SouthRamp', T = 1300., F = 0.75 /
&RAMP ID = 'SouthRamp', T = 1550., F = 0.48 /
&RAMP ID = 'SouthRamp', T = 1700., F = 0.19 /
&RAMP ID = 'SouthRamp', T = 1800., F = 0.00 /

--------------
 OUTPUT PLOTS
--------------

&SLCF PBX =  0.0,  QUANTITY = 'TEMPERATURE' /
&SLCF PBX =  0.0,  QUANTITY = 'U-VELOCITY', VECTOR = .TRUE. /
&SLCF PBX =  0.0,  QUANTITY = 'V-VELOCITY'  /
&SLCF PBX =  0.0,  QUANTITY = 'W-VELOCITY'  /
```

```
&SLCF PBX =  0.0,  QUANTITY = 'VELOCITY'    /
&SLCF PBX =  0.0,  QUANTITY = 'HRRPUV'      /
&SLCF PBX =  0.0,  QUANTITY = 'DIVERGENCE'  /

&SLCF PBY =  0.0,  QUANTITY = 'TEMPERATURE' /
&SLCF PBY =  0.0,  QUANTITY = 'U-VELOCITY'  /
&SLCF PBY =  0.0,  QUANTITY = 'V-VELOCITY'  /
&SLCF PBY =  0.0,  QUANTITY = 'W-VELOCITY'  /
&SLCF PBY =  0.0,  QUANTITY = 'VELOCITY'    /
&SLCF PBY =  0.0,  QUANTITY = 'HRRPUV'      /
&SLCF PBY =  0.0,  QUANTITY = 'DIVERGENCE'  /

&SLCF PBY = 37.8,  QUANTITY = 'TEMPERATURE' /
&SLCF PBY = 37.8,  QUANTITY = 'U-VELOCITY'  /
&SLCF PBY = 37.8,  QUANTITY = 'V-VELOCITY'  /
&SLCF PBY = 37.8,  QUANTITY = 'W-VELOCITY'  /
&SLCF PBY = 37.8,  QUANTITY = 'VELOCITY'    /
&SLCF PBY = 37.8,  QUANTITY = 'HRRPUV'      /
&SLCF PBY = 37.8,  QUANTITY = 'DIVERGENCE'  /

&SLCF PBZ = 10.0,  QUANTITY = 'TEMPERATURE' /
&SLCF PBZ = 10.0,  QUANTITY = 'U-VELOCITY'  /
&SLCF PBZ = 10.0,  QUANTITY = 'V-VELOCITY'  /
&SLCF PBZ = 10.0,  QUANTITY = 'W-VELOCITY'  /
&SLCF PBZ = 10.0,  QUANTITY = 'VELOCITY'    /
&SLCF PBZ = 10.0,  QUANTITY = 'HRRPUV'      /
&SLCF PBZ = 10.0,  QUANTITY = 'DIVERGENCE'  /

&SLCF PBZ = 40.95, QUANTITY = 'TEMPERATURE' /
&SLCF PBZ = 40.95, QUANTITY = 'U-VELOCITY'  /
&SLCF PBZ = 40.95, QUANTITY = 'V-VELOCITY'  /
&SLCF PBZ = 40.95, QUANTITY = 'W-VELOCITY'  /
&SLCF PBZ = 40.95, QUANTITY = 'VELOCITY'    /
&SLCF PBZ = 40.95, QUANTITY = 'HRRPUV'      /
&SLCF PBZ = 40.95, QUANTITY = 'DIVERGENCE'  /

--------------------------------
 FIRE THERMOCOUPLE DATA - TOWERS
--------------------------------
```

```
&THCP XYZ = -3.0, -1.2,  1.2, QUANTITY = 'TEMPERATURE', LABEL = 'TWR A-1' / Tower A
&THCP XYZ = -3.0, -1.2,  2.4, QUANTITY = 'TEMPERATURE', LABEL = 'TWR A-2' /

&THCP XYZ = -3.0,  1.2,  1.2, QUANTITY = 'TEMPERATURE', LABEL = 'TWR B-1' / Tower B
&THCP XYZ = -3.0,  1.2,  2.4, QUANTITY = 'TEMPERATURE', LABEL = 'TWR B-2' /

&THCP XYZ =  3.7,  0.0,  1.2, QUANTITY = 'TEMPERATURE', LABEL = 'TWR C-1' / Tower C
&THCP XYZ =  3.7,  0.0,  2.4, QUANTITY = 'TEMPERATURE', LABEL = 'TWR C-2' /

&THCP XYZ =  0.3,  1.2,  1.2, QUANTITY = 'TEMPERATURE', LABEL = 'TWR 2-1' / Tower 2
&THCP XYZ =  0.3,  1.2,  2.4, QUANTITY = 'TEMPERATURE', LABEL = 'TWR 2-2' /
&THCP XYZ =  0.3,  1.2,  5.3, QUANTITY = 'TEMPERATURE', LABEL = 'TWR 2-3' /
&THCP XYZ =  0.3,  1.2, 11.0, QUANTITY = 'TEMPERATURE', LABEL = 'TWR 2-4' /

&THCP XYZ = -4.7,  0.0,  1.2, QUANTITY = 'TEMPERATURE', LABEL = 'TWR 3-1' / Tower 3
&THCP XYZ = -4.7,  0.0,  2.4, QUANTITY = 'TEMPERATURE', LABEL = 'TWR 3-2' /
&THCP XYZ = -4.7,  0.0,  5.3, QUANTITY = 'TEMPERATURE', LABEL = 'TWR 3-3' /
&THCP XYZ = -4.7,  0.0, 11.0, QUANTITY = 'TEMPERATURE', LABEL = 'TWR 3-4' /

&THCP XYZ =  0.3, -1.2,  1.2, QUANTITY = 'TEMPERATURE', LABEL = 'TWR 4-1' / Tower 4
&THCP XYZ =  0.3, -1.2,  2.4, QUANTITY = 'TEMPERATURE', LABEL = 'TWR 4-2' /
&THCP XYZ =  0.3, -1.2,  5.3, QUANTITY = 'TEMPERATURE', LABEL = 'TWR 4-3' /
&THCP XYZ =  0.3, -1.2, 11.0, QUANTITY = 'TEMPERATURE', LABEL = 'TWR 4-4' /

&THCP XYZ =  2.5, -1.2,  1.2, QUANTITY = 'TEMPERATURE', LABEL = 'TWR 6-1' / Tower 6
&THCP XYZ =  2.5, -1.2,  2.4, QUANTITY = 'TEMPERATURE', LABEL = 'TWR 6-2' /
&THCP XYZ =  2.5, -1.2,  5.3, QUANTITY = 'TEMPERATURE', LABEL = 'TWR 6-3' /
&THCP XYZ =  2.5, -1.2, 11.0, QUANTITY = 'TEMPERATURE', LABEL = 'TWR 6-4' /

&THCP XYZ =  2.5,  1.2,  1.2, QUANTITY = 'TEMPERATURE', LABEL = 'TWR 7-1' / Tower 7
&THCP XYZ =  2.5,  1.2,  2.4, QUANTITY = 'TEMPERATURE', LABEL = 'TWR 7-2' /
&THCP XYZ =  2.5,  1.2,  5.3, QUANTITY = 'TEMPERATURE', LABEL = 'TWR 7-3' /
&THCP XYZ =  2.5,  1.2, 11.0, QUANTITY = 'TEMPERATURE', LABEL = 'TWR 7-4' /

------------------------------------------------------------------
 LARGE CALORIMETER THERMOCOUPLE DATA - FIRE TEMPERATURE NEAR SURFACE
------------------------------------------------------------------

&THCP XYZ =  2.7,   0.00, 0.65, QUANTITY = 'TEMPERATURE', LABEL = 'FT 1-000'  / Station 1
&THCP XYZ =  2.7,  -0.75, 1.40, QUANTITY = 'TEMPERATURE', LABEL = 'FT 1-090'  /
```

```
&THCP XYZ =  2.7,   0.00, 2.15, QUANTITY = 'TEMPERATURE', LABEL = 'FT 1-180'  /
&THCP XYZ =  2.7,   0.75, 1.40, QUANTITY = 'TEMPERATURE', LABEL = 'FT 1-270'  /

&THCP XYZ = -0.08,  0.00, 0.65, QUANTITY = 'TEMPERATURE', LABEL = 'FT 2-000'  / Station 2
&THCP XYZ = -0.08, -0.75, 1.40, QUANTITY = 'TEMPERATURE', LABEL = 'FT 2-090'  /
&THCP XYZ = -0.08,  0.00, 2.15, QUANTITY = 'TEMPERATURE', LABEL = 'FT 2-180'  /
&THCP XYZ = -0.08,  0.75, 1.40, QUANTITY = 'TEMPERATURE', LABEL = 'FT 2-270'  /

&THCP XYZ = -2.7,   0.00, 0.65, QUANTITY = 'TEMPERATURE', LABEL = 'FT 3-000'  / Station 3
&THCP XYZ = -2.7,  -0.75, 1.40, QUANTITY = 'TEMPERATURE', LABEL = 'FT 3-090'  /
&THCP XYZ = -2.7,   0.00, 2.15, QUANTITY = 'TEMPERATURE', LABEL = 'FT 3-180'  /
&THCP XYZ = -2.7,   0.75, 1.40, QUANTITY = 'TEMPERATURE', LABEL = 'FT 3-270'  /

&THCP XYZ =  3.2,   0.0,  1.4,  QUANTITY = 'TEMPERATURE', LABEL = 'FT E ndcp' / End Caps
&THCP XYZ = -3.2,   0.0,  1.4,  QUANTITY = 'TEMPERATURE', LABEL = 'FT W ndcp' /

------------------------------------------------------------
 LARGE CALORIMETER THERMOCOUPLE DATA - BACKFACE TEMPERATURES
------------------------------------------------------------

&THCP XYZ =  2.7,   0.0,  0.7, QUANTITY = 'INSIDE_WALL_TEMPERATURE',
      IOR = -3, DEPTH = 0.03175,                          LABEL = 'BF 1-000'  / Station 1
&THCP XYZ =  2.7,  -0.7,  1.4, QUANTITY = 'INSIDE_WALL_TEMPERATURE',
      IOR = -2, DEPTH = 0.03175,                          LABEL = 'BF 1-090'  /
&THCP XYZ =  2.7,   0.0,  2.1, QUANTITY = 'INSIDE_WALL_TEMPERATURE',
      IOR =  3, DEPTH = 0.03175,                          LABEL = 'BF 1-180'  /
&THCP XYZ =  2.7,   0.7,  1.4, QUANTITY = 'INSIDE_WALL_TEMPERATURE',
      IOR =  2, DEPTH = 0.03175,                          LABEL = 'BF 1-270'  /

&THCP XYZ = -0.08,  0.0,  0.7, QUANTITY = 'INSIDE_WALL_TEMPERATURE',
      IOR = -3, DEPTH = 0.03175,                          LABEL = 'BF 2-000'  / Station 2
&THCP XYZ = -0.08, -0.7,  1.4, QUANTITY = 'INSIDE_WALL_TEMPERATURE',
      IOR = -2, DEPTH = 0.03175,                          LABEL = 'BF 2-090'  /
&THCP XYZ = -0.08,   0.0,  2.1, QUANTITY = 'INSIDE_WALL_TEMPERATURE',
      IOR =  3, DEPTH = 0.03175,                          LABEL = 'BF 2-180'  /
&THCP XYZ = -0.08,  0.7,  1.4, QUANTITY = 'INSIDE_WALL_TEMPERATURE',
      IOR =  2, DEPTH = 0.03175,                          LABEL = 'BF 2-270'  /

&THCP XYZ = -2.7,   0.0,  0.7, QUANTITY = 'INSIDE_WALL_TEMPERATURE',
      IOR = -3, DEPTH = 0.03175,                          LABEL = 'BF 3-000'  / Station 3
```

```
&THCP XYZ = -2.7,  -0.7,  1.4, QUANTITY = 'INSIDE_WALL_TEMPERATURE',
      IOR = -2, DEPTH = 0.03175,                          LABEL = 'BF 3-090'  /
&THCP XYZ = -2.7,   0.0,  2.1, QUANTITY = 'INSIDE_WALL_TEMPERATURE',
      IOR =  3, DEPTH = 0.03175,                          LABEL = 'BF 3-180'  /
&THCP XYZ = -2.7,   0.7,  1.4, QUANTITY = 'INSIDE_WALL_TEMPERATURE',
      IOR =  2, DEPTH = 0.03175,                          LABEL = 'BF 3-270'  /

&THCP XYZ =  3.15,  0.0, 1.4, QUANTITY = 'INSIDE_WALL_TEMPERATURE',
      IOR = 1, DEPTH = 0.0127,                            LABEL = 'BF E ndcp' / End Caps
&THCP XYZ = -3.15,  0.0, 1.4, QUANTITY = 'INSIDE_WALL_TEMPERATURE',
      IOR = -1, DEPTH = 0.0127,                           LABEL = 'BF W ndcp' /

-----------------
 WIND FIELD DATA
-----------------

&THCP XYZ =   0,   0, 10, QUANTITY = 'U-VELOCITY', LABEL = 'U ctl' /
&THCP XYZ =   0,   0, 10, QUANTITY = 'V-VELOCITY', LABEL = 'V ctl' /
&THCP XYZ =   0,   0, 10, QUANTITY = 'W-VELOCITY', LABEL = 'W ctl' /

&THCP XYZ =  20,   0, 10, QUANTITY = 'U-VELOCITY', LABEL = 'U X+2' /
&THCP XYZ =  20,   0, 10, QUANTITY = 'V-VELOCITY', LABEL = 'V X+2' /
&THCP XYZ =  20,   0, 10, QUANTITY = 'W-VELOCITY', LABEL = 'W X+2' /

&THCP XYZ = -20,   0, 10, QUANTITY = 'U-VELOCITY', LABEL = 'U X-2' /
&THCP XYZ = -20,   0, 10, QUANTITY = 'V-VELOCITY', LABEL = 'V X-2' /
&THCP XYZ = -20,   0, 10, QUANTITY = 'W-VELOCITY', LABEL = 'W X-2' /

&THCP XYZ =   0,  20, 10, QUANTITY = 'U-VELOCITY', LABEL = 'U Y+2' /
&THCP XYZ =   0,  20, 10, QUANTITY = 'V-VELOCITY', LABEL = 'V Y+2' /
&THCP XYZ =   0,  20, 10, QUANTITY = 'W-VELOCITY', LABEL = 'W Y+2' /

&THCP XYZ =   0, -20, 10, QUANTITY = 'U-VELOCITY', LABEL = 'U Y-2' /
&THCP XYZ =   0, -20, 10, QUANTITY = 'V-VELOCITY', LABEL = 'W Y-2' /
&THCP XYZ =   0, -20, 10, QUANTITY = 'W-VELOCITY', LABEL = 'W Y-2' /

&THCP XYZ =  30,   0, 10, QUANTITY = 'U-VELOCITY', LABEL = 'U X+3' /
&THCP XYZ =  30,   0, 10, QUANTITY = 'V-VELOCITY', LABEL = 'V X+3' /
&THCP XYZ =  30,   0, 10, QUANTITY = 'W-VELOCITY', LABEL = 'W X+3' /
```

```
&THCP XYZ = -30,   0, 10, QUANTITY = 'U-VELOCITY', LABEL = 'U X-3' /
&THCP XYZ = -30,   0, 10, QUANTITY = 'V-VELOCITY', LABEL = 'V X-3' /
&THCP XYZ = -30,   0, 10, QUANTITY = 'W-VELOCITY', LABEL = 'W X-3' /

&THCP XYZ =   0,  30, 10, QUANTITY = 'U-VELOCITY', LABEL = 'U Y+3' /
&THCP XYZ =   0,  30, 10, QUANTITY = 'V-VELOCITY', LABEL = 'V Y+3' /
&THCP XYZ =   0,  30, 10, QUANTITY = 'W-VELOCITY', LABEL = 'W Y+3' /

&THCP XYZ =   0, -30, 10, QUANTITY = 'U-VELOCITY', LABEL = 'U Y-3' /
&THCP XYZ =   0, -30, 10, QUANTITY = 'V-VELOCITY', LABEL = 'W Y-3' /
&THCP XYZ =   0, -30, 10, QUANTITY = 'W-VELOCITY', LABEL = 'W Y-3' /

--------------------
 FLAME HEIGHT DATA
--------------------

&THCP XYZ = 0.0, 0.0,  8., QUANTITY = 'HRRPUV', LABEL = 'HRRPUV  8' /
&THCP XYZ = 0.0, 0.0, 12., QUANTITY = 'HRRPUV', LABEL = 'HRRPUV 12' /
&THCP XYZ = 0.0, 0.0, 16., QUANTITY = 'HRRPUV', LABEL = 'HRRPUV 16' /
&THCP XYZ = 0.0, 0.0, 20., QUANTITY = 'HRRPUV', LABEL = 'HRRPUV 20' /
&THCP XYZ = 0.0, 0.0, 24., QUANTITY = 'HRRPUV', LABEL = 'HRRPUV 24' /
&THCP XYZ = 0.0, 0.0, 28., QUANTITY = 'HRRPUV', LABEL = 'HRRPUV 28' /
&THCP XYZ = 0.0, 0.0, 32., QUANTITY = 'HRRPUV', LABEL = 'HRRPUV 32' /
&THCP XYZ = 0.0, 0.0, 36., QUANTITY = 'HRRPUV', LABEL = 'HRRPUV 36' /
&THCP XYZ = 0.0, 0.0, 40., QUANTITY = 'HRRPUV', LABEL = 'HRRPUV 40' /
```

APPENDIX C. SANDIA FIRE TEST C DATA AND C-175d RESULTS

This appendix presents pairs of charts comparing Test C data (top of each page) to FDS3 simulation results for Case C-175d (bottom of each page). The figure number for the corresponding chart in the Sandia report is provided on each page.

Sandia Figure B20

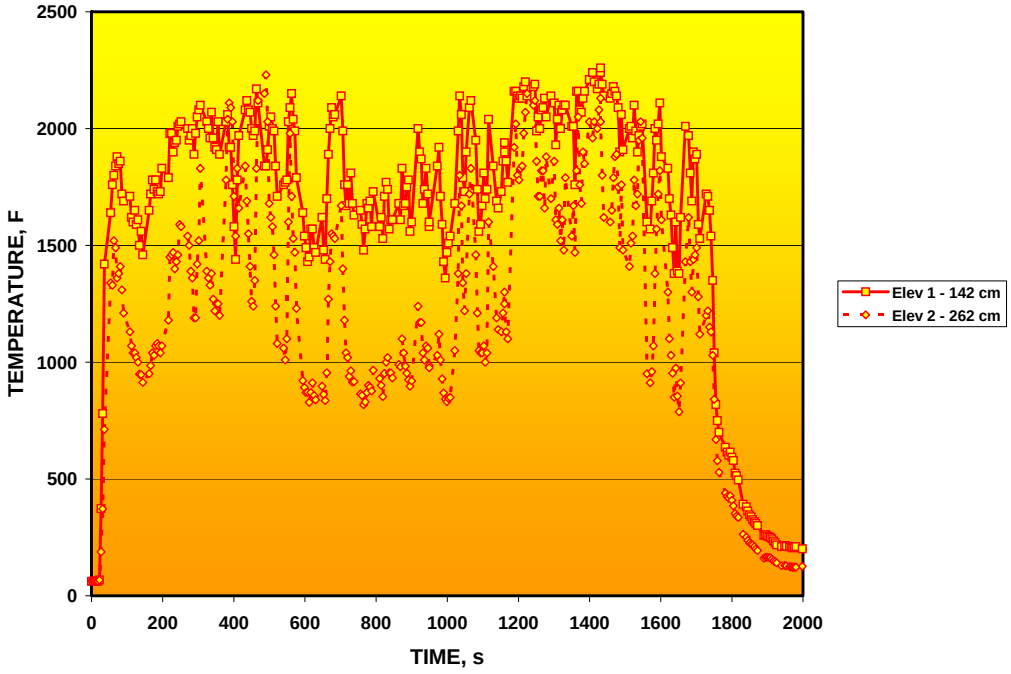

FDS3 Case C-175d

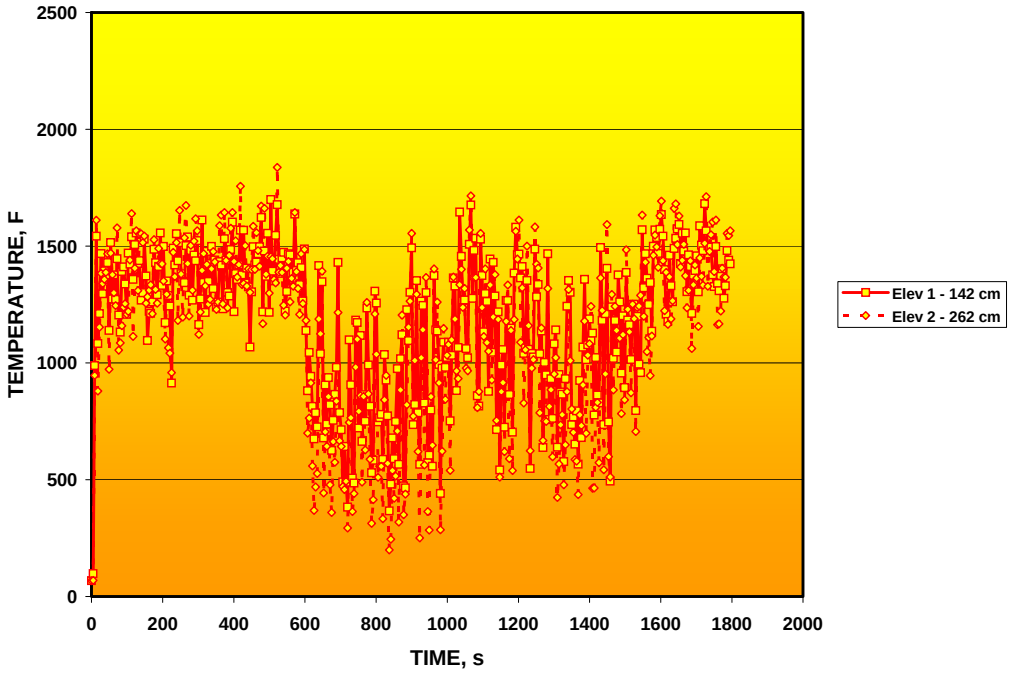

Fig. C.1. Flame temperatures – Tower A.

Sandia Figure B21

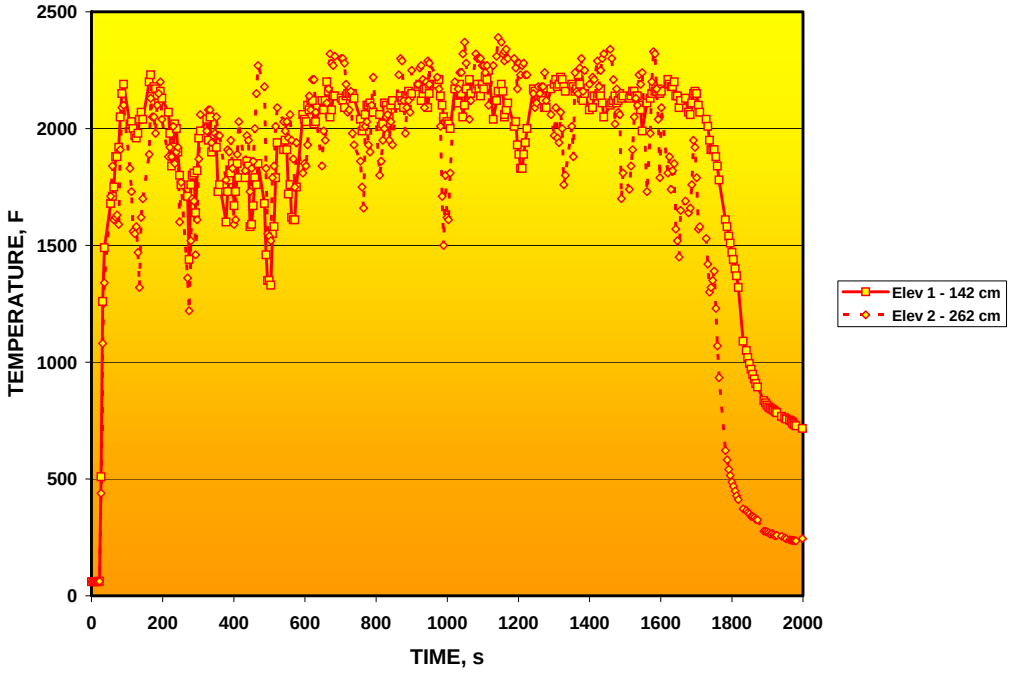

FDS3 Case C-175d

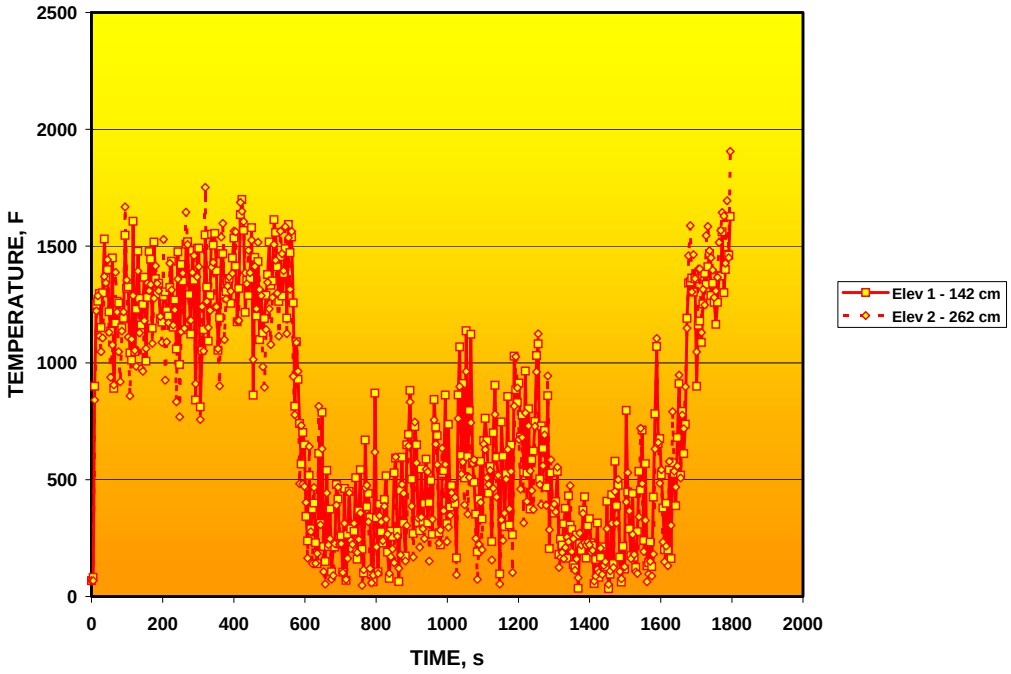

Fig. C.2. Flame temperatures – Tower B.

Sandia Figure B22

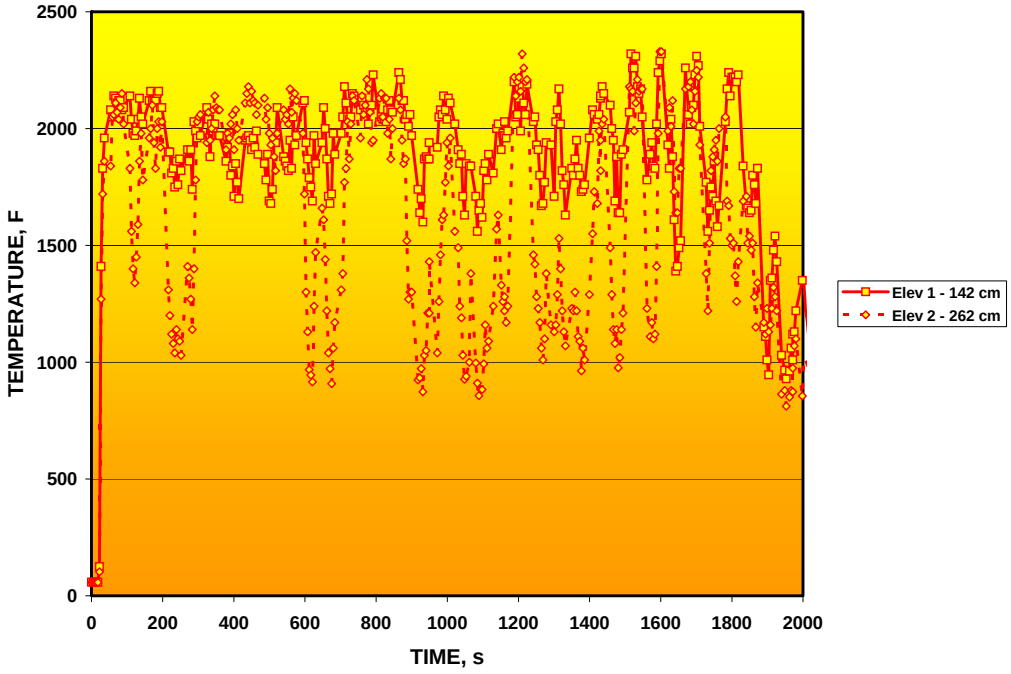

FDS3 Case C-175d

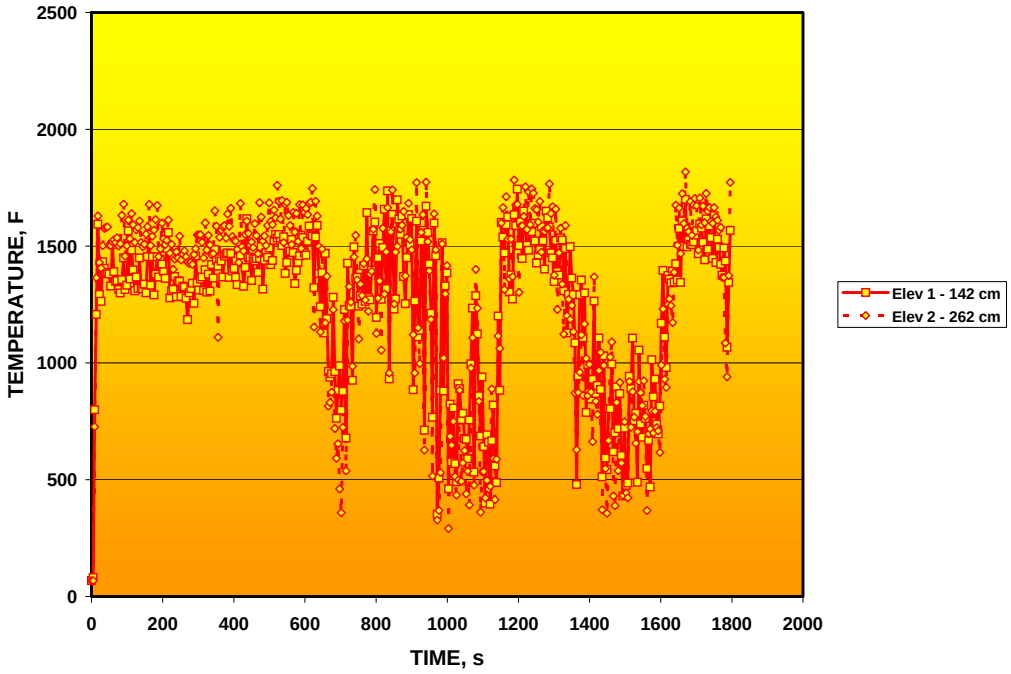

Fig. C.3. Flame temperatures – Tower C.

Sandia Figure B23

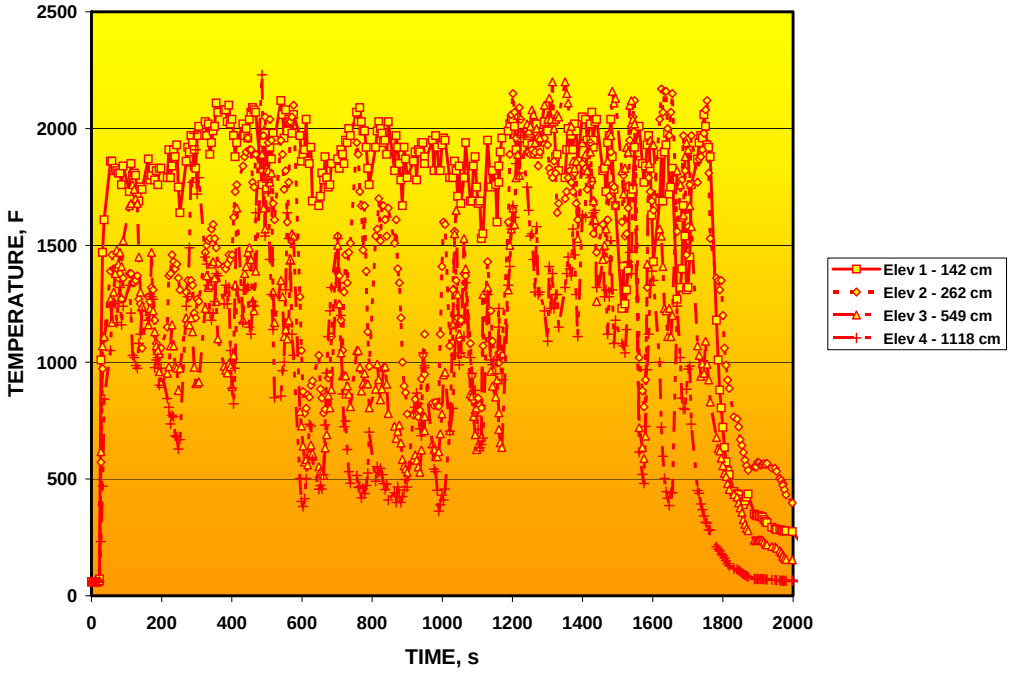

FDS3 Case C-175d

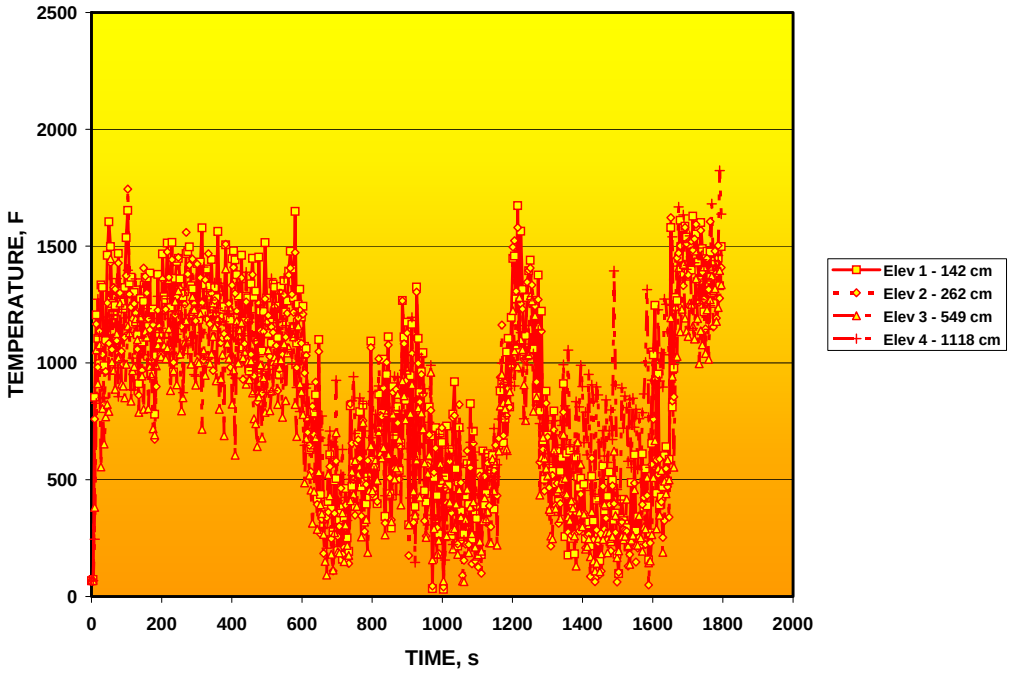

Fig. C.4. Flame temperatures – Tower 2.

Sandia Figure B24

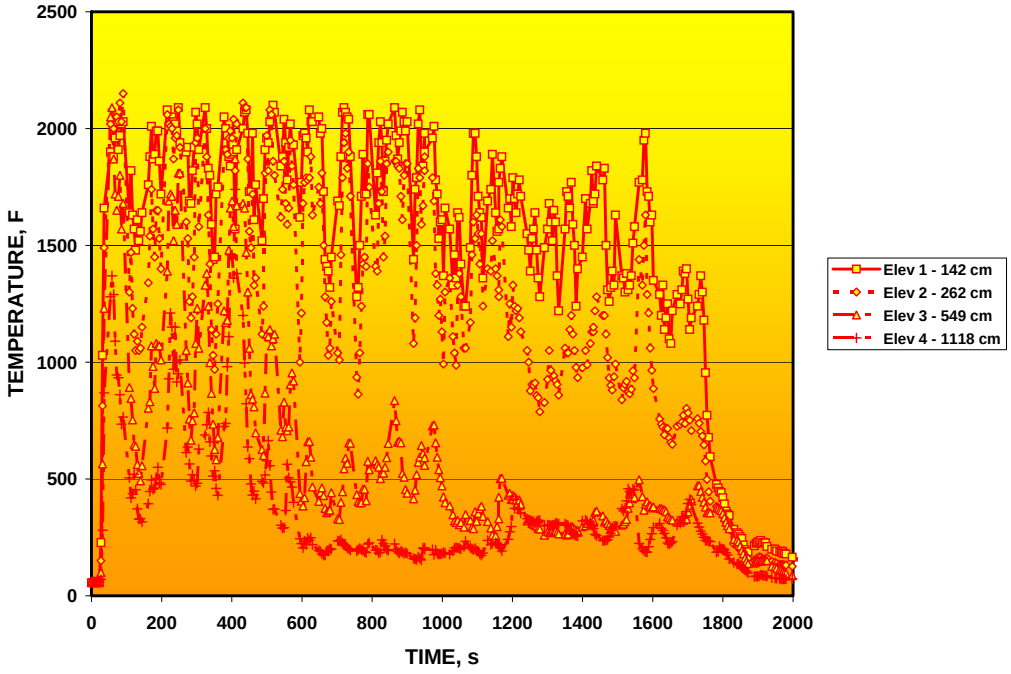

FDS3 Case C-175d

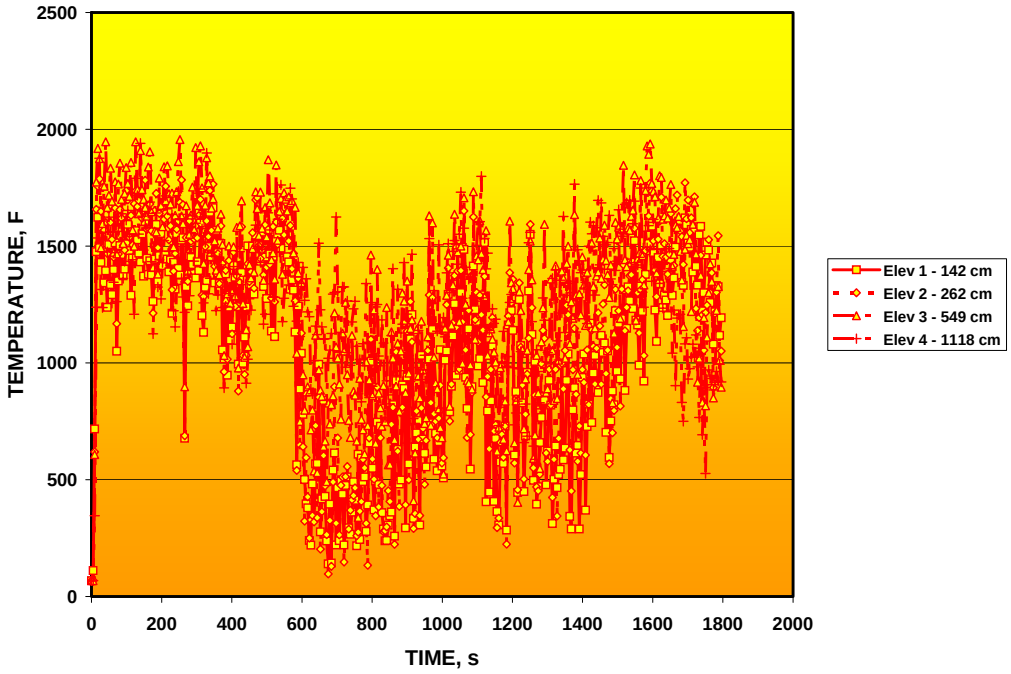

Fig. C.5. Flame temperatures – Tower 3.

Sandia Figure B25

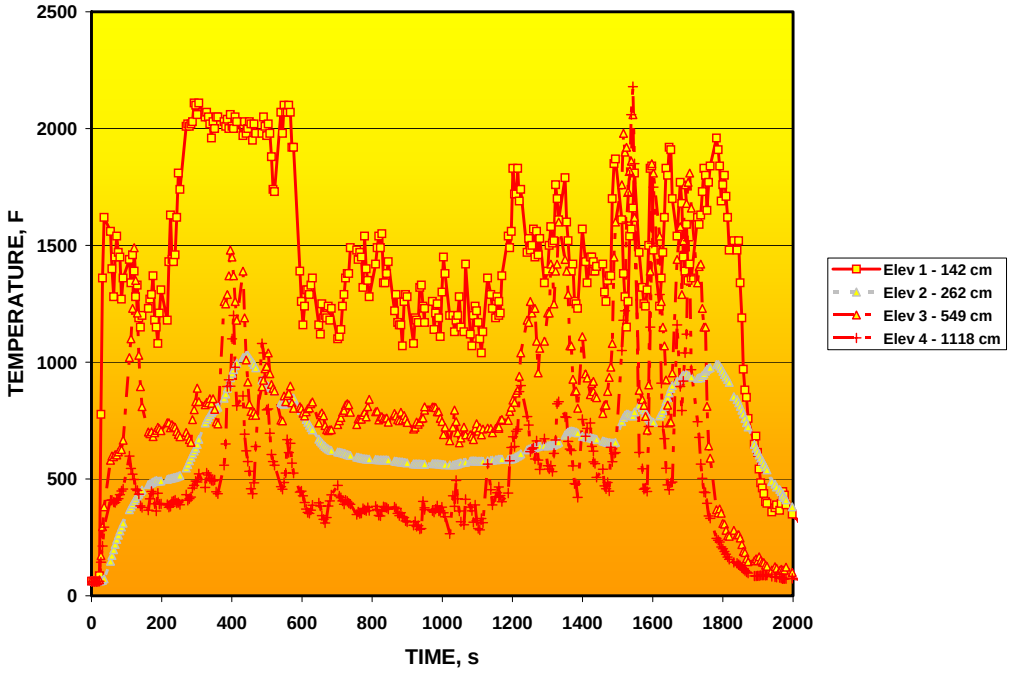

FDS3 Case C-175d

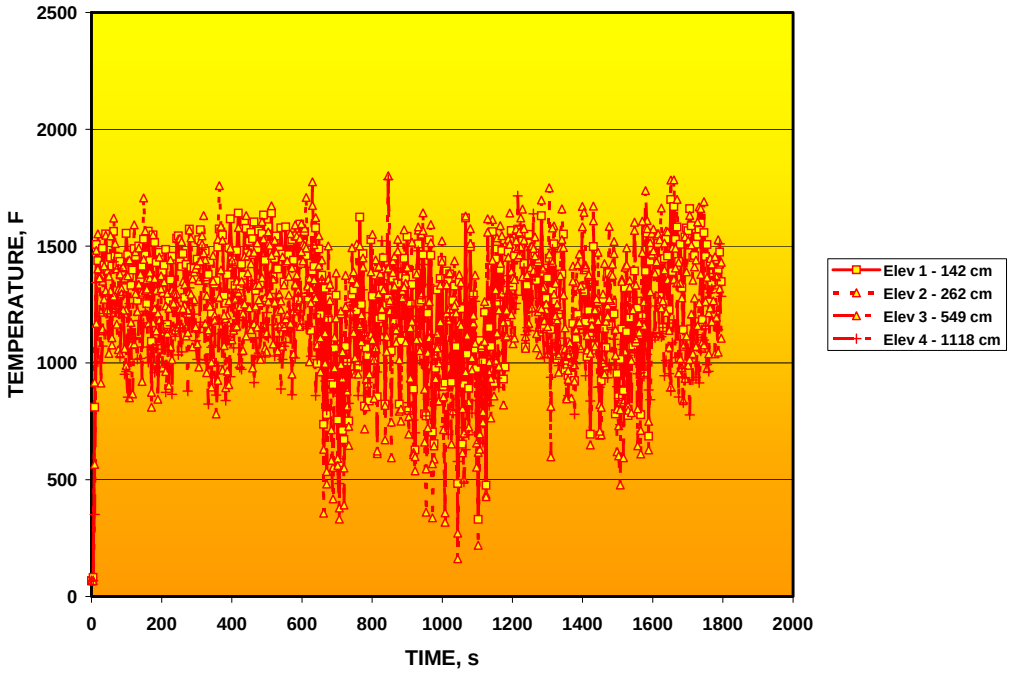

Fig. C.6. Flame temperatures – Tower 4.

Sandia Figure B26

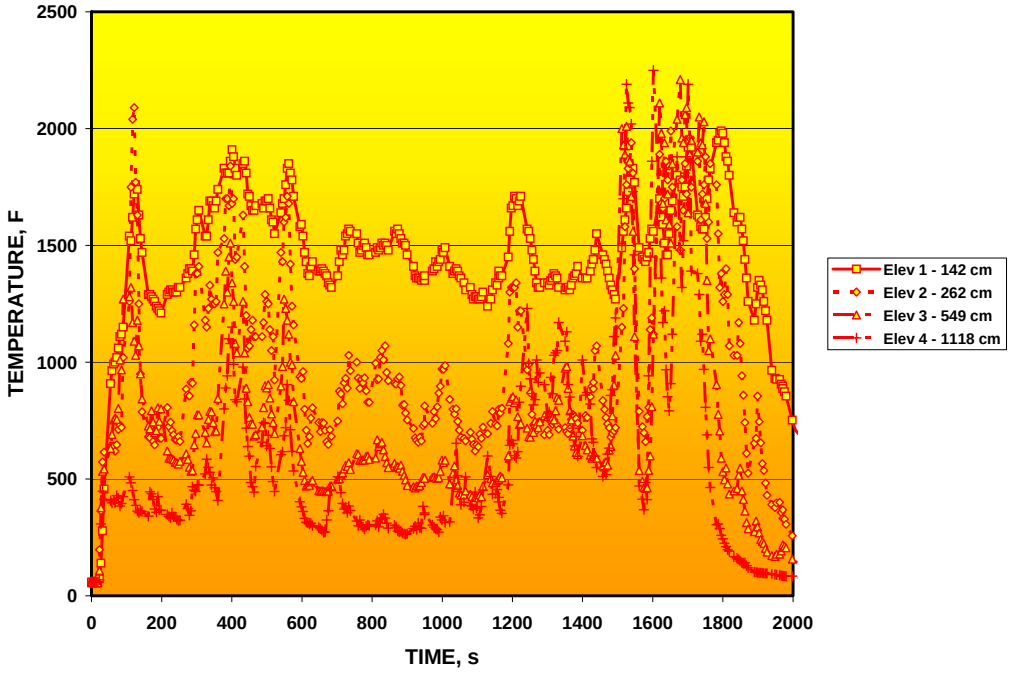

FDS3 Case C-175d

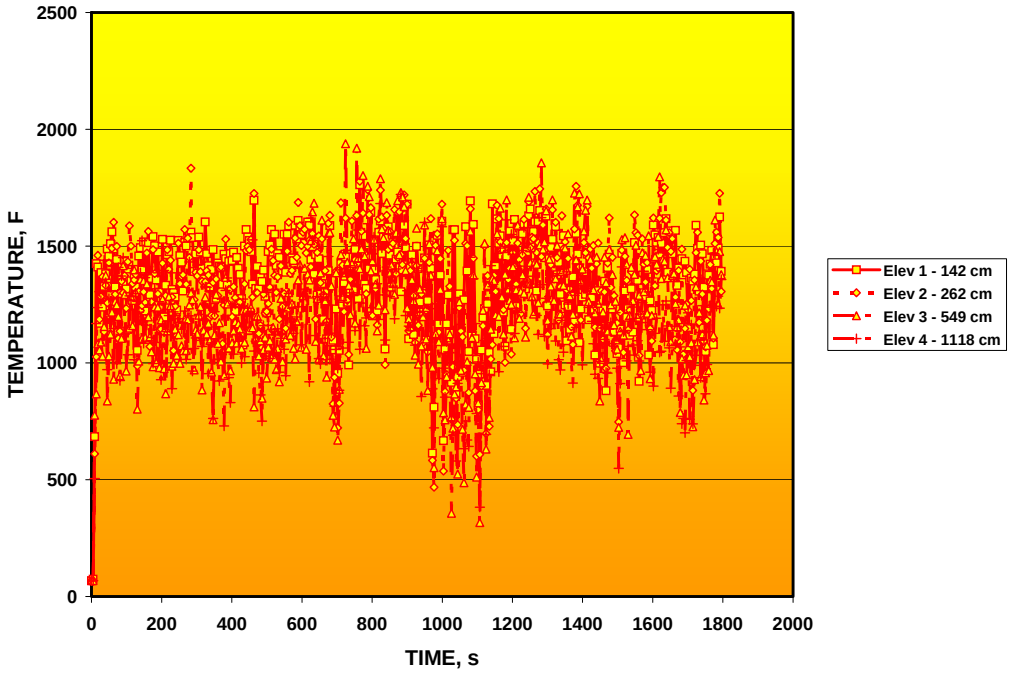

Fig. C.7. Flame temperatures – Tower 6.

Sandia Figure B27

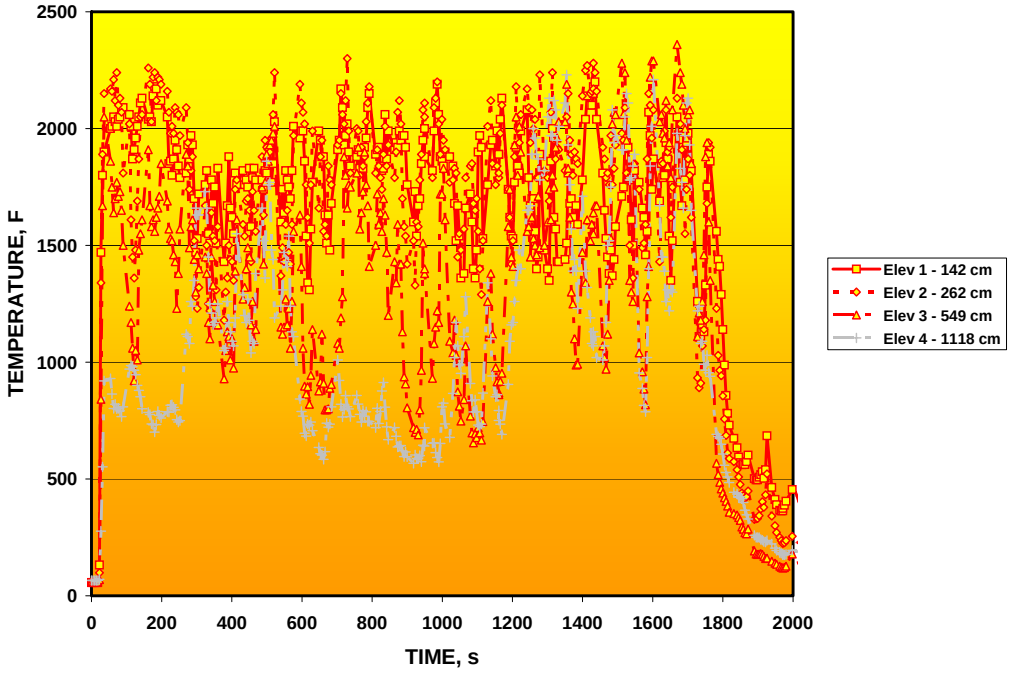

FDS3 Case C-175d

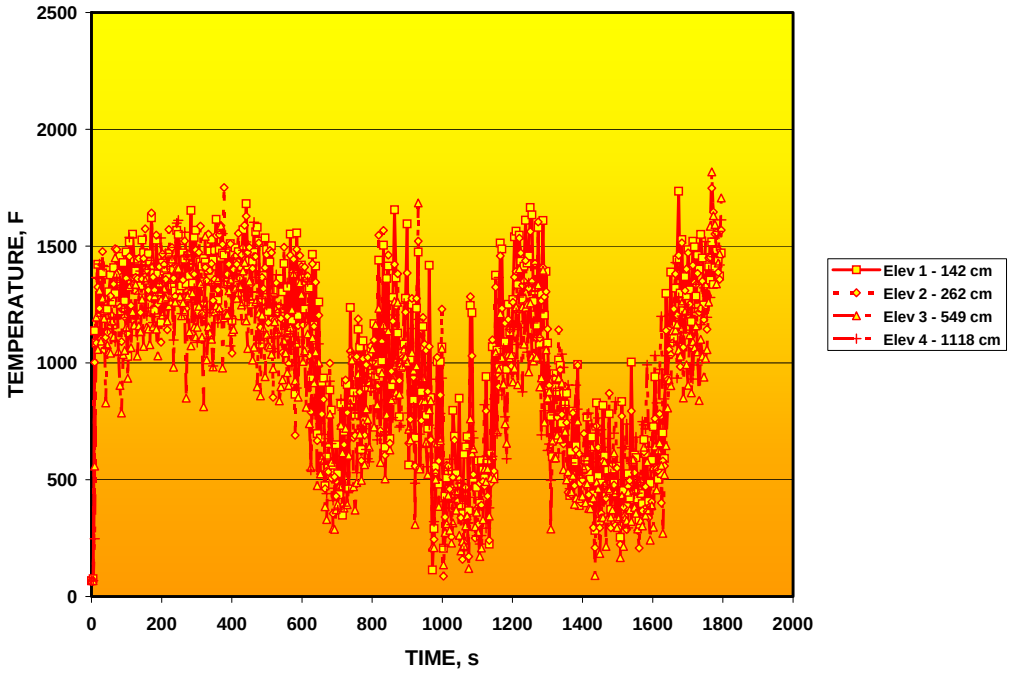

Fig. C.8. Flame temperatures – Tower 7.

Sandia Figure B52

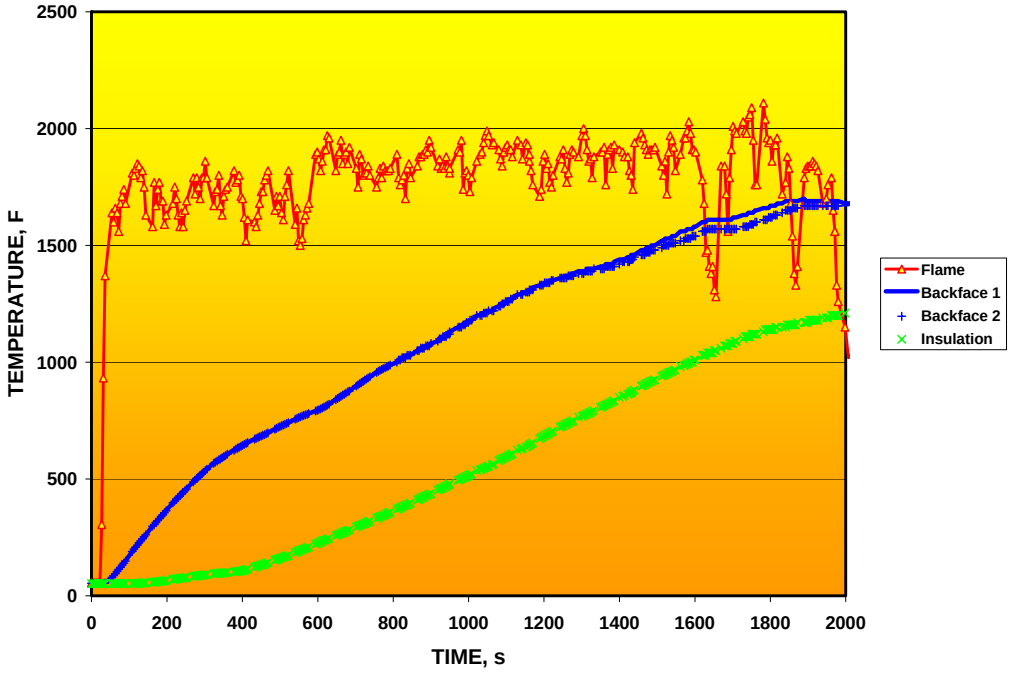

FDS3 Case C-175d

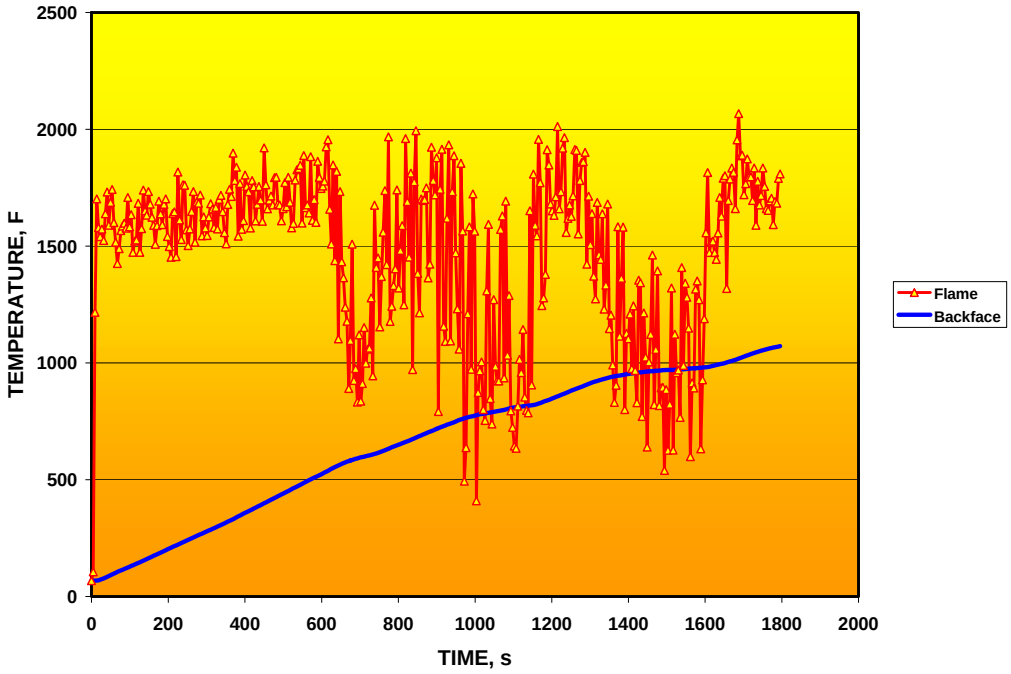

Fig. C.9. Calorimeter temperatures – Position 1-000.

Sandia Figure B53

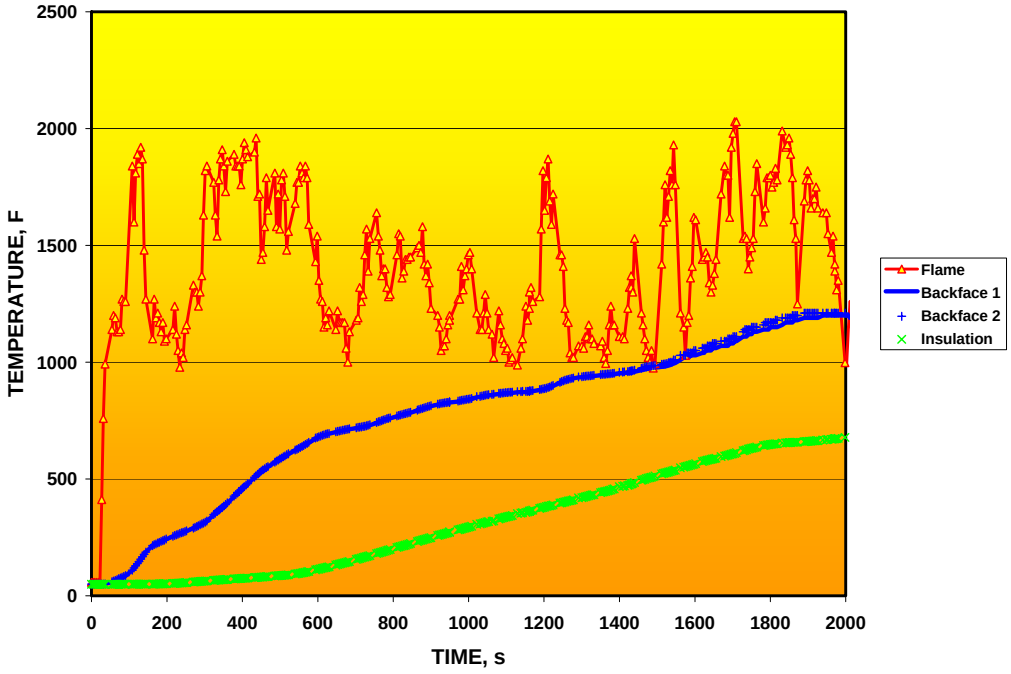

FDS3 Case C-175d

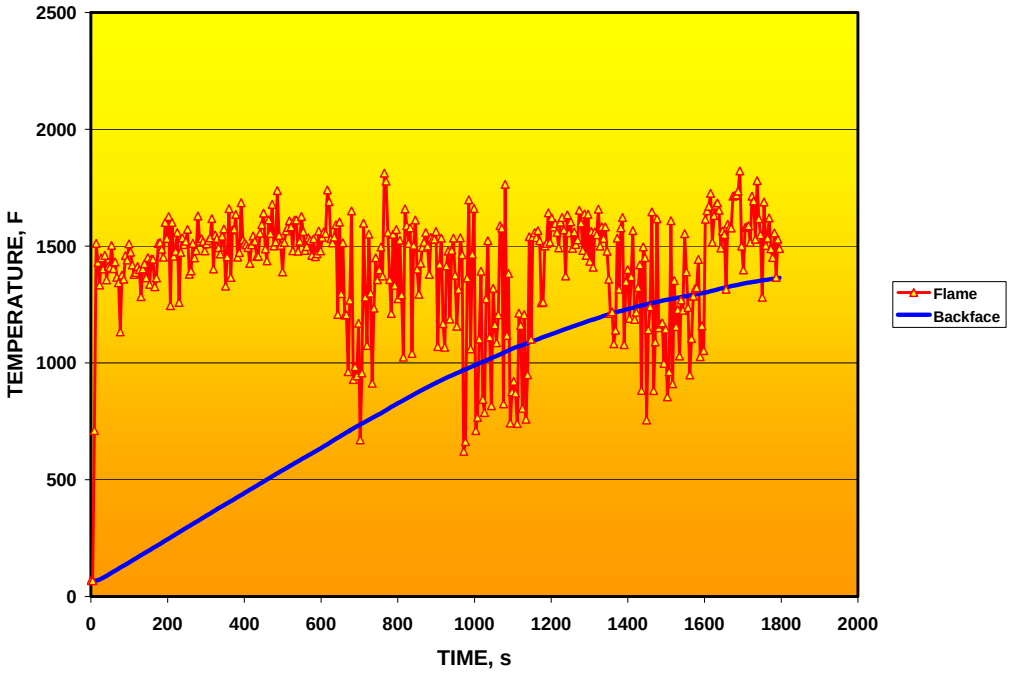

Fig. C.10. Calorimeter temperatures – Position 1-090.

Sandia Figure B54

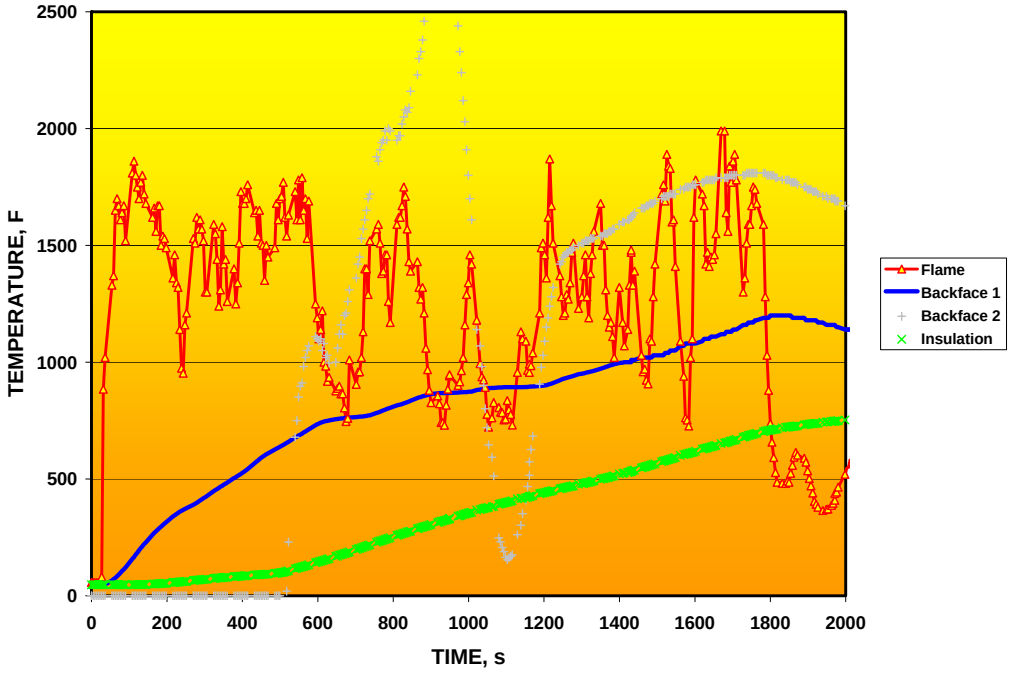

FDS3 Case C-175d

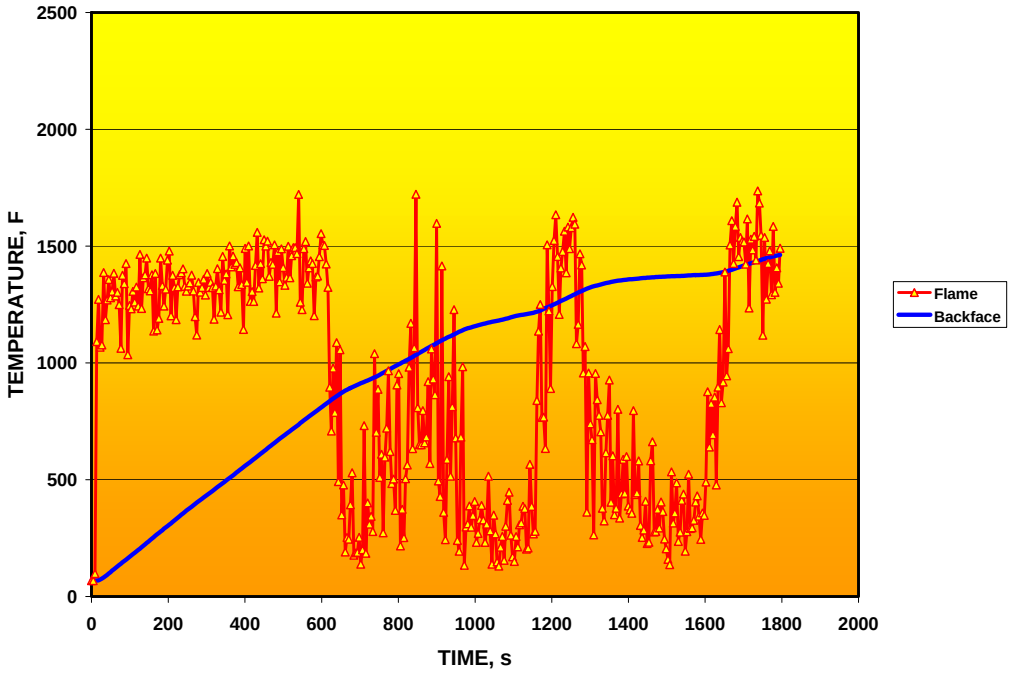

Fig. C.11. Calorimeter temperatures – Position 1-180.

Sandia Figure B55

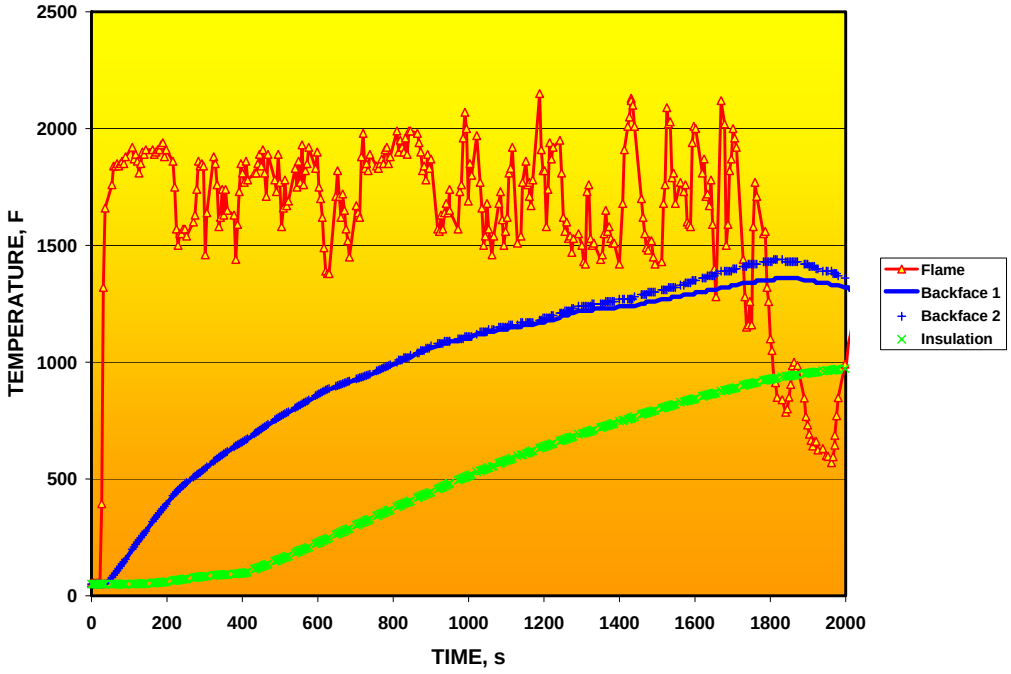

FDS3 Case C-175d

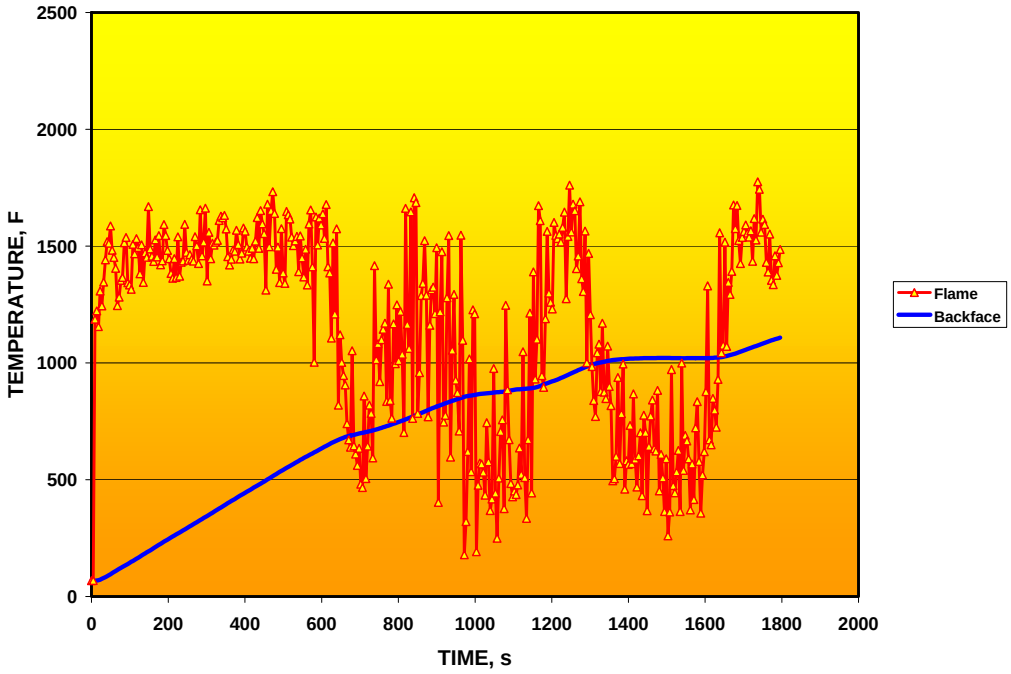

Fig. C.12. Calorimeter temperatures – Position 1-270.

Sandia Figure B56

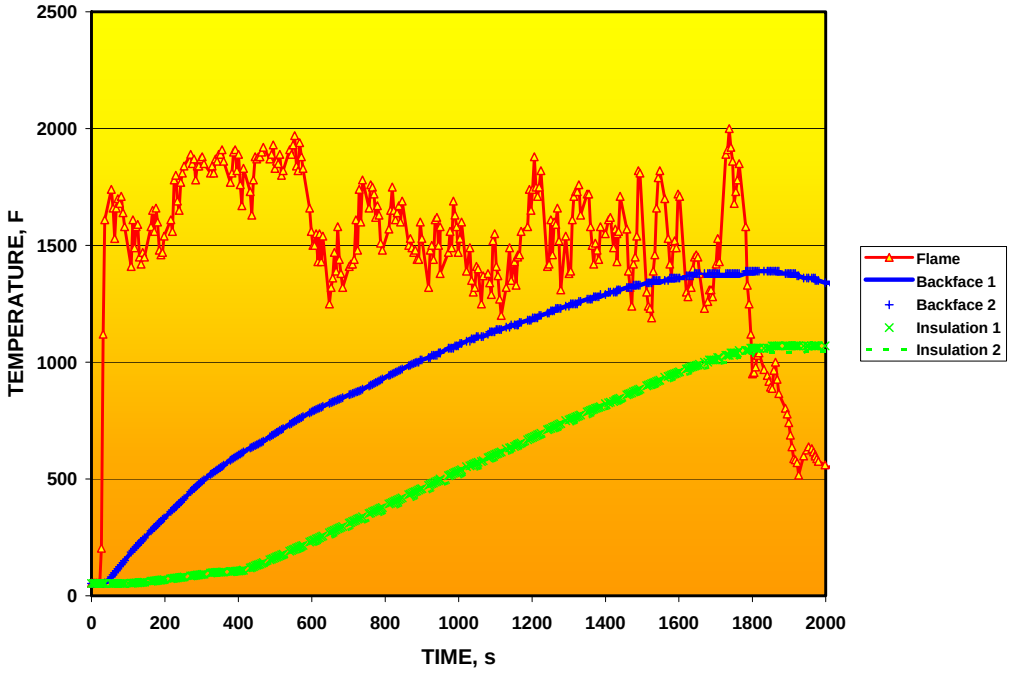

FDS3 Case C-175d

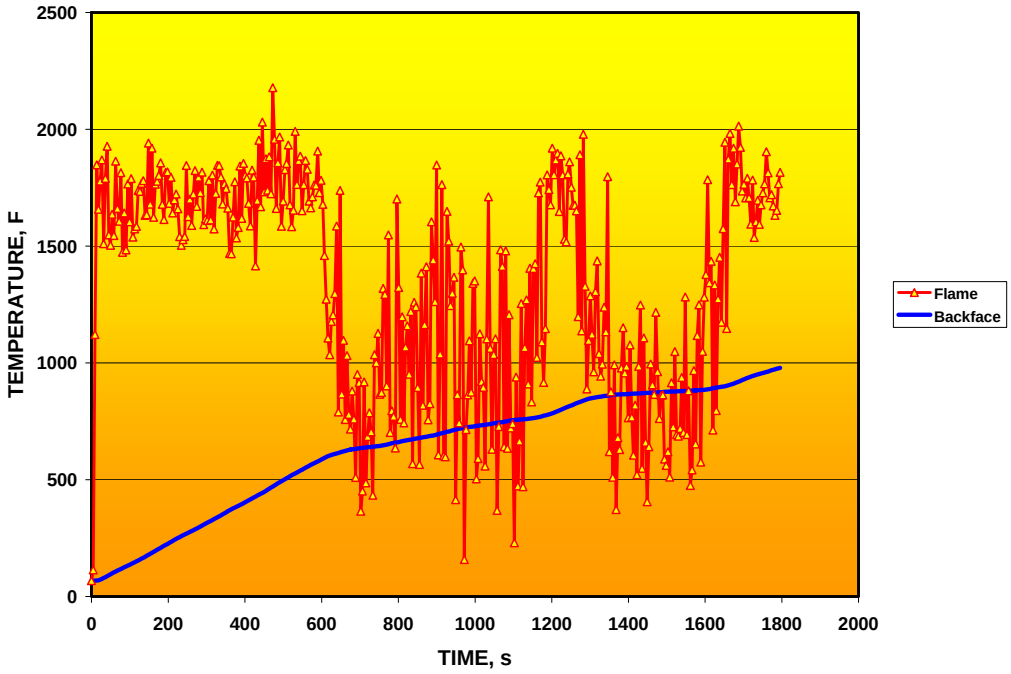

Fig. C.13. Calorimeter temperatures – Position 2-000.

Sandia Figure B57

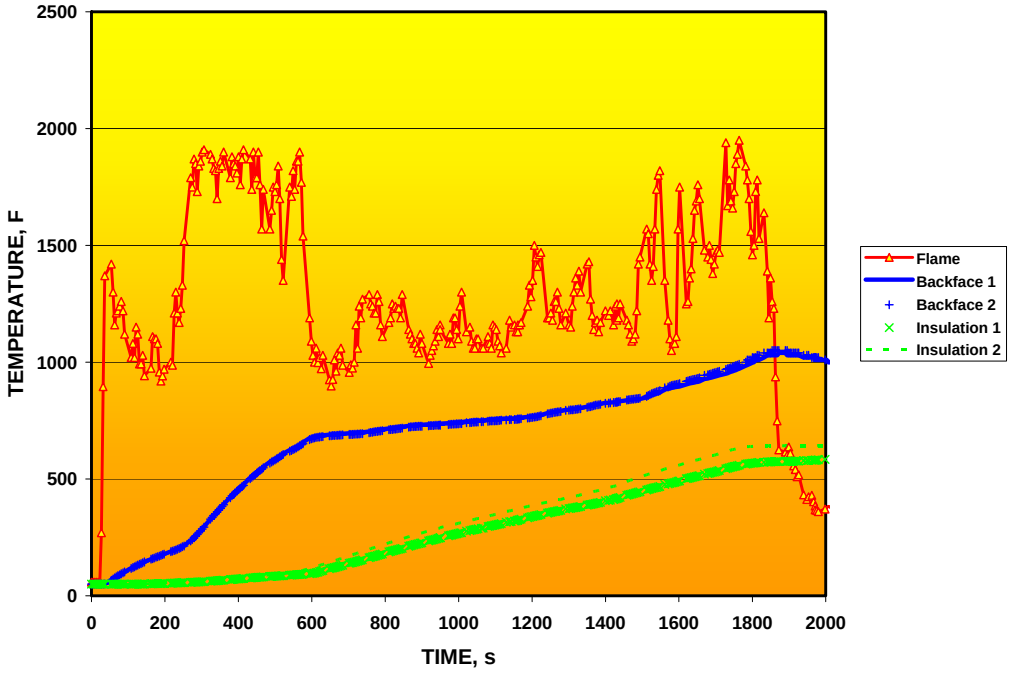

FDS3 Case C-175d

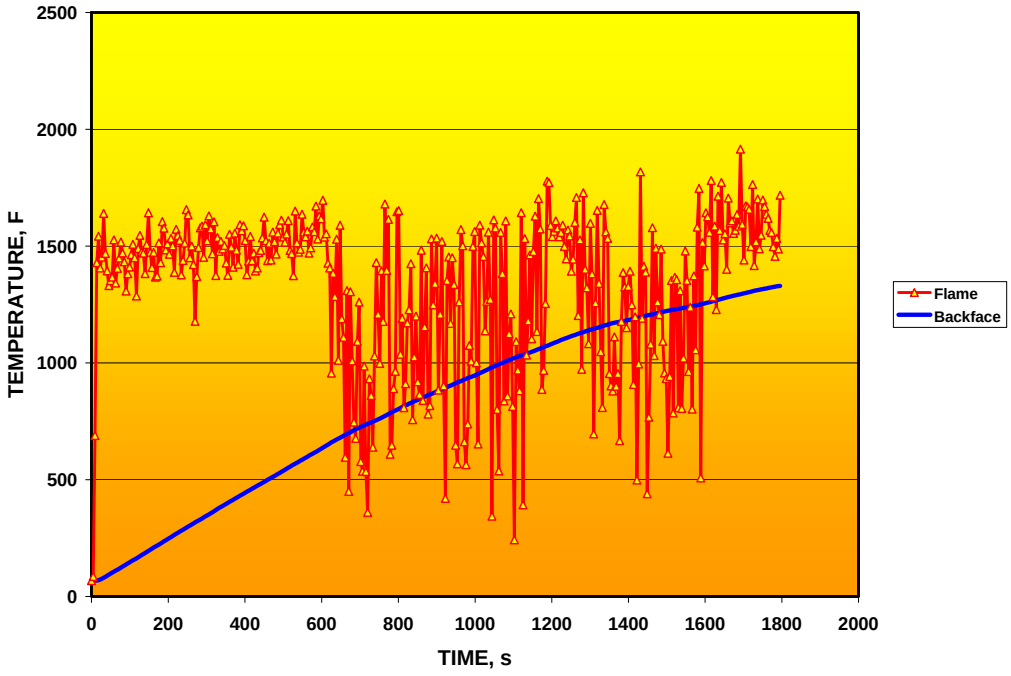

Fig. C.14. Calorimeter temperatures – Position 2-090.

Sandia Figure B58

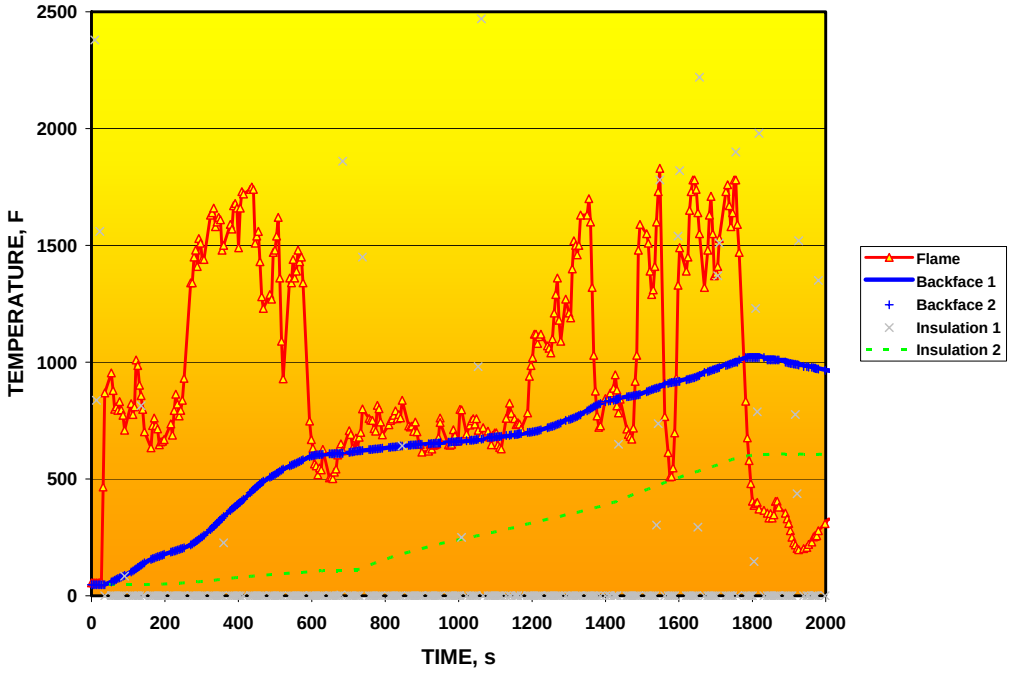

FDS3 Case C-175d

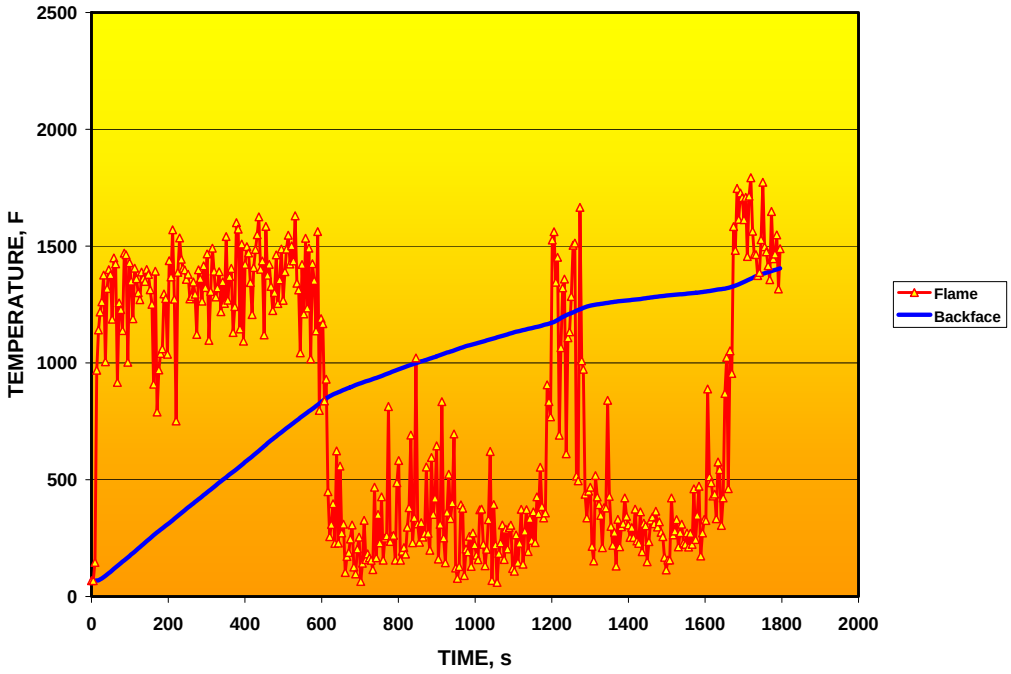

Fig. C.15. Calorimeter temperatures – Position 2-180.

Sandia Figure B59

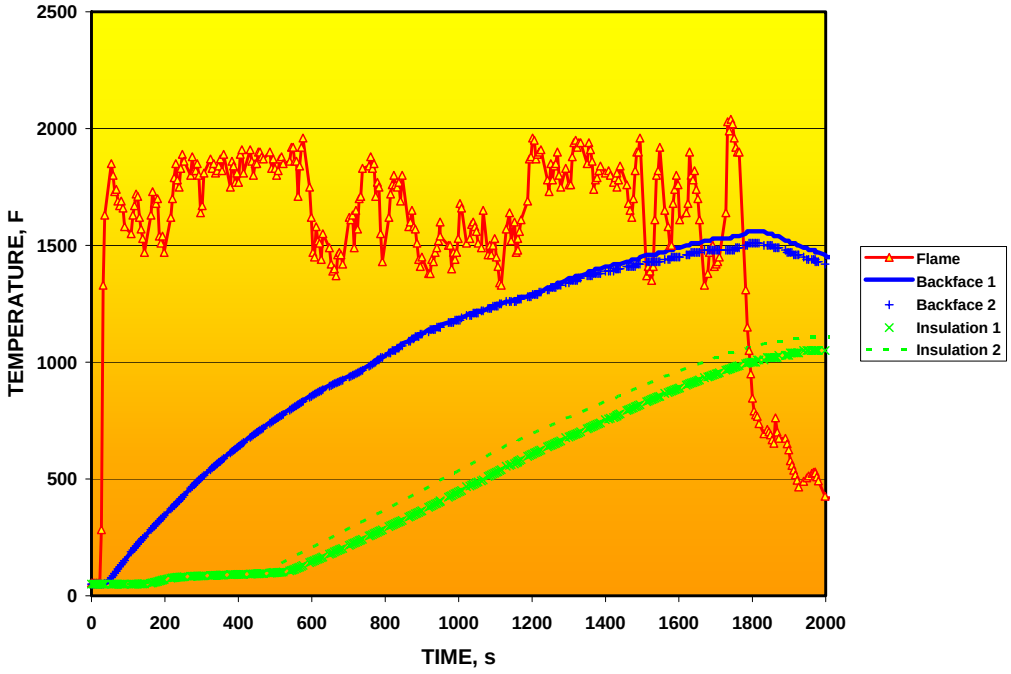

FDS3 Case C-175d

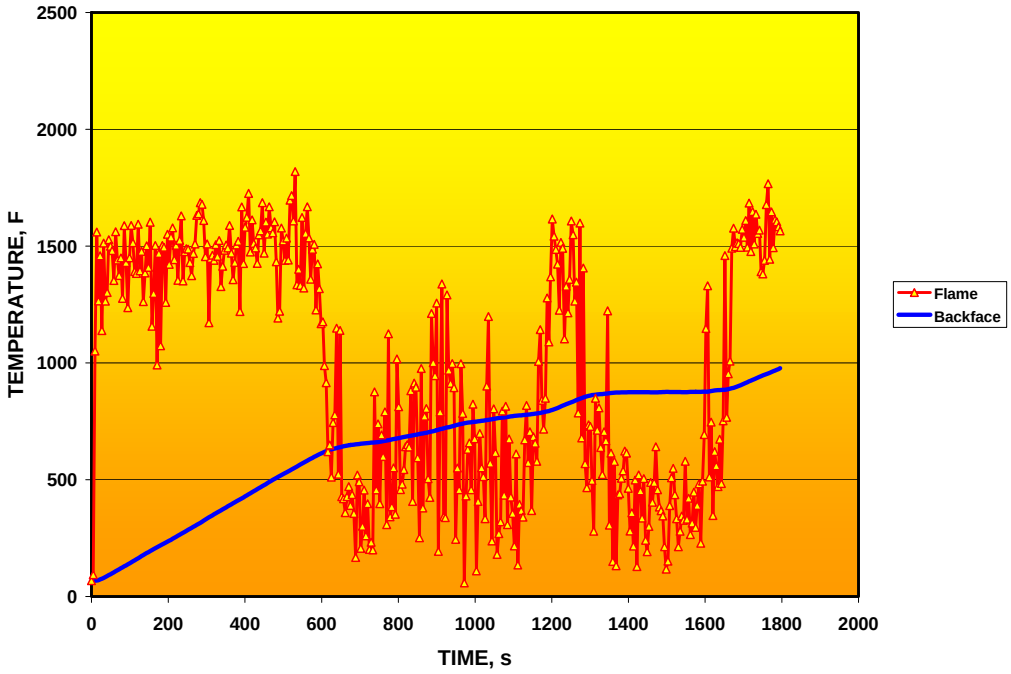

Fig. C.16. Calorimeter temperatures – Position 2-270.

Sandia Figure B60

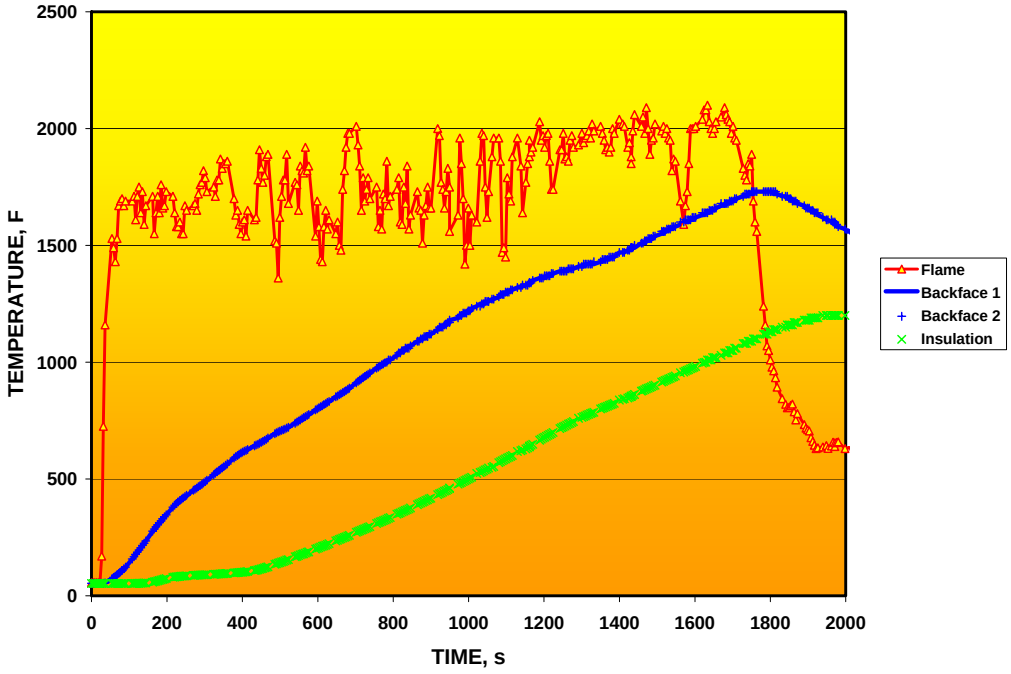

FDS3 Case C-175d

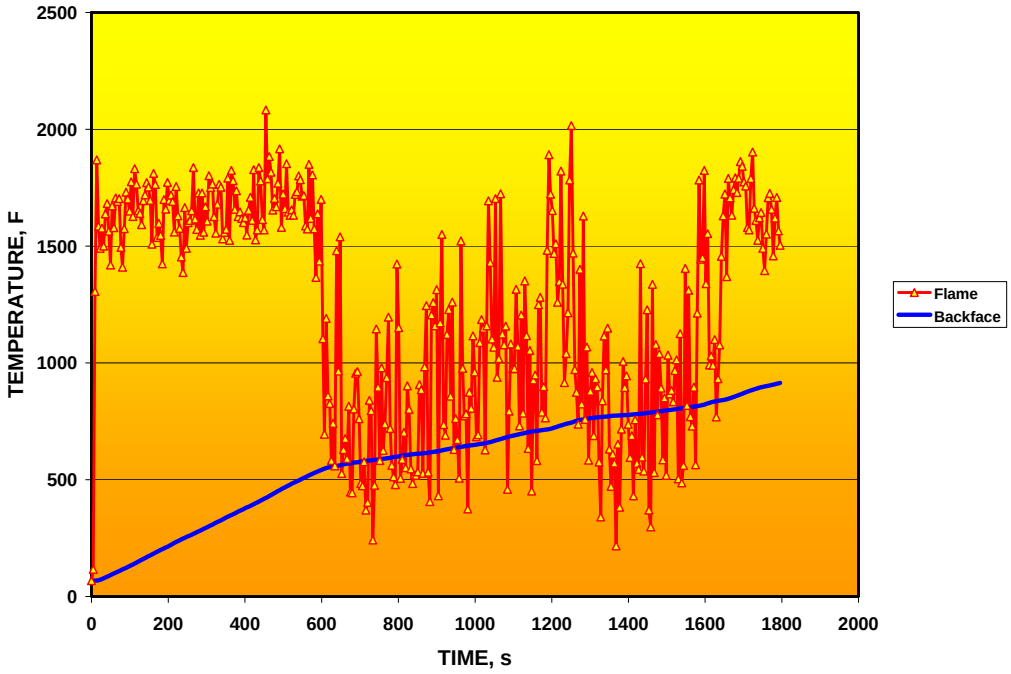

Fig. C.17. Calorimeter temperatures – Position 3-000.

Sandia Figure B61

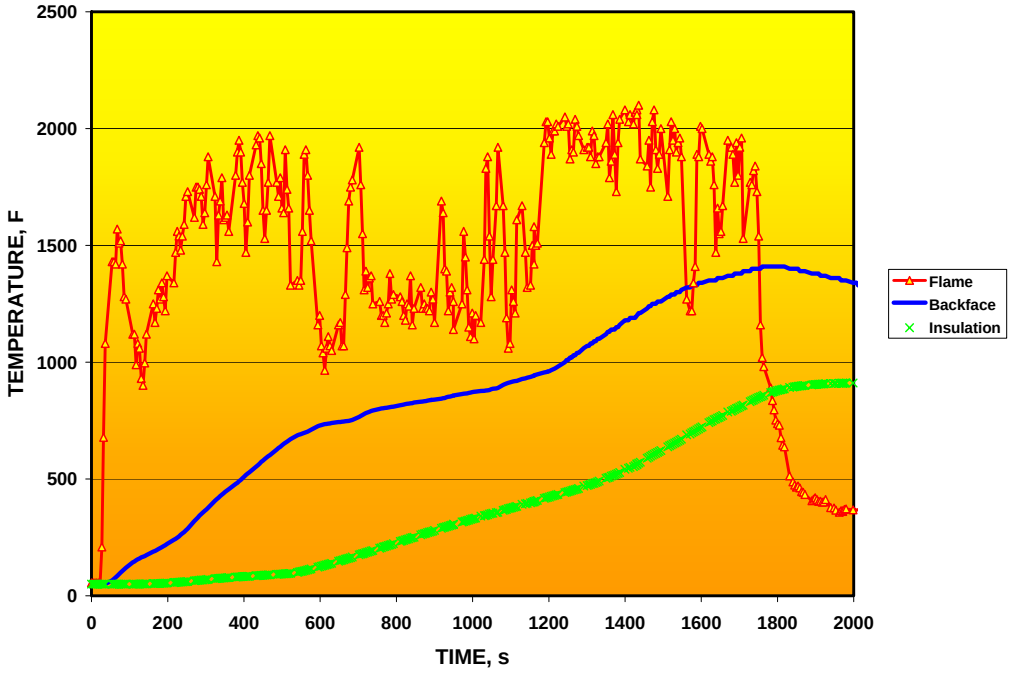

FDS3 Case C-175d

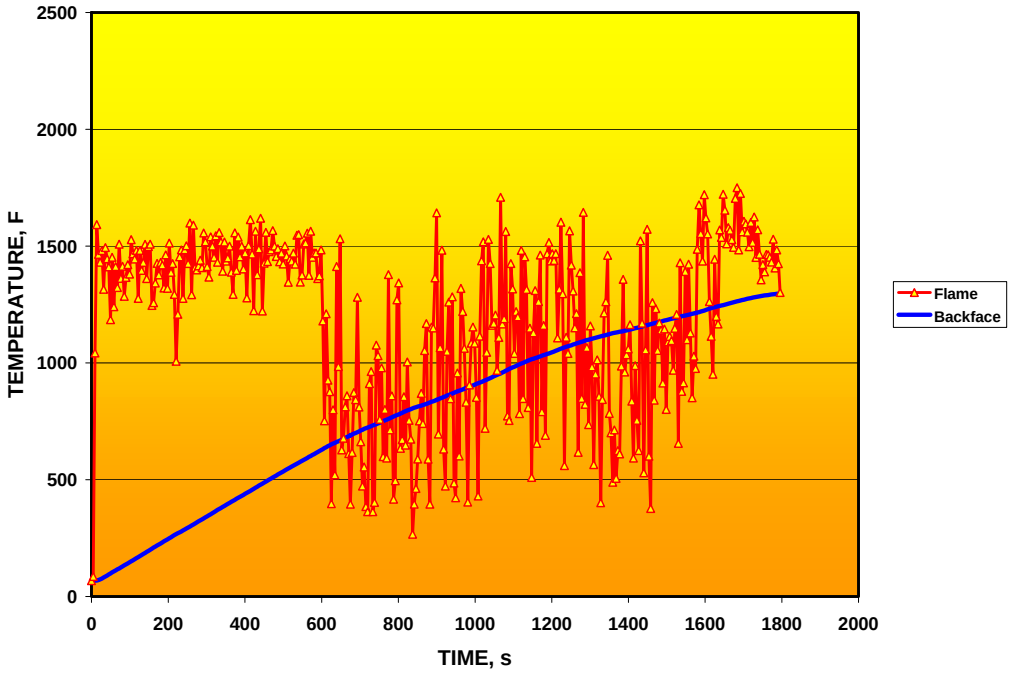

Fig. C.18. Calorimeter temperatures – Position 3-090.

Sandia Figure B62

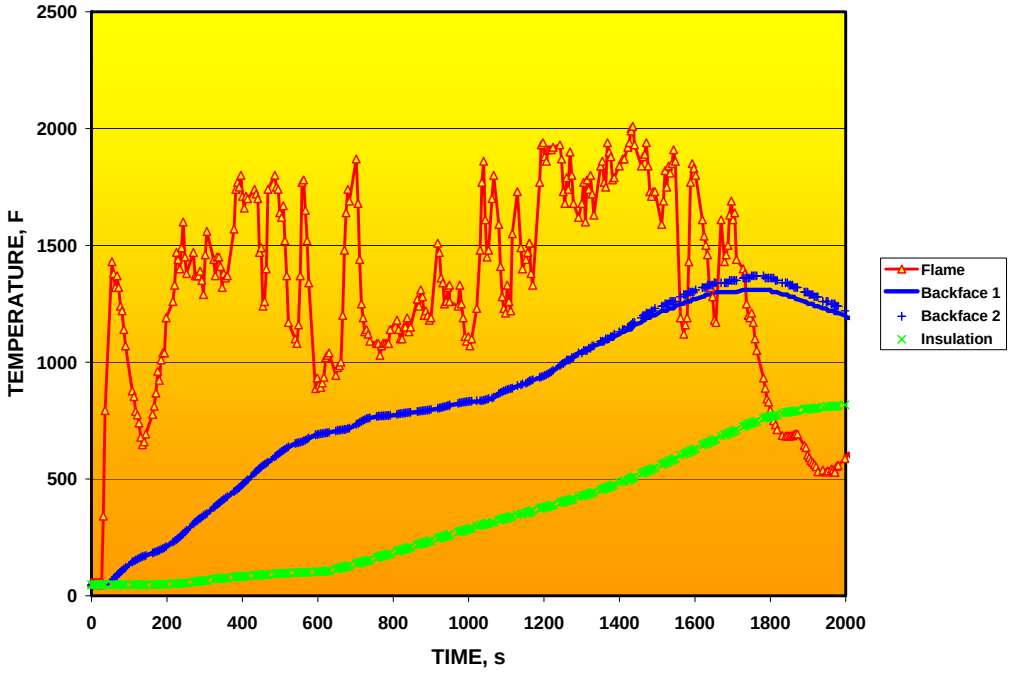

FDS3 Case C-175d

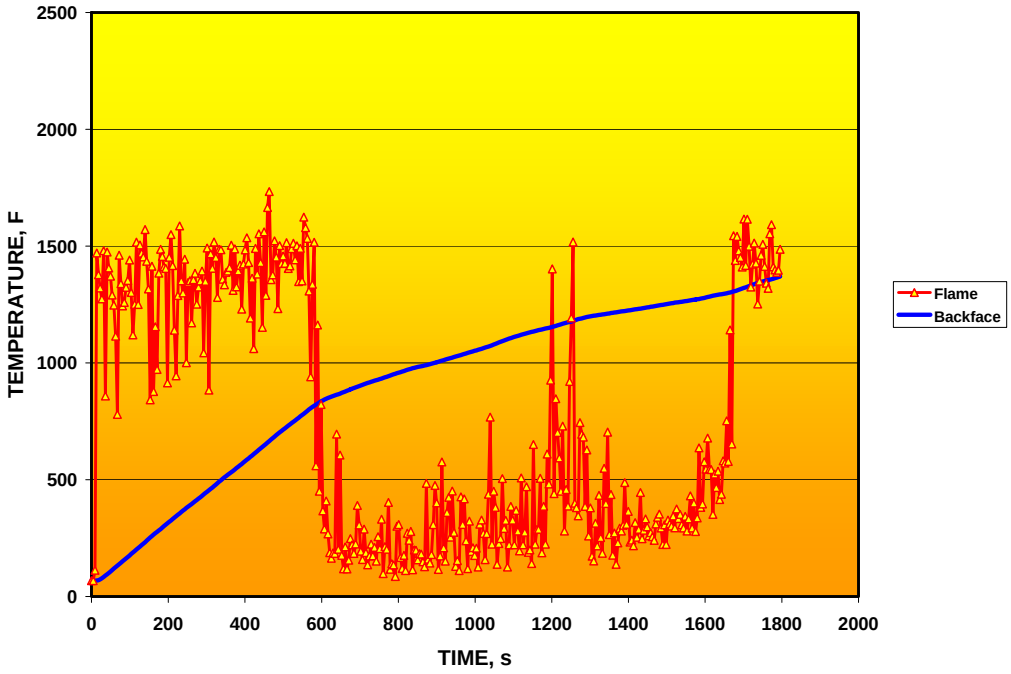

Fig. C.19. Calorimeter temperatures – Position 3-180.

Sandia Figure B63

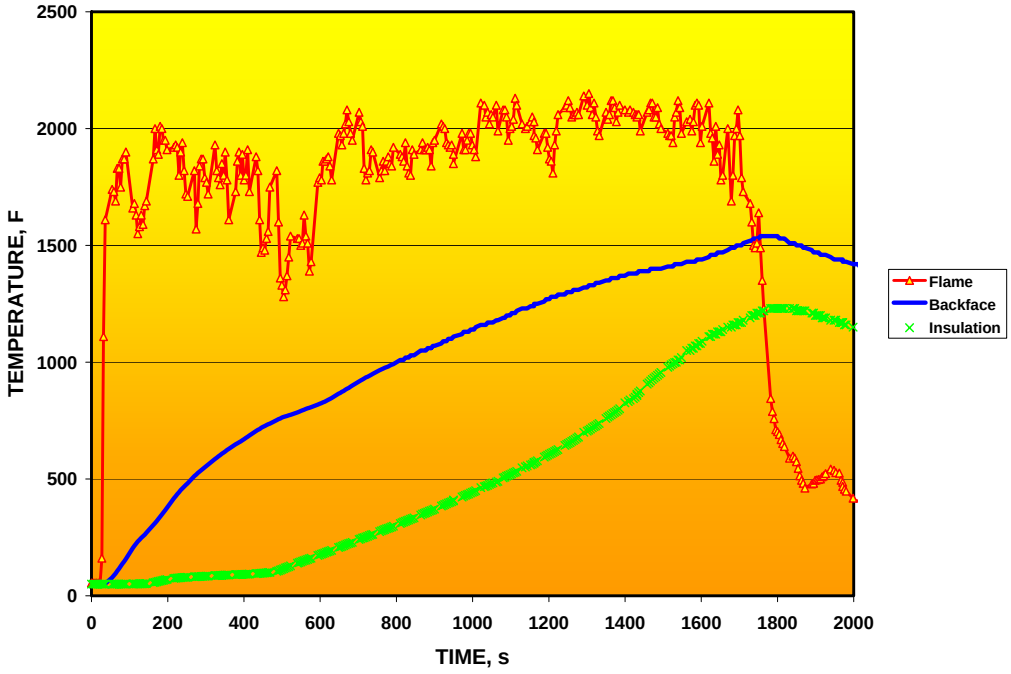

FDS3 Case C-175d

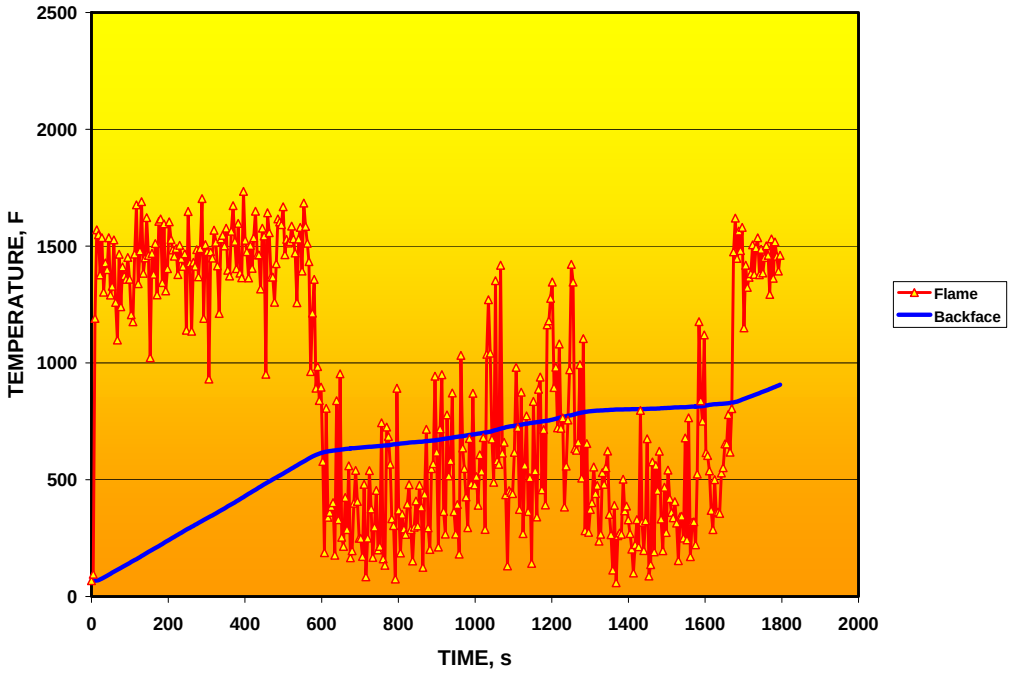

Fig. C.20. Calorimeter temperatures – Position 3-270.

Sandia Figure B77

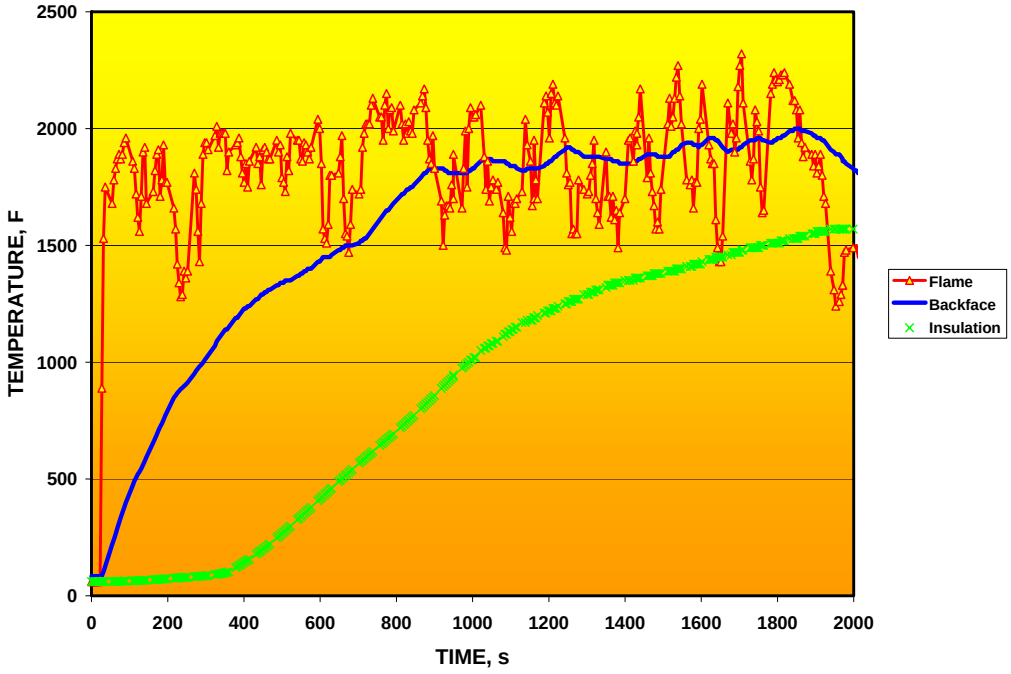

FDS3 Case C-175d

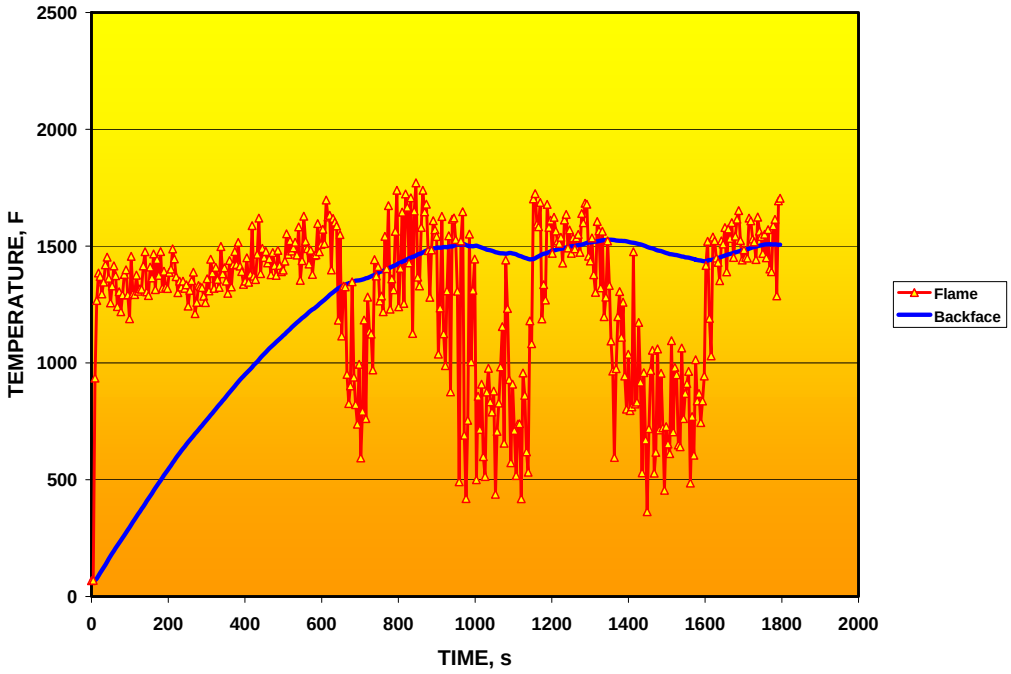

Fig. C.21. Calorimeter temperatures – East end cap.

Sandia Figure B78

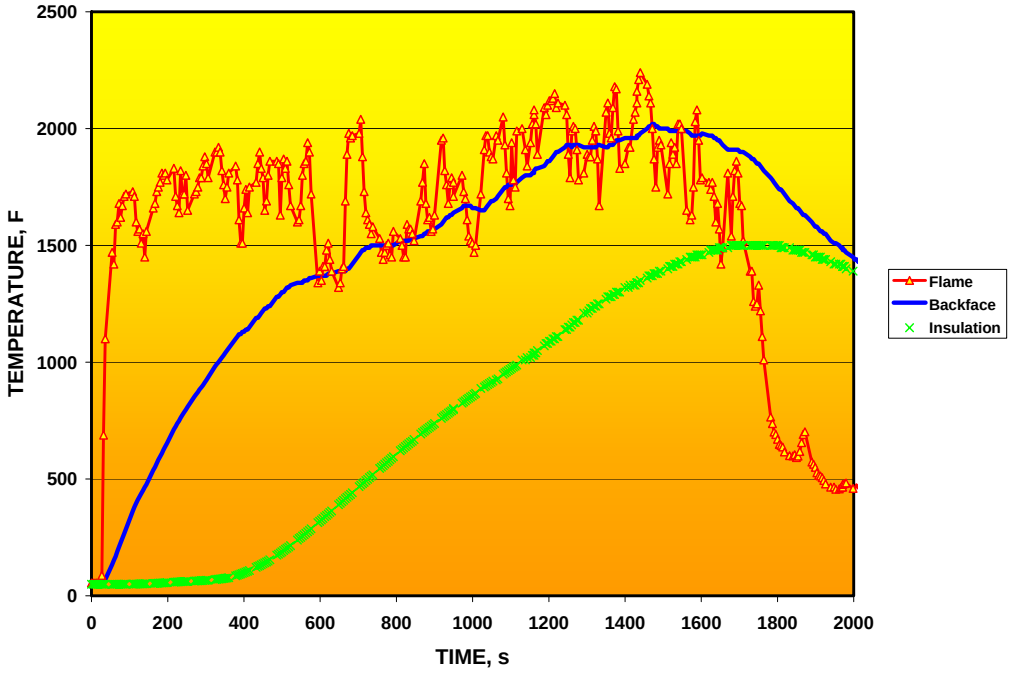

FDS3 Case C-175d

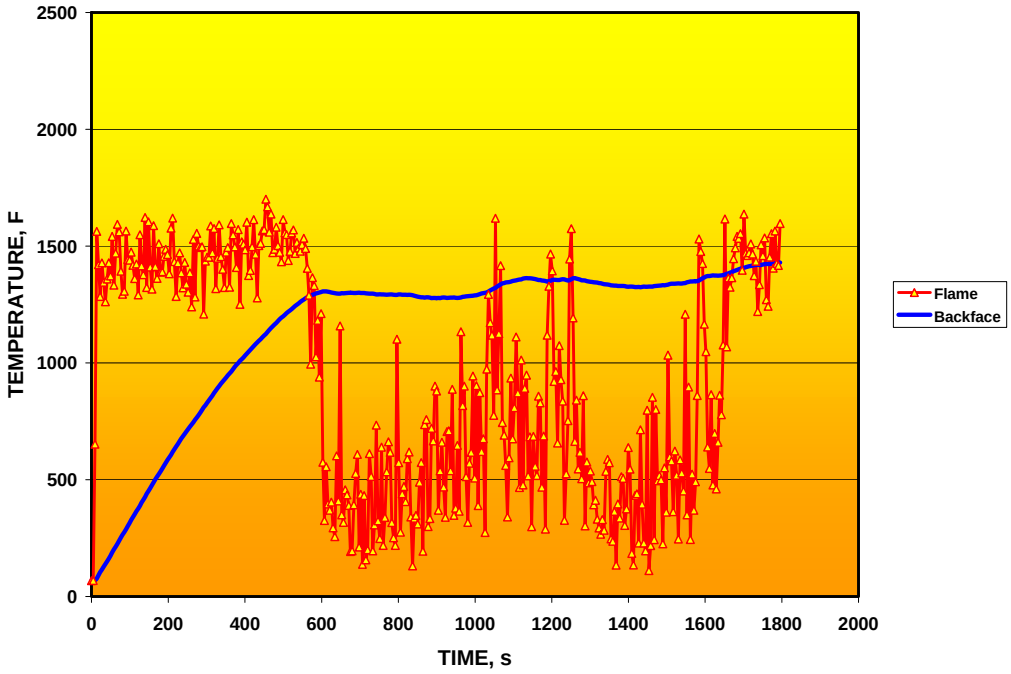

Fig. C.22. Calorimeter temperatures – West end cap

VITA

W. Reid Williams was born July 28, 1952, in Greensboro, North Carolina; was raised in Chattanooga, Tennessee, graduating from Brainerd Senior High School in 1970; and now lives in Knoxville, Tennessee.

In 1975, he received a Bachelor of Chemical Engineering, Cooperative Plan, With Highest Honors, from the Georgia Institute of Technology in Atlanta, Georgia. He co-oped at E. I. DuPont de Nemours and Co. in Chattanooga, Tennessee. While at Georgia Tech, he was elected to Tau Beta Pi.

Since graduation, he has been employed by operating contractors of the Department of Energy facilities in Oak Ridge, Tennessee: Union Carbide Corporation, Nuclear Division; Martin Marietta Energy Systems; Lockheed Martin Energy Systems; and BWXT Y-12. Principal areas of interest have been atmospheric dispersion and thermal analysis, including fire modeling of uranium hexafluoride cylinders and sulfuric acid tanks engulfed in fire and the effects of extended combustion of insulating material in damaged packages. In 1998, he received the Lockheed Martin Energy Systems Technical Achievement Award.

Mr. Williams is a Registered Professional Engineer, TN 14,242.